SKB

# TECHNICAL REPORT 85-08

## In situ one-year burial experiments with simulated nuclear waste glasses

Larry L Hench, Derek Spilman and T Buonaquisti
Collage of Engineering, Univ. of Florida, Gainesville, USA
Alexander Lodding
Chalmers Univ. of Technology, Gothenburg, Sweden
Lars Werme
SKB, Stockholm, Sweden

**SVENSK KÄRNBRÄNSLEHANTERING AB**
*SWEDISH NUCLEAR FUEL AND WASTE MANAGEMENT CO*

BOX 5864 S-102 48 STOCKHOLM
TEL 08-67 95 40 TELEX 13108-SKB
TEL 08-665 28 00

SKB

# TECHNICAL REPORT 85-08

## In situ one-year burial experiments with simulated nuclear waste glasses

Larry L Hench, Derek Spilman and T Buonaquisti
Collage of Engineering, Univ. of Florida, Gainesville, USA
Alexander Lodding
Chalmers Univ. of Technology, Gothenburg, Sweden
Lars Werme
SKB, Stockholm, Sweden

**SVENSK KÄRNBRÄNSLEHANTERING AB**
*SWEDISH NUCLEAR FUEL AND WASTE MANAGEMENT CO*

BOX 5864 S-102 48 STOCKHOLM
TEL 08-665 28 00 TELEX 13108-SKB

# IN SITU ONE-YEAR BURIAL EXPERIMENTS

# WITH

# SIMULATED NUCLEAR WASTE GLASSES

Larry L Hench, Derek Spilman and T Buonaquisti
College of Engineering, Univ. of Florida, Gainesville, USA

Alexander Lodding
Chalmers Univ. of Technology, Gothenburg, Sweden

Lars Werme
SKB, Stockholm, Sweden

## ABSTRACT

Two simulated nuclear waste glasses were corroded in an in-situ experiment in the Stripa mine up to one year at 90°C and ambient temperature. Changes in compositional in-depth profiles were measured using Fourier transform infrared reflection spectroscopy, SIMS and Rutherford back-scattering.

For glass/glass interfaces, both glasses showed depletion of Na, Cs and B, but for the more corrosion resistant glass, the lower depletion is ascribed to the formation of a thin (0.2 nm) coherent and dense outer layer, enriched in Mg, Ca, Sr, Ba, Zn-Al), and Si, which impedes both ion exchange and network attack of the bulk underneath.

For the bentonite interfaces, cation exchange of Ca, Mg, Al and Fe from the bentonite for primarily Na and B is found to produce a glass surface that has three silicate-rich layers. The larger concentrations of $M^{2+}$ and $M^{3+}$ cations and the high silica content of the reaction layers result in a considerably retarded rate of ion exchange after the formation of these layers during the first three months of burial.

The granite interfaces showed the lowest rate of attack. This appears to be due to a large increase of Fe and Al within the glass surfaces exposed to granite.

The results obtained using Rutherford back-scattering confirm the results obtained using the other techniques for surface analysis.

Analysis of burial samples cast in steel mini-canisters show no significant effects associated with the steel canister-glass interface.

TABLE OF CONTENT

# IN-SITU ONE-YEAR BURIAL EXPERIMENTS WITH SIMULATED NUCLEAR WASTE GLASSES

## FOREWORD

In 1981 a series of burial experiments using simulated nuclear waste glasses started in Stripa mine. In this experimental study the corrosion of several glass compositions have been studied in contact with groundwater, granite, bentonite and overpack materials under realistic conditions. To date results for exposure times up to one year have been evaluated, but the study is still in progress and results for longer exposure times will be presented in forthcoming reports as well as results from studies using glass compositions other than the ones reported here.

The present report contains a decription of the experimental set-up, together with four papers discussing the specific interactions for the glass/glass, glass/bentonite and glass/granite interfaces followed by a paper on the application of Rutherford back-scattering for surface analysis.

## EXPERIMENTAL SET-UP

For the study, two configurations of glass, canister, overpack and buffer/backfill materials were designed (Figs, 1 and 2). Both configurations were inserted into 56 mm diameter, 3 m deep boreholes in the Stripa mine at the 340 m level and maintained at 90°C. One of the configurations (Fig. 2) was also kept at ambient temperature, approx. 10°C. In the experiments reported here, two glass types were used, ABS 39 and ABS 41 (Table 1).

TABLE 1

GLASS COMPOSITION (WEIGHT %)

| Oxide | ABS 39 | ABS 41 |
|---|---|---|
| $SiO_2$ | 48.5 | 52.0 |
| $B_2O_3$ | 19.1 | 15.9 |
| $Al_2O_3$ | 3.1 | 2.5 |
| $Na_2O$ | 12.9 | 9.9 |
| $Fe_2O_3$ | 5.7 | 3.0 |
| ZnO | 0 | 3.0 |
| $Li_2O$ | 0 | 3.0 |
| $UO_2$ | 1.7 | 1.7 |
| Simulated fission products | 9.0 | 9.0 |

One configuration, Fig. 1, is designed to simulate closely a waste package in a disposal hole. The glass specimens, referred to as "mini-canisters", contain ABS 39 or ABS 41 glass cast into chromium-nickel steel cylinders. The upper and lower surfaces of the mini-canisters are polished to to a 600 grit surface finish after a concentric center hole is bored for a center heater rod. The mini-canisters are then arranged to provide glass/glass and glass/bentonite interfaces as is shown schematically in Fig. 3. Sleeves of lead and titanium or copper overpacks are placed around the steel wall of the mini-canister, and a bentonite buffer sleeve separates the waste package form the granite walls of the borehole in the granitic rock.

In the second configuration (called "pineapple slices"), right cicular discs of glass, granite, bentonite and various overpack are stacked around a central tube containing a heater rod, to maximize the number of interfaces between glass and other materials (Fig. 2). The sequence of interfaces are shown schematically in Fig. 4. One side of each glass sample is polished to 600 grit. The alternate side is left rough in order to avoid mixing the interfaces during disassembly.

Both configurations provide interfaces between the glass and the other components in the KBS waste storage concept. However, the the number of interfaces are maximized in the "pineapple slice" configuration (28 vs 8) and consequently most experiments are performed using that configuration.

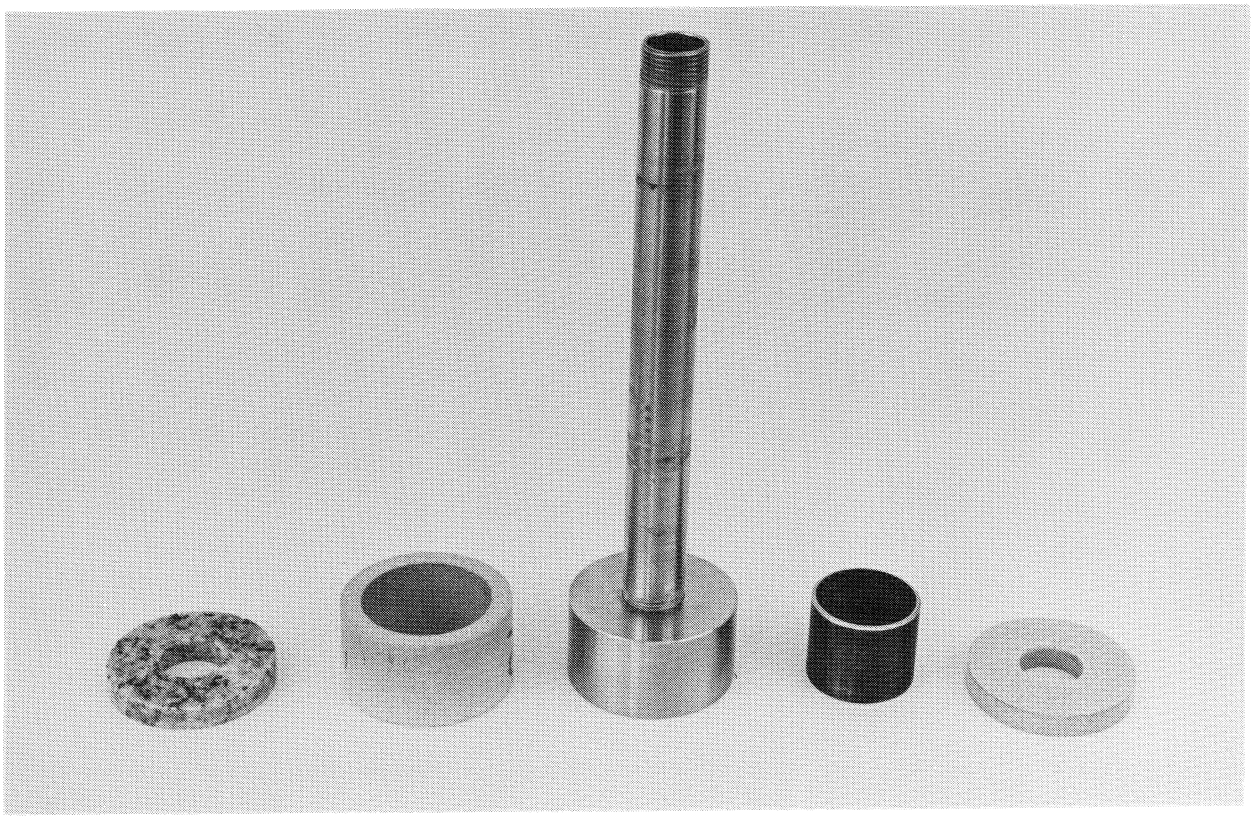

Figure 1. Mini-canister experiment; Photograph of: granite disc, bentonite sleeve, holder, glass canister, and bentonite disc.

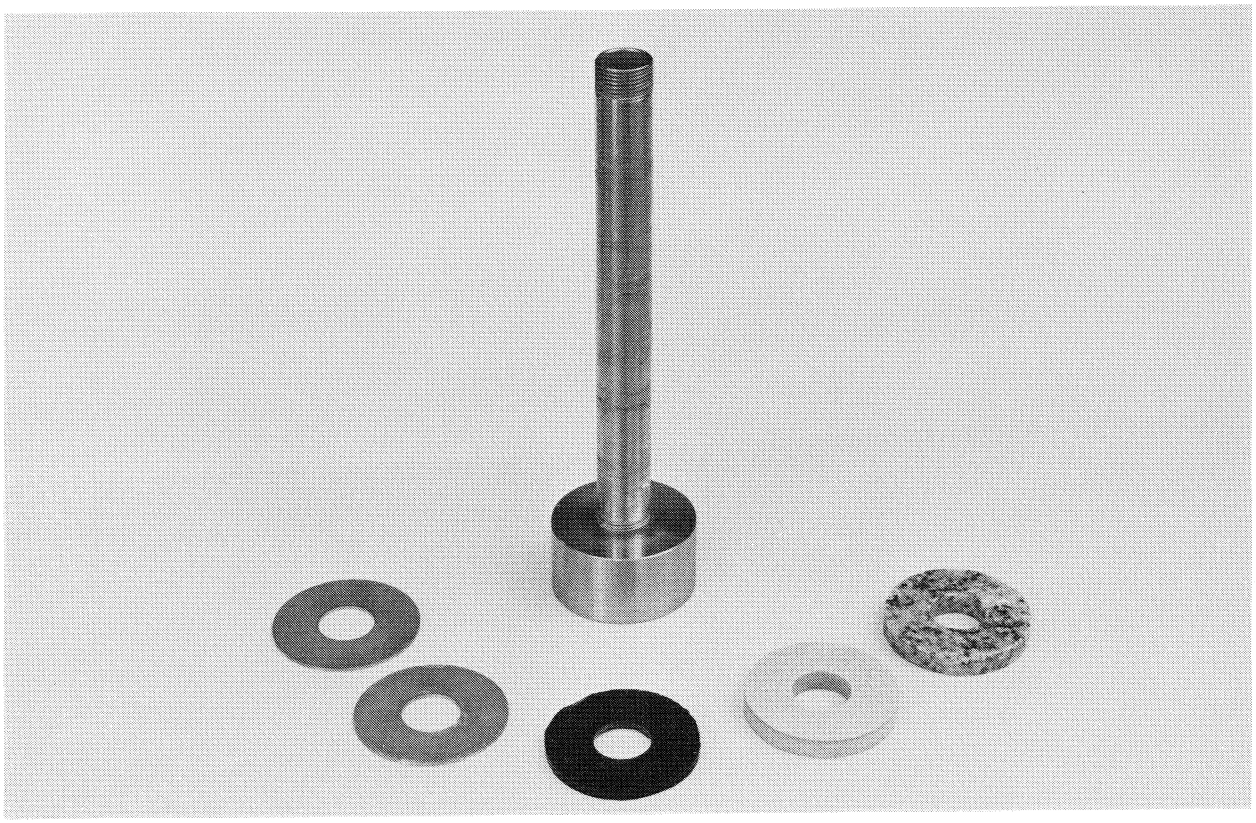

Figure 2. Parts of a "pineapple slice" stack.

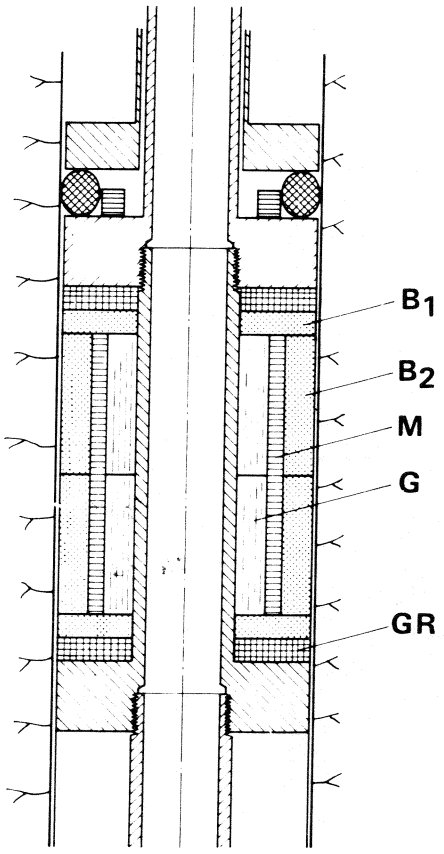


$B_1$ = Highly compacted bentonite plate

$B_2$ = Highly compacted bentonite (ring)

M = Metal comp. (Steel 253 MA lead titanium copper)

G = Glass

GR= Granite

Figure 3. Schematic view of a mini-canister in a borehole.

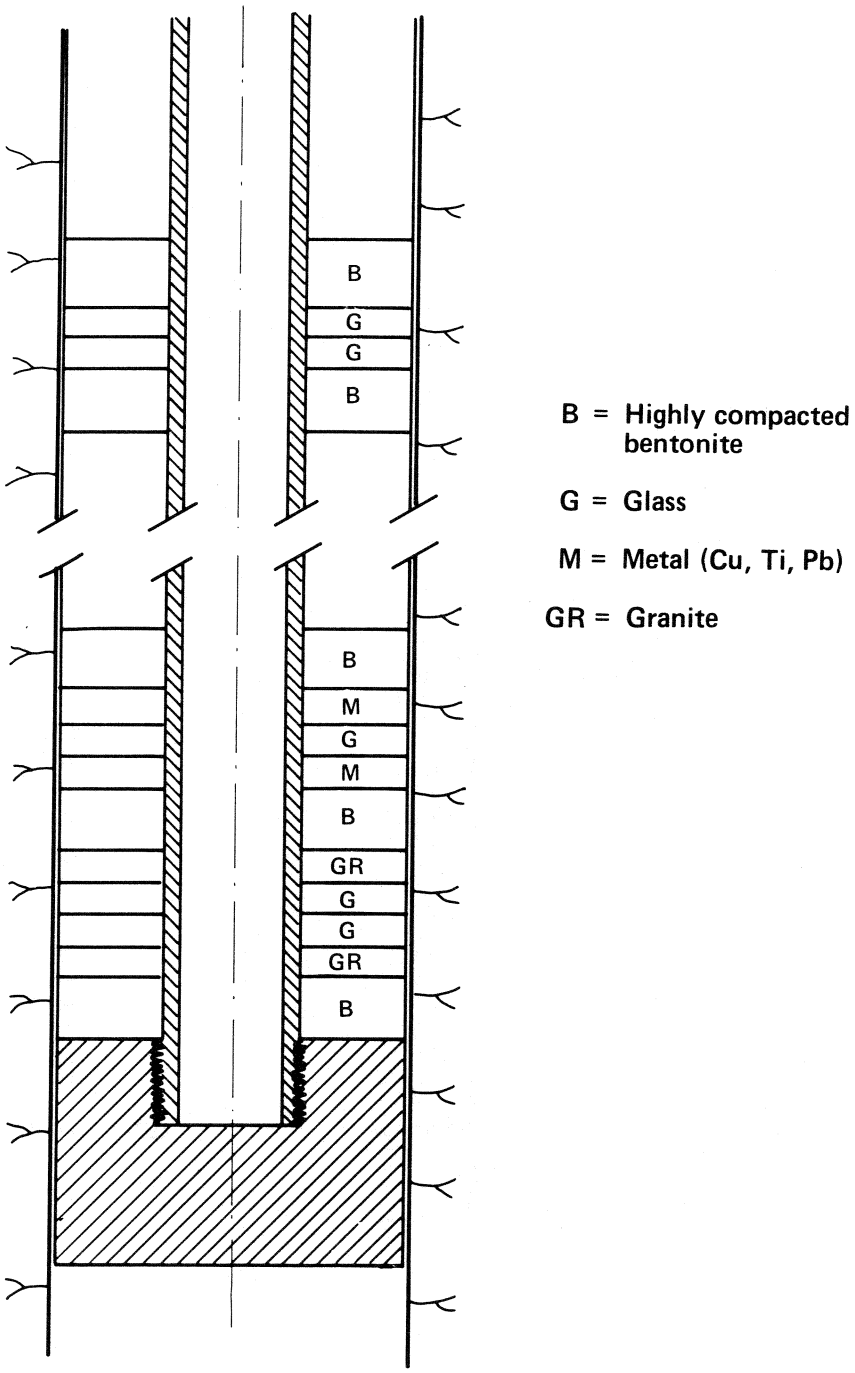


Figure 4. Sequence of glass interfaces in the "pineapple slice" burial configuration.

# NUCLEAR WASTE GLASS INTERFACES

# AFTER ONE YEAR BURIAL IN STRIPA

# PART 1: GLASS/GLASS

by

Larry L. Hench
Department of Materials Science and Engineering
University of Florida
Gainesville, Florida 32611

Alexander Lodding
Chalmers University of Technology
Gothenburg, Sweden

Lars Werme
SKBF/KBS
Stockholm, Sweden

August 1983

## Introduction

The long term reliability of nuclear waste glasses will depend upon the interaction of water with glass and various components of the storage system. An experiment designed to test nuclear waste storage system interactions in deep granite burial has been in place for more than one year. Two configurations of glass, canister, overpack and backfill material were inserted into 56 mm x 3 m deep boreholes located at the 330 m level in the STRIPA mine. One configuration (called "pineapple slices") involved thin, right circular discs of glass with a central hole for a heater rod. These glass discs were stacked together with similar discs of the other materials to form a sequence of interfaces. The second configuration, called minicans, was designed to simulate closely a waste package in a disposal hole. The minicans contain glass cast into steel cylinders and arranged to provide glass-glass and glass-bentonite interfaces. Sleeves of lead and titanium or copper overpacks were placed around the steel wall of the minican and a bentonite sleeve separated the waste package from the walls of the borehole. The thermal period of storage is modeled by use of 90°C centerline heaters. Equivalent burial samples are maintained at the 8 to 10°C ambient of the STRIPA mine in Sweden. A more detailed description of the experimental design can be found in previous papers by authors where one month data from glass-glass and glass-bentonite interfaces (1) and several glass-metal overpack interfaces have been reported (2). The time dependence of the glass interfacial reactions, after 1, 3 and 12 months, has also been recently reported (3).

Each of these reports showed a significant difference between the rate of attack of the two alkali borosilicate glass compositions investigated in the burial experiment (Table 1). The purpose of this paper is to examine the difference in surface compositional gradients between the two glasses after one year 90°C burial. Polished glass interfaces in contact with polished glass of the same composition are discussed herein. Subsequent papers will discuss glass-bentonite and glass-granite interfaces.

## Method

Data from glass-glass interfaces were obtained from the "pineapple slice" samples (1,2) after one year burial at 90°C in STRIPA at 330 m depth. Duplicate one-year assemblies were buried and the results described in this paper came from samples located in the B position, as discussed in detail elsewhere (3). Previous investigations involved surface analysis by Fourier transform IR reflection spectroscopy (FTIRRS) of more than 100 glass-glass interfaces after one year 90° C burial (3). The interfaces described in this papper are representative of this large area of glass studied.

Compositional profiles were obtained from the samples using the SIMS method described previously (1-4). Data were obtained for 17 elements.

## Results

The FTIRRS spectra representative of the two glass compositions (Table 1) shows considerable difference after one year burial at 90°C. Glass ABS 41 has changed very little, with only a slight shift in the primary Si-=-Si molecular stretching vibration to a higher wavenumber (Fig. 1). In contrast, glass ABS 39 shows both a greater shift upwards in the stretching vibration and a considerable loss in spectral intensity in the region from 1000 $cm^{-1}$ to 800 $cm^{-1}$. Based upon previous IRRS investigations of glass-water interactions (5,6) these spectral differences can be attributed to

extensive loss of alkali and alkaline earth cations from the ABS 39 glass surface and formation of a $SiO_2$-rich surface layer. The absence of the spectral changes for glass ABS 41 shows that there is very much less alteration of the relative proportion of bridging oxygen and non-bridging oxygen bonds in the glass surface.

The SIMS data provide a quantitative explanation of the FTIRRS surface spectral differences between the two glasses. Figures 2-5 show the compositional depth profiles for both glass compositions. Figure 2 summarizes results for the $m^{+1}$ cations; Fig. 3 for $M^{4+}$ and rare earths; Fig. 4 for $M^{2+}$; and Fig. 5 for the other $M^{3+}$ cations. (The oxidation state for multivalent species such as $Fe^{3+}$ or $U^{4+}$ is only assumed for simplicity when assigning the data to respective figures as SIMS analyses is for the elemental concentration (4).

It is evident from Figs. 2-5 that two distinctive surface regions are present on each glass. Adjacent to the bulk glass i a plateau enriched in Si and depleted in a number of other species. This is the so-called silica-rich gel layer reported for many glasses (5,6). The thickness of this gel layer is approximately 3.5 μm for glass ABS 39 and approximately 1.5 μm for glass ABS 41. Table 1 compares the composition of the gel layer at mid-plateau; i.e., 2 μm for glass 39 and 0.6 μm for glass 41, with the bulk blass composition.

A second, outer layer of considerably different composition is present at the glass-water-glass interface. The thickness of the outer layer is only about 0,2 μm for both glasses. Table 1 compares the elemental composition of the outer layer with the gel layer and the bulk composition.

The data in Table 1 for the "mid-plateau" gel layer correspond to a particular point on the abscissa of the profiles, and do not (especially where marked with a, b, or c) more than qualitatively relate to the average concentrations in the whole plateau region. Also, the elemental concentrations presented for the outer layer corresponds only to a particular probe area, 40 μm in diameter. Some variation from point to point on the surface can be expected, based upon our previous FTIRRS results (3).

Surface dealkalization of glass ABS 39 extends about 3.5X deeper than glass ABS 41. The shape of the compositional profiles for Na, Cs and Li (Fig. 2) between the bulk glass and the plateau region is similar for each element and each glass and corresponds in part to a diffusional grandient. The plateau shapes are similar. However, the outer surface layer differs for the two glasses (see Table 1). Both Na and Li are depleted in the outer layer for ABS 41 whereas Cs has a concentration increase. In contrast Na seems somewhat enhanced in the outer layer for ABS 39 and Cs is depleted compared with ABS 41.

A dramatic result shown in Fig. 2 is the reverse concentration gradient of K in the surface of both glasses. The depth of the K-rich layer corresponds to the depth of Na, Cs and in (ABS 41) Li depletion indicating there has been an ion-exchange counter diffusion gradient throughout the burial period.

The alkali exchange results in nearly equivalent thickness of silica enrichment (Fig. 3 and Table 1). Glass ABS 41 shows a 1.2 μm silicarich layer and ABS 39 has a 3.5 μm layer. This difference between the two glasses is roughly equivalent to the difference in depth of dealkalization.

Multiple valence species such as La, Zr, Y and U all behave similarly for both glasses (Fig. 3). There is a gradual depletion of these elements throughout the plateau layer, without the sharp diffusional gradient exhibited byg the alkali species. At the outer surface ( 0.2 μm), the concentration of these higher valence elements decreases for both glasses. However, for glass ABS 41 the change in elemental concentration of the outer layer is associated with an increase in Si and $M^{2+}$ species (Fig. 4), whereas glass ABS 39 shows only an enhanced Si concentration (Fig. 3).

Surface compositional profiles of the $M^{2+}$ elements (Fig. 4) show the most striking difference between the two glasses. There is an extensive Ca ion exchange layer on ABS 39 to the same depth (3.5 μm) as the dealkalization and silica-rich layer. The Ca concentration in the outer layer is decreased for glass ABS 39, however. In contrast, glass ABS 41 has a continously increasing Ca concentration from the bulk to the surface. At least three distinct regions of enhanced Ca appear to be present on the surface of glass ABS 41 after the 1 year burial. Glass ABS 41 shows three regions of Mg enhancement as well. (Mg was not measured on ABS 39 for technical reasons).

The most marked finding of this study is the behavior of Ba, Sr, and Zn on the two glasses. Glass ABS 39 has compositional profiles for Ba and Sr that are very similar to the alkali profiles of that glass (Fig.2). There is no Zn in ABS 39. In contrast, all three elements in glass ABS 41 depleted from the bulk have concentration within the outer layer on the glass. In fact, Zn has concentrated in the surface several fold over the bulk concentration.

Behavior of B, A1 and Fe during burial is approximately the same for both glasses (Fig. 5), although quite different from element to element. Boron is depleted from the surface to a depth equivalent to the loss of alkali ions. Again, a significant difference between the two glasses is the

elemental concentration of the outer layer formed. The 0.2 μm outer layer on ABS 41 appears to have more present even though the bulk composition has less B than ABS 39. More strikingly, the gel plateau region of ABS 41 has more than twice the B content than ABS 39 (Table 1).

Aluminium remains constant in the glass/glass interface for both glasses. This behavior is different from the A1 surface enhancement observed for glass/bentonite interfaces (7) which is evidence that there was no bentonite intrusion between the glass/glass interfaces reported herein. This is an important observation since another study has shown considerable variation in glass/glass interfacial results due to intrusion of bentonite solutions (3).

Iron concentrates within the gel plateau region (Fig. 5) for both glasses to a depth equivalent to the dealkalization layer. However, the relative enhancement of Fe is slightly greater for ABS 41. Although the Fe/Si ratio is lower in the outer region (Fig.5) the elemental concentration of Fe is enhanced over the bulk by 50% for both glasses.

## Discussion

Previous laboratory static leaching studies of glasses ABS 39 and 41 in DI $H_2O$ at 90°C showed that ABS 41 was 3 to 4X more leach resistant (8). This superior performance of ABS 41 is duplicated in the STRIPA burial tests at 1, 3 and 12 month (3). Although various studies of the compositional dependence of leaching of alkali borosilicate glasses show that a critical concentration of network

forming oxides is needed for good leach resistance (9-11), the role of specific elements is still unclear (12). Current theories of nuclear waste glass leaching behavior indicate that saturation of various elements in the glass-water interface will produce multiple reaction layers on the glass surface (12,14). This type of surface has been denoted a type IIIB surface and the kinetics conditions necessary to produce such surfaces have been identified (12). Numerous studies of a wide variety of nuclear waste glass compositions have shown evidence of surface layer formation and concentration of Fe and other heavy elements in the surface (14-17).

The SIMS profiles shown in Figs. 2-5 show that the improved leach resistance of ABS 41 is due to a combination of several of the above factors. Two distinct reaction layers form on both glasses. Ion exchange of $Ca^{2+}$, $K^{+}$, as well as $H^{+}$ or $H_3O^{+}$ for the $M^{+}$ species in the glass determines the thickness of the deepest layer. The $Ca^{2+}$ and $K^{+}$ come respectively from the compacted bonteonite and dissolution of the K-rich feldspar in the STRIPA granite. Laboratory leaching of ABS 39 in contact with bentonite and STRIPA granite also results in large concentrations of K and Ca on the surface, analyzed by SEM-EDS and similar SIMS proviles for all the elements (18).

One of the factors responsible for the improved leach resistance of ABS 41 may be the co-existence of Na and Li in the bulk glass. Even though the total concentration of alkali is greater for ABS 41 (25% vs 21 %), the presence of Na and Li together is likely to result in a mixed alkali reduction of the rate of ion exchange (19). In addition, it has been shown that divalent cations in the glass can interact with the mixed alkali effect and further decrease the rate of ion exchange (5). It also has been demonstrated that $Li^{+}$ will combine with $Al^{3+}$ to form a corrosion

resistant tetrahedral network complex and greatly retard dealkalization (20,21). Consequently the depth of Na and Li dealkalization and ion exchange with K, Ca and $H^+$, $H_3O^+$ is no more than 1. μm after the one year 90°C burial for glass ABS 41. For glass ABS 39 with only Na as the frit flux the depth of ion exchange is approximately 3.5X greater.

The second major factor probably responsible for the better leach resistance of ABS 41 is the formation of a 0,2 μm outer film enriched in $M^{2+}$ species. All divalent ions; Mg, Ca, Sr, Ba, Zn, have concentrated within the thin outer film of glass ABS 41. A total concentration of 9.2% by weight of the divalent cations is present in the ABS 41 outer film and less than 1% for ABS 39 (Table 1). It is well known in glass technology (22) and has been demonstrated in the corrosion of model $Na_2O$-CaO-$SiO_2$ glasses (5) that the presence of 10w/o $M^{2+}$ cations in a glass greatly retards the rate of nedwork dissolution.

It is now established that solution saturation of $M^{2+}$ species gives rise to formation of a surface layer concentrated in these species (13). At a certain pH level the saturated species must come out of solution and precipitate on the glass surface (12,23). It has also been shown that the rate of change of solution pH, which is a function of flow rate, residence time, SA/V (surface area of glass/volume of solution), will affect the rate at which precipitation will take place (24). Thus, the very slow rate of deal kalization of ABS 41, discussed above, results in very slow increase in solution pH at the glass-glass interface. Consequently when saturation of $M^{2+}$ species occurs and the outer layer forms on the glass there is very little attack under the layer or through the layer. The presence of 10% of $M^{2+}$ and 6.5% $Al^{3+}$, $Fe^{3+}$ cations in the outer layer

from network dissolution and the slow formation of the layer enables it to form as a coherent and dense film on the glass, as shown by Fig. 1 and ref (3). Consequently, diffusion through the dense coherent $MO\text{-}SiO_2$ layer is slow and dealkalization or network dissolution from under the film is impeded.

## Conclusions

One year 90°C burial of two similar alkali borosilicate glasses in STRIPA granite produces markedly different rates of surface attack. Glass ABS 41 has approximately 3.5X less depth of ion exchange of Na, Cs and B for K, Ca, $H^+$, $H_3O^+$ than glass ABS 39. The difference in depletion depth is ascribed mainly to formation of a thin ( 0.2 μm) coherent and dense outer layer on glass ABS 41 enriched in Mg, Ca, Sr, Ba, Zn-Al, Fe and Si. This outer film is resistant to network dissolution and impedes both ion exchange and network attack of the bulk glass underneath it.

## Acknowledgments

The authors gratefully acknowledge the financial support of SKBF/Project KBS during the course of this study. They also appreciate the SIMS analytical assistance of H. Odelius. One of the authors (LLH) acknowledges support of the U.S. Department of Energy during this investigation.

References


1. L. L. Hench, L. Werme and A. Lodding, "Burial Effects on Nuclear Waste Glass," in Scientific Basis for Nuclear Waste Management-V, W. Lutze, ed., Elsevier Science Pub. Co., New York, 153-162 (1982).

2. L. Werme, L. L. Hench and A. Lodding, "Effect of Overpack Materials on Glass Leaching in Geological Burial," in Scientific Basis for Nuclear Waste Management-V, W. Lutze, ed., Elsevier Science Pub. Co., New York, 135-144 (1982).

3. L. L. Hench, A. Lodding and L. Werme, "Analysis of One Year In-Situ Burial of Nuclear Waste Glasses in STRIPA," in Advances in Ceramics, G. Wicks, ed., Am. Ceram. Soc., Columbus, Ohio (1983).

4. A. Lodding and H. Odelius, "Applications of SIMS in Interdisciplinary Materials Characterization," Microchim. Acta (1983).

5. D. E. Clark, C. G. Pantano and L. L. Hench, Glass Corrosion, Books for Industry, New York (1979).

6. L. L. Hench and D. E. Clark, "Physical Chemistry of Glass Surfaces," J. Non-Crystalline Solids, 28(1), 83-105 (1978).

7. L. L. Hench, A. Lodding and L. Werme, "Nuclear Waste Glass Interfaces After One-Year Burial in STRIPA, Part 2: Glass/Bentonite," to be published.

8. D. E. Clark, H. Christensen, H-P. Hermansson, S-B. Sundvall and L. Werme, "Effects of Flow on Corrosion and Surface Film Formation on an Alkali Borosilicate Glass," presented at the Second International Symposium on Ceramics in Nuclear Waste Management, April 24-27, 1983, Chicago, Illinois.

9. J. L. Nogues, L. L. Hench and J. Zarzycki, "Comparative Study of Seven Glasses for Solidification of Nuclear Wastes," in Scientific Basis for Nuclear Waste Managment-V, W. Lutze, ed., Elsevier Science Pub. Co., New York, 211-218 (1982).

10. D. E. Clark, C. A. Mauer, A. R. Jurgensen and L. Urwongse, "Effects of Waste Composition and Loading on the Chemical Durability of a Borosilicate Glass," in Scientific Basis for Nuclear Waste Management-V, W. Lutze, ed., Elsevier Science Pub. Co., New York, 1-14 (1982).

11. G. G. Wicks, B. M. Robnett and W. E. Rankin, "Chemical Durability of Glass Containing SRP Waste--Leachability Characteristics, Protective Layer Formation, and Repository System Interactions," in Scientific Basis for Nuclear Waste Management-V, W. Lutze, ed., Elsevier Science Pub. Co., New York, 15-24 (1982).

12. L. L. Hench, "Glass Surfaces - 1982," J. de Physique, Colloque C9, Suppl. au. no. 12, Tome 43, 625-636 (1982).

13. B. Grambow, "The Role of Metal Ion Solubility in Leaching of Nuclear Waste Glasses," in Scientific Basis for Nuclear Waste Management-V, W. Lutze, ed., Elsevier Science Pub. Co., New York, 93-102 (1982).

14. R. M. Wallace and G. G. Wicks, "Leaching Chemistry of Defense Borosilicate Glass," in Scientific Basis for Nuclear Waste Management-VI, D. G. Brookins, ed., Elsevier Pub. Co., New York, 167-174 (1983).

15. L. L. Hench, D. E. Clark, and E. Lue Yen-Bower, "Corrosion of Glasses and Glass-Ceramics," Nuclear and Chemical Waste Management, 1, 59-75 (1980).

16. G. Malow, "The Mechanisms for Hydrothermal Leaching of Nuclear Waste Glasses: Properties and Evaluation of Surface Layers," in Scientific Basis for Radioactive Waste Management-V, W. Lutze, eds., Elsevier Sci. Pub. Co, New York, 347-354 (1982).

17. G. L. McVay and C. Q. Buckwalter, Nuclear Technologies, 51 (1980).

18. H. Christensen, H-P. Hermansson, D. E. Clark and L. Werme, "Surface Reactions Occurring on an Alakali Borosilicate Glass Immersed in Aqueous Solutions Containing Bentonite, Granite and Stainless Steel Corrosion Products," to be published.

19. M. F. Dilmore, D. E. Clark and L. L. Hench, "Chemical Durability of a $Na_2O$-$K_2O$-CaO-$SiO_2$ Glass," Bull. Am. Ceram. Soc., 61(9-10), 439-443 (1978).

20. M. F. Dilmore, D. E. Clark and L. L. Hench, "Aqueous Corrosion of Lithia-Alumina-Silicate Glasses," Bull. Am. Ceram. Soc. 57, 1040-1044 (1978).

21. M. F. Dilmore, D. E. Clark and L. L. Hench, "Corrosion Behavior of Lithia Disilicate Glass in Aqueous Solutions of Aluminum Compounds," Am. Ceram. Soc. Bull, 58(11), 1111-1114 (1979).

22. R. H. Doremus, Glass Science, John Wiley & Sons, New York (1973).

23. L. O. Werme, L. L. Hench, J. L. Nogues, M. Odelius, and A. Lodding, "On the pH-Dependence of Leaching of Nuclear Waste Glasses," J. Nucl. Mat. 116, 69-77 (1983).

24. D. E. Clark (to be published).

Figure Captions

1. FTIRRS spectra of nuclear waste glasses ABS 41 and ABS 39 after 1 year 90°C burial in STRIPA; glass/glass interface.

2. SIMS compositional profiles of ABS 41 glass/glass interface (light or open lines) and ABS 39 glass/glass interface (dark or full lines) after one year 90°C burial in STRIPA; $Na^+$, $Cs^+$, $K^+$, and $Li^+$, normalized to $Si^+$.

3. SIMS compositional profiles of ABS 41 glass/glass interface (light or open lines) and ABS 39 glass/glass interface (dark or full lines) after one year 90°C burial in STRIPA; $Si^+$, $La^+$, $Zr^+$, $U^+$, and $Y^+$, normalized to $Si^+$.

4. SIMS compositional profiles of ABS 41 glass/glass interface (light or open lines) and ABS 39 glass/glass interface (dark or full lines) after one year 90°C burial in STRIPA; $Ba^+$, $Sr^+$, $Zn^+$, $Ca^+$, and $Mg^+$, normalized to $Si^+$.

5. SIMS compositional profiles of ABS 41 glass/glass interface (light or open lines) and ABS 39 glass/glass interface (dark or full lines) after one year 90°C burial in STRIPA; $B^+$, $Al^+$, and $Fe^+$, normalized to $Si^+$.

TABLE 1
90°C
Glass Against Glass
SIMS Surface Compositional Analysis

| | ABS 41 | "Gel", mid-plateau | "Outer region" | ABS 39 | "Gel," mid-plateau | "Outer region" | |
|---|---|---|---|---|---|---|---|
| | Bulk | 1 yr. | 1 yr. | Bulk | 1 yr. | 1 yr. | |
| Si | 42.1 | 66.2 | 67.1 | 40.7 | 69.3 | 70.8 | Si |
| Li | 9.8 | 1.55 | 1.1 | (0.01) | | | Li |
| Na | 15.55 | 11.0 | 8.7 | 20.85 | 9.25 | 7.6 | Na |
| K | 0.05 | 0.40 | 0.40 | 0.04 | 0.45 | 0.35 | K |
| Cs | 0.30 | 0.25[b] | 0.55 | 0.30 | 0.09 | 0.06 | Cs |
| Mg | 0.03 | 0.12[c] | 2.8 | 0.02 | n.m. | n.m. | Mg |
| Ca | 0.01 | 0.4 | 0.5 | (0.01) | 1.0 | 0.45 | Ca |
| Sr | 0.10 | 0.06[b] | 0.07 | 0.10 | 0.06 | 0.04 | Sr |
| Ba | 0.15 | 0.25[b] | 0.15 | 0.15 | 0.02 | 0.01 | Ba |
| Zn | 1.80 | 2.1 | 5.7 | | | | Zn |
| B | 22.2 | 4.9[a] | 1.75 | 27.45 | 2.1 | 1.35 | B |
| Al | 2.4 | 3.95 | 3.85 | 3.05 | 5.0 | 5.3 | Al |
| Mn | 0.45 | n.m. | n.m. | 0.45 | n.m. | n.m. | Mn |
| Fe | 1.80 | 3.95 | 2.6 | 3.60 | 7.05 | 5.75 | Fe |
| Zr | 0.55 | 0.95 | 0.7 | 0.55 | 0.9 | 0.8 | Zr |
| Mo | 0.75 | n.m. | n.m. | 0.80 | n.m. | n.m. | Mo |
| Y | 0.06 | 0.09 | 0.04 | 0.70 | 0.07 | 0.05 | Y |
| La | 0.20 | 0.3 | 0.15 | 0.20 | 0.25 | 0.15 | La |
| U | 0.30 | 0.35 | 0.26 | 0.30 | 0.4 | 0.2 | U |
| $x_{\mu m}$ | | 1.0 | | | 4.0 | | |

a: Conc. increasing with depth in "gel".
b: Conc. varies; minimum in "gel" zone.
c: Conc. decreasing throughout "plateau" region.
$x_{\mu m}$: Approx. depth of leached layer.
n.m.: Not measured.

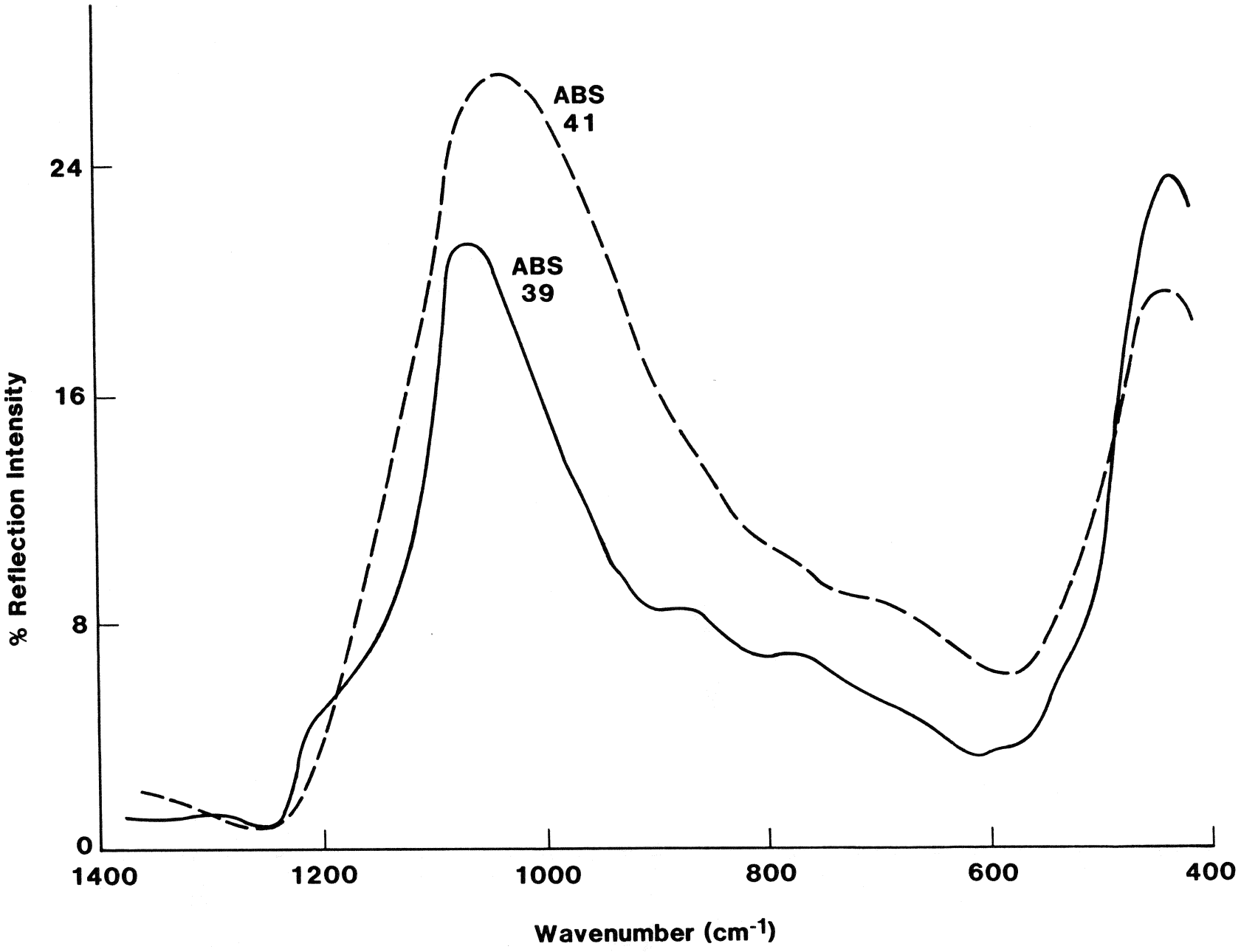
ABS
41
ABS
39
24
16
8
0
% Reflection Intensity
1400
1200
1000
800
600
400
Wavenumber (cm-1)

Fig. 1

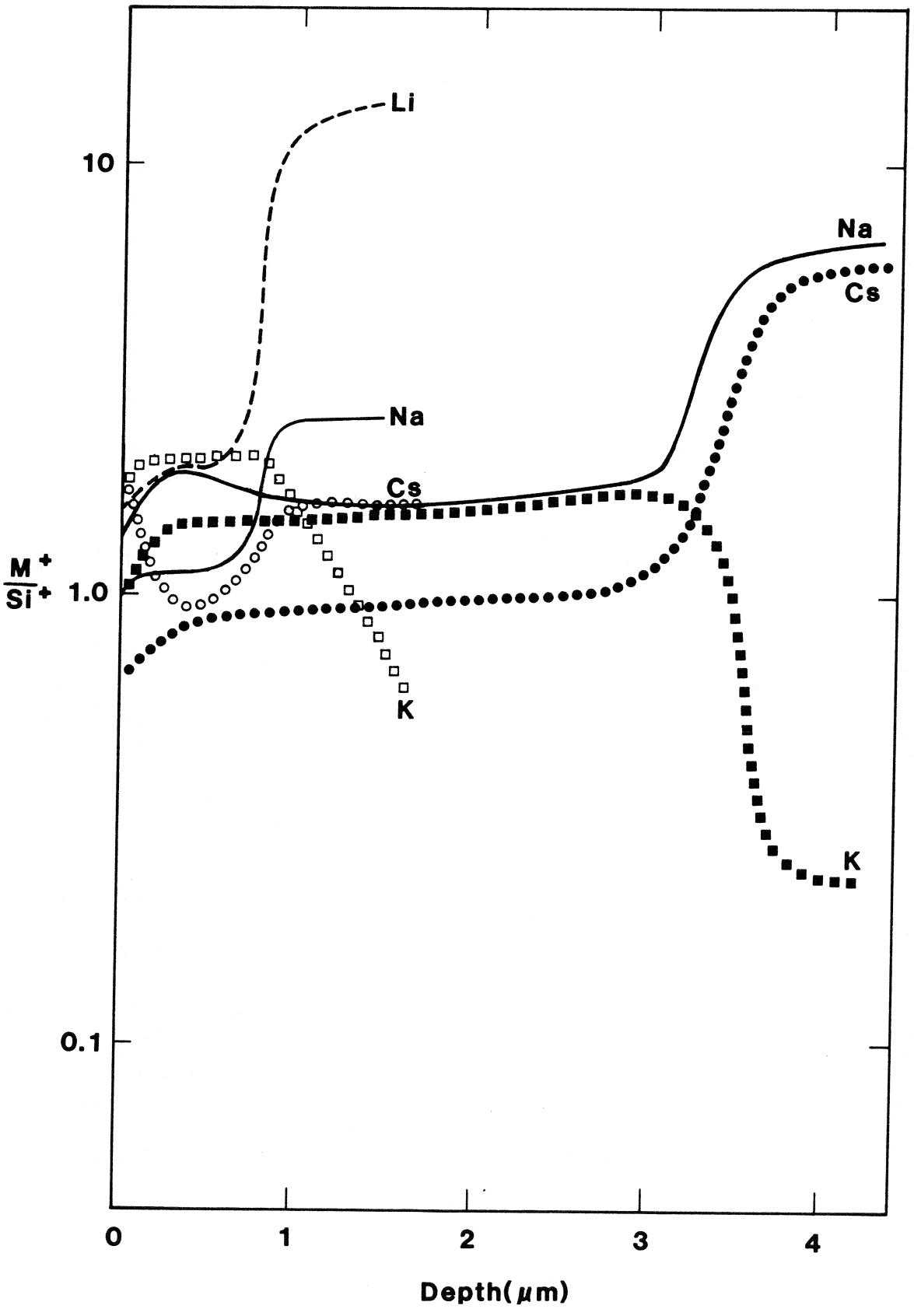


Fig. 2

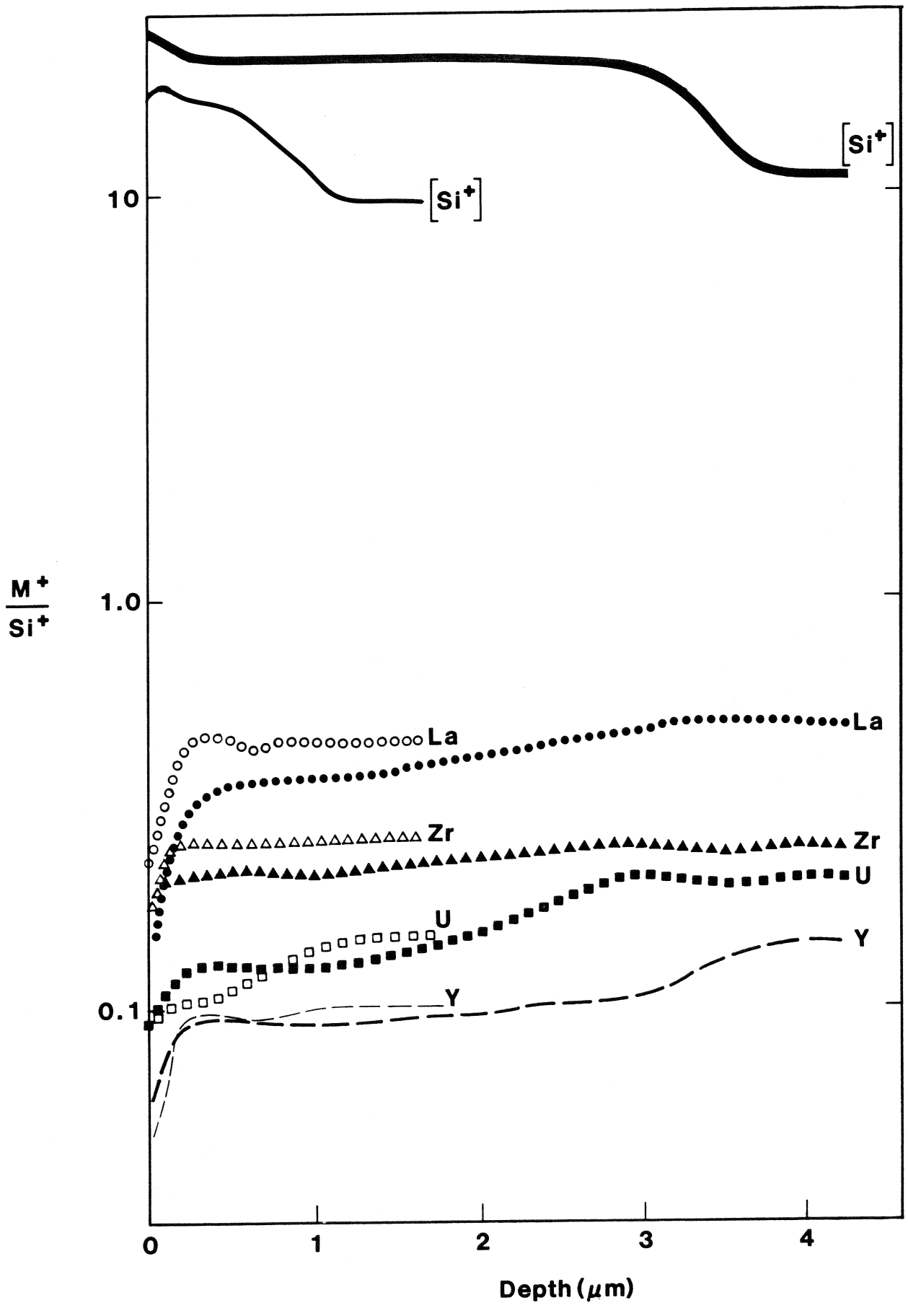


Fig. 3

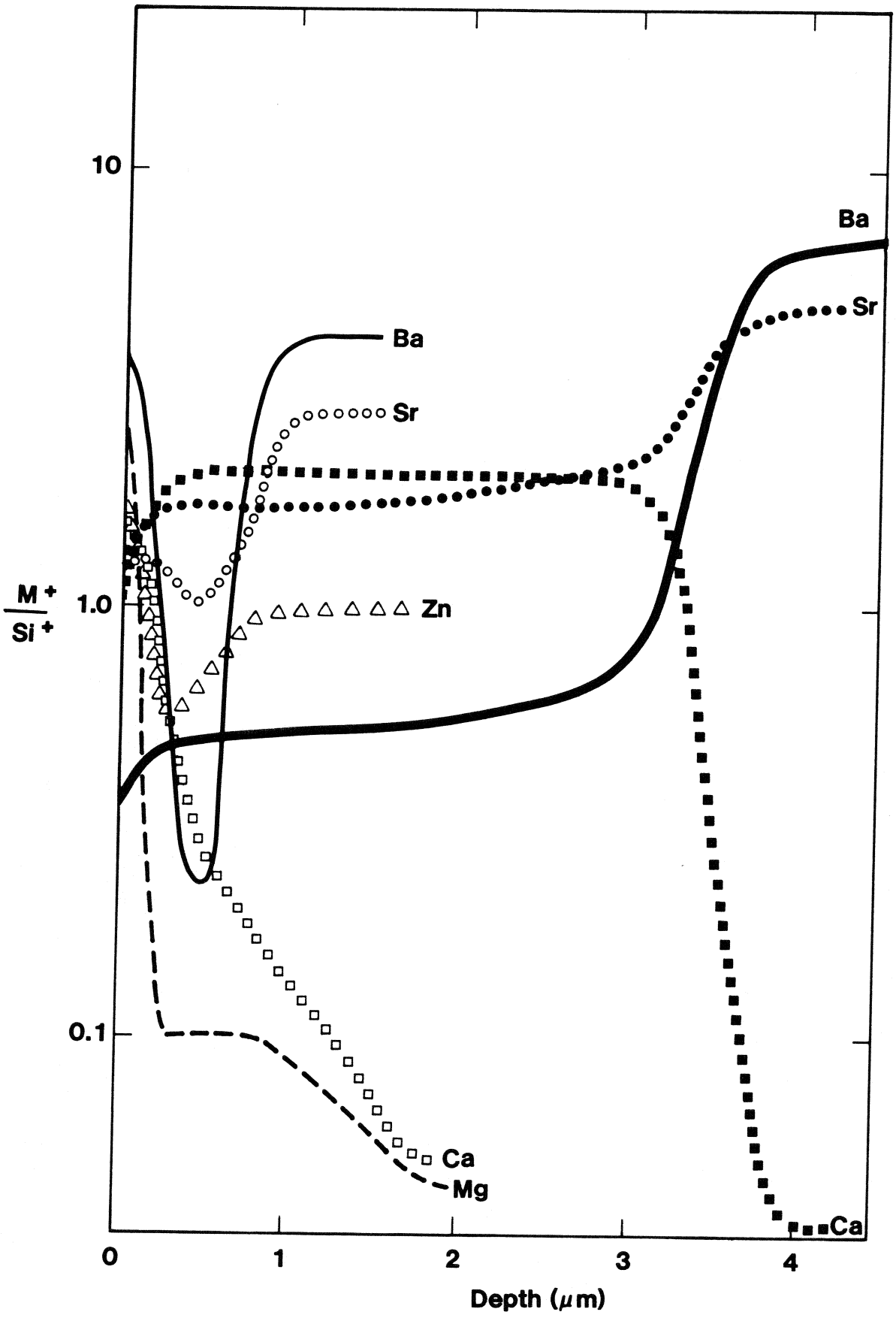


Fig. 4

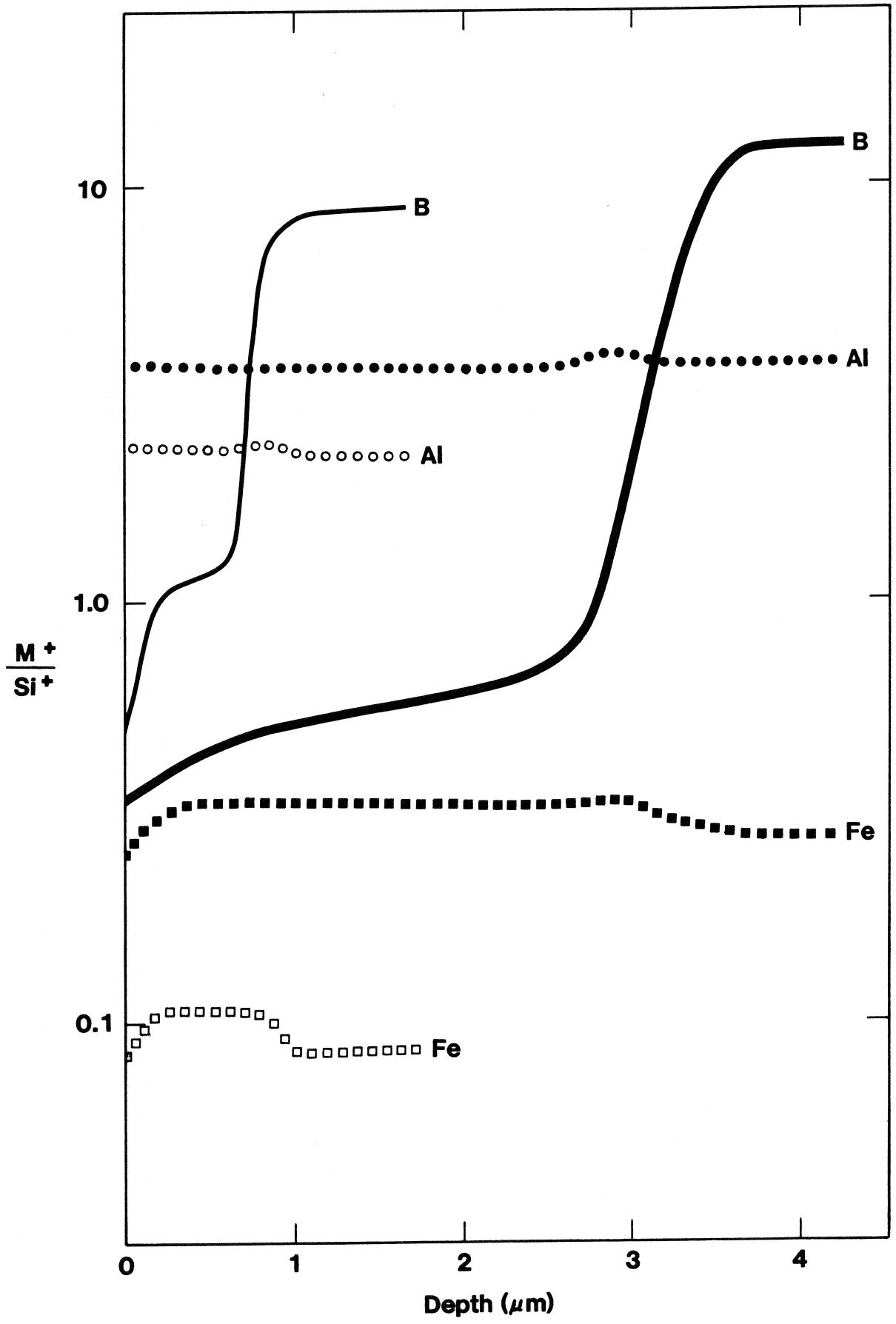


Fig. 5

# NUCLEAR WASTE GLASS INTERFACES

# AFTER ONE YEAR BURIAL IN STRIPA

# PART 2: GLASS/BENTONITE

by

Alexander Lodding
Chalmers University of Technology
Gothenburg, Sweden

Larry L. Hench
Department of Materials Science and Engineering
University of Florida
Gainesville, Florida 32611

Lars Werme
SKBF/KBS
Stockholm, Sweden

August 1983

## Introduction

Previous studies of the authors have described an in-situ burial experiment at the 350 m level in STRIPA granite where repository conditions are simulated by 90°C center-line heaters.[1-3] Two alkali borosilicate glass compositions (Table 1) ABS 39 and 41 are compared in the experiment. This paper describes the difference in surface layers formed by the two glasses when they have been in contact with compacted bentonite saturated with 90°C water for one year under burial conditions in a borehole in the STRIPA mine. The configuration of the glass and compacted bentonite samples is the so-called "pineapple slice" arrangement which permits 28 interfaces to be studied after disassembly.[1-3]

Earlier reports from this experiment emphasized that the glass/bentonite interface resulted in a substantially greater depth of alkali and boron removal from the galss.[1,3] One of the objectives of this paper is to show the effect of compacted bentonite on the surface behavior of a number of cations of differing valence. Another objective is to compare the chemical nature of the surface layer(s) formed on glass/glass and water interfaces. Finally, results from glass/bentonite interfaces after burial are compared with laboratory simulations, reported elsewhere.[4]

## Method

The nature of the burial experiment, glass and compacted bentonite characteristics, and use of Fourier transform IR spectroscopy (FTIRRS) and secondary ion mass spectroscopy (SIMS) surface analyses, to study the chan-es in glass surface have been described previously.[1,2,3,5] Previous studies also presented representative optical microscopy of the

glass surface after 1, 3 and 12 mo. contact with compacted bentonite.[1,3] The results shown herein help explain the features of these optical micrographs. The statistical variation in the glass burial surfaces in contact with bentonite has also been presented.[6] Data discussed in this paper are judged to be representative of the mean of the more than 24 glass/bentonite interfacial areas investigated in this one year burial experiment. Duplicated one year burial assemblies were used to confirm the results.

The compositional profiles shown herein come from SIMS analysis areas, 40 μm diameter. Therefore the profiles represent an average composition of several "phase regions" on the outer surface layer (Table 1). Spot to spot analyses came from 10 $\mu m^2$ areas which are small enough to show compositional differences characteristic of three different "phase regions", labeled A, B and C in Table 1.

## Results

Figure 1 compares the FTIRRS spectra of ABS 39 and 41 before and after exposure to compacted bentonite during the one year 90°C burial. Glass ABS 39 shows loss of a large fraction of non bridging oxygen-alkali and alkaline earth bonds in the region between 800 and 950 $cm^{-1}$. The peak remaining after the one year burial is composed primarily of Si-O-Si bonds, based upon previous spectral analyses of silicate glasses.[7-9]

The FTIRRS spectrum of glass ABS 41 differs markedly from ABS 39 after burial in contact with bentonite (Fig. 1). Although a silica-rich layer formed during the first 3 mo. of burial (see refs. 1 and 3), the spectrum after one year shows a considerable fraction of $Si-OM^{+}$ and $Si-O-M^{2+}$ bonds present in the surface.

SIMS compositional profiles of the two glasses also show major differences in both the depth of ion exchange and the chemical species in the surface layers (Figs. 2-5). Figure 2 compares the profiles of $M^{+}$ species in the surface, Fig. 3 compares $M^{2+}$ species, Fig. 4 compares $M^{3+}$, and Fig. 5 compares La and higher valence species. Since SIMS produces an elemental analysis, the assignment here of a single valence state for elements, such as Fe, with variable oxidation states is only an estimate used for comparative purposes.

Alkali ion exchange extends to nearly 15 μm for glass ABS 39 (Fig. 2 and Table 1) whereas it is less than 4 μm for glass ABS 41. All three alkali species in the glass (Na, Cs, Li) are nearly uniformly depleted for glass ABS 39.

In contrast, Na and Cs both show extensive build-up in the outer 1 μm layer of glass ABS 41, although Li is completely depleted (Fig. 2). As a consequence ABS 41 has three distinctly different surface layers present; one depleted in alkali sandwiched between two others of higher alkali content. Each of these layers is only 1 m or less thick.

A counter diffusion of K into the surface layers of both glasses is also observed (Fig. 2). This is due to the low K content of the glass and a high K concentration in the STRIPA granite ground water. [10] The thickness of the K gradient is equivalent to the extent of depletion of the other $M^{+}$ species.

Table 1 shows that there are at least two "phases", each identifiable on a 100 $\mu m^2$ area, which make-up the outer layer formed on glass ABS 41 and three "phases" on ABS 39. The alkali content is appreciably different for each "phase". Region A on ABS 41 has 3X less Na than region B and

is very much richer in $M^{2+}$ and $M^{3+}$ cations. The three phases formed on ABS 39 show more than a 2X variation in Na and K content.

There is also a substantial difference in the $M^{2+}$ profiles for the two glasses (Fig. 3), although not as much as is observed for glass/glass interfaces. [10] Depletion depths for Ba and Sr (14 μm) in ABS 39 is equivalent to the depths for the $M^{+}$ ions. A counter diffusion zone of Ca, more than 2 atom percent extends throughout the ion exchange region, although Ca is nearly negligible in the bulk.

Glass ABS 41, Fig. 3, also shows Ca in exchange for Ba and Sr and probably the alkali ion (Fig. 2). Magnesium, likewise coming from the bentonite is expceially dominant in the outer surface phases of both glasses. One of the phases on ABS 41 shows as much as 6% Mg as do two of the surface phases on ABS 39 (Table 1).

The profile for Zn (ABS 41) comes the closest to matching the outer layer concentration of $M^{2+}$ species observed for glass/glass interfaces observed after one year burial. [10] There are three distinct surface layers with varying Zn content. The thickness of these layers corresponds to the thickness of the variable alkali layers formed on ABS 41 (Fig. 2).

One of the most dramatic findings of this study is the extensive Al ion exchange within the gel layer (Fig. 4). The depth of the Al exchange for the $M^{+}$ and $M^{2+}$ ions is nearly the same depth for ABS 41 (4 μm), but is possibly less than the exchange for lower valence species for ABS 39. No Al ion exchange was observed for glass/glass interfaces after one year [11] which indicats that the origin of the Al ions is also the compacted bentonite.

The thick layer of Fe incorporated within the gel layer (Fig. 4) arises via ion-exchange from the bentonite as well. (A typical chemical analysis of the bentonite used is given in Table 2). There is an approximately 12 μm deep Fe enriched layer on ABS 39 and 4 μm ABS 41. Three distinct regions of the Fe concentration exists on both glasses. The thickness of the separate layers of ABS 41 is in the range of 1 μm, the same as the $M^{+}$ and $M^{2+}$ layers. The increase of Fe within the outer surface for glass/bentonite is qualitatively similar to glass/granite interfaces, [10] whereas it is dissimilar to the glass/glass interfaces.[11]

For each glass, Fig. 4 shows that the ion exchange of Al, Fe, Ca, and K is at the expense of B as well as Na, and other lower valence species in the glass, all depleted to the same depth, i.e., 14-15 μm for ABS 39 and 4 μm for ABS 41. Of the alkali metals, Na appears to deplete less than Cs or Li probably because of the presence of Na in the bentonite.

A consequence of the surface ion exchange is the formation of three layers which have differing Si content as well as variable $M^{+}$, $M^{2+}$ and $M^{3+}$ concentrations (Fig. 5). These layers are especially distinct for ABS 41 where they are only 1 to 2 μm thick. The outermost surface phases of the ABS 41 glass appear higher in Si than those of ABS 39 (Table 1). This difference, although small, may be significant enough to affect the glass corrosion rate.[12,13]

Uranium is lost from both glasses; as deep as the greater part of the ion exchange layer for ABS 41 but is only approximately 70% of the layer for ABS 39. Lanthanum is also lost to about the same depth as U for both glasses but gets concentrated in the outer surface layer to some extent whereas U does not. Thus the 4 to 5X greater rate of alkali and

B ion exchange for glass ABS 39, compared with ABS 41, is a factor of only 2X for La and U loss. Zirconium behaves like a network forming oxide and is accumulated thrughout the entire ion-exchange layer for both glases. The similarity of the Fe profile (Fig. 4) to that of Zr may suggest that Fe is associated with network formation as well.

## Discussion

The net effect of the ion exchange of Na and B (and Li for ABS 41) from the glass network with solution ions from compacted bentonite is the development of multiple surface layers that are rich in $(Mg,Ca)O$-$Al_2O_3$-$Fe_2O_3$-$SiO_2$. Table 1 shows that the Si content of the plateau gel layer is increased by 19-24%, the Al and Fe content is increased by 3 to 5X and the Ca and Mg content is increased by several orders of magnitude in comparison with the bulk glass. The increase in the outer layers is even greater, expecially for Fe and Mg.

As reported previously,[3] and summarized in Fig. 6, the rate of ion exchange from bentonite is very much more rapid during the first month of burial, begins to slow during 1 to 3 months, and decreases substantially thereafter. The rapid rate of attack at the glass/bentonite interface within one month has also been reported in laboratory simulations. Christensen et al.[4] have shown that weight loss of ABS 39 after 28d, 90°C static leaching was 1.5 to 2X higher in the presence of bentonite and crushed granite. SEM-EDS analyses of the reacted surfaces showed deposits containing K, Ca and Fe. A second phase of 10 μm particles was also observed which contained larger concentrations of rare earths. Larger area scans (40 $\mu m^2$), equivalent to this paper, by SIMS showed that the laboratory leached glass in content with bentonite and granite had three

compositionally distinct layers on the glass, similar to those shown herein. However, the thickness of the lab layers were somewhat less than observed in our burial experiments. Possible explanations for these differences are discussed by Clark et al. [14] Recent mapping and depth profiling studies by SIMS at higher surface resolution, by Clark et al. [15] have revealed similar phase formations in ABS 39 leached under different laboratory conditions.

Quantitatively though the findings of the lab simulations in these studies and previous lab data on glass/bentonite interactions reported by the authors [1] all confirm the presence of a short term rapid ion exchange process. Similar static laboratory leaching experiments of other nuclear waste glass compositions in the presence of clays, [16] gran diorite, [17] and hydrous silicates [18] show equivalent effects.

The high initial rate for ABS 39 compared to ABS 41 is attributed mainly to its larger Na and B content which gives a 3X greater rate of surface depletion for glass/glass interfaces. [11] Bentonite provides a solution saturated in soluble Ca-Mg, Fe, A1, etc. and a high base exchange capacity for the Na and B. Consequently, the rate of cation exchange increases markedly for both glasses over the rate observed for a glass-water-glass interface. However, the incorporation of divalent and trivalent ions within the silicate network as Na and B is exchanged results in a progressively more effective barrier to diffusion. Consequently, the longer term rate of surface depletion and ion exchange with bentonite present is nearly equivalent to that without bentonite, as shown in Fig. 6.

## Conclusions

Cation exchange of Ca, Mg, Al and Fe from compacted bentonite for primarily Na (Li) and B produces a glass surface zone after one year 90°C burial that has three silicate-rich layers. The thickness of these layers is approximately 1 m each for glass ABS 41 and approximately 2, 6 and 6 m (in inward order) for ABS 39. The larger concentration of $M^{2+}$ and $M^{3+}$ cations and high silica content of the reaction layers results in a considerably retarded rate of ion exchange after the formation of these layers during the first three months of burial. The loss of simulated radionuclides, U, La and Cs from the glass is slowed by the reaction layers.

## Acknowledgments

The authors gratefully acknowledge the financial support of SKBF/Project KBS during the course of this study. They also appreciate the SIMS analytical assistance of H. Odelius. One of the authors (LLH) acknowledges support of the U.S. Department of Energy during this investigation. Part of the work was supported by a grant (to AL) from the Swedish Board of Technical Development.

References


1. L. L. Hench, L. Werme and A. Lodding, "Burial Effects in Nuclear Waste Glass," in Scientific Basis for Radioactive Waste Management-V, W. Lutze, ed., Elsevier Science Pub. Co., New York, 153-162 (1982).

2. L. Werme, L. L. Hench and A. Lodding, "Effect of Overpack Materials on Glass Leaching in Geological Burial," in Scientific Basis for Radioactive Waste Management-V, W. Lutze, ed., Elsevier Science Pub. Co., New York, 135-144 (1982).

3. L. L. Hench, Alexander Lodding and Lars Werme, "Analysis of One Year In Situ Burial of Nuclear Waste Glasses in STRIPA," to be published in Second International Symp. on Ceramics in Nuclear Waste Management, Am. Ceram. Soc., Columbus, Ohio, 1983.

4. H. Christensen, H-P. Hermansson, D. E. Clark and L. Werme, "Surface Reactions Occurring on an Alkali Borosilicate Glass Immersed in Aqueous Solutions Containing Bentonite, Granite and Stainless Steel Corrosion Products," to be published in Second International Symp. on Ceramics in Nuclear Waste Management, Am. Ceram. Soc., Columbus, Ohio, 1983.

5. A. Lodding and H. Odelius, "Applications of SIMS in Interdisciplinary Materials Characterization," Microchim. Acta (1983).

6. L. L. Hench et al., to be published.

7. D. M. Sanders, W. B. Person and L. L. Hench, "Quantitative Analysis of Glass Structure Using Infrared Reflection Spectra," Appl. Spectroscopy, 28(3), 247-255 (1974).

8. D. E. Clark, E. C. Ethridge and L. L. Hench, "Effects of Glass Surface Area to Solution Volume Ratio on Glass Corrosion," Physics and Chemistry of Glass, 20(2), 35-40 (1979).

9. D. E. Clark, C. G. Pantano and L. L. Hench, in Glass Corrosion, Books for Industry, New York (1979).

10. L. L. Hench, A. Lodding and L. Werme, "Nuclear Waste Glass Interfaces After One Year Burial in STRIPA, Part 3: Glass/Granite," to be published.

11. L. L. Hench, A. Lodding and L. Werme, "Nuclear Waste Glass Interfaces After One Year Burial in STRIPA, Part 1: Glass/Glass," to be published.

12. J. L. Nogues, L. L. Hench and J. Zarzycki, "Comparative Study of Seven Glasses for Solidification of Nuclear Wastes," in Scientific Basis for Radioactive Waste Management-V, W. Lutze, ed., Elsevier Science Pub. Co., New York, 211-218 (1982).

13. Alan A. Hench and Larry L. Hench, "Computer Analysis of Nuclear Waste Glass Composition Effects on Leaching," to be published in J. Nuclear and Chemical Waste Management (1983).

14. D. E. Clark, H. Christensen, H-P. Hermansson, S. B. Sundvall and L. Werme, "Effects of Flow on Corrosion and Surface Film Formation on an Alkali Borosilicate Glass," to be published in Second International Symp. on Ceramics in Nuclear Waste Management, Am. Ceram. Soc., Columbus, Ohio, 1983.

15. D. E. Clark, A. Lodding, and L. Werme, to be published.

16. P. van Iseghem, W. Timmers and R. de Batist, "Chemical Stability of Simulated HLW Forms in Contact with Clay Media," in Scientific Basis for Radioactive Waste Management-V, W. Lutze, ed., Elsevier Science Pub. Co., New York, 219-228 (1982).

17. D. Savage and J. E. Robbins, "The Interaction of Borosilicate Glass and Granodiarite at 100°C, 50 MKPa: Implications for Models of Radionuclide Release," in Scientific Basis for Radioactive Waste Management-V, W. Lutze, ed., Elsevier Science Pub. Co., New York, 145-152 (1982).

18. G. G. Wicks, D. M. Robnett and W. E. Rankin, "Chemical Durability of Glass Containing SRP Waste—Leachability Characteristics, Protective Layer Formation and Repository System Interactions," in Scientific Basis for Radioactive Waste Management-V, W. Lutze, ed., Elsevier Science Pub. Co., New York, 15-24 (1982).

Figure Captions

1. FTIRRS spectra of nuclear waste glasses ABS 41 and ABS 39 after 1 year, 90°C burial in STRIPA, glass bentonite interface.

2. SIMS compositional profiles of ABS 39 glass/bentonite interface (light or open lines) and ABS 41 glass/bentonite interface (dark or full lines) after one year, 90°C burial in STRIPA; $Na^+$, $CS^+$, $Li^+$ and $K^+$ normalized to $Si^+$.

3. SIMS compositional profiles of ABS 39 glass/bontonite interface (light or open lines) and ABS 41 glass/bentonite interface (dark or full lines) after one year, 90°C burial in STRIPA; $Mg^+$, $Ba^+$, $Sr^+$, $Zn^+$ and $Ca^+$, normalized to $Si^+$.

4. SIMS compositional profiles of ABS 39 glass/bontonite interface (light or open lines) and ABS 41 glass/bentonite interface (dark or full lines) after one year, 90°C burial in STRIPA; $B^+$, $Al^+$, $Fe^+$ and $Y^+$ nromalized to $Si^+$.

5. SIMS compositional profiles of ABS 39 glass/bentonite interface (light or open lines) and ABS 41 glass/bentonite interface (dark or full lines) after one year, 90°C burial in STRIPA; $Si^+$, $U^+$, $La^+$ and $Zr^+$ normalized to $Si^+$.

6. Comparison of time dependent change of B depletion depth of ABS 39 and ABS 41 glass/bentonite interfaces during 90°C STRIPA burial.

TABLE 1

Glass in Contact with Bentonite

| | ABS 41 Bulk | "Gel", mid-plateau 1 Yr. | "Outer Region" 1 Yr. | 1 Yr. Surface Phase A | 1 Yr. Surface Phase B | ABS 39 Bulk | "Gel", mid-plateau 1 Yr | "Outer Region" 1 Yr. | 1 Yr Surface Phase A | 1 Yr Surface Phase B | 1 Yr Surface Phase C |
|---|---|---|---|---|---|---|---|---|---|---|---|
| Si | 42.1 | 64.0 | 61.2 | 62.9 | 68.9 | 40.7 | 64.5 | 58.8 | 59.9 | 61.0 | 59.3 |
| Li | 9.80 | 0.65[a] | 0.3 | 0.15 | 0.35 | (0.01) | | | | | |
| Na | 15.55 | 6.6 | 7.4 | 2.6 | 7.9 | 20.85 | 7.5 | 7.25 | 4.95 | 10.65 | 4.25 |
| K | 0.05 | 1.2 | 1.0 | 1.0 | 0.75 | 0.04 | 1.0 | 1.2 | 1.3 | 0.6 | 0.65 |
| Cs | 0.30 | 0.02[b] | 0.06 | 0.02 | 0.001 | 0.30 | 0.07 | 0.06 | 0.02 | 0.003 | 0.005 |
| Mg | 0.03 | 2.2 | 4.0 | 6.0 | 0.7 | 0.02 | n.m. | n.m. | 5.9 | 0.8 | 5.8 |
| Ca | 0.01 | 2.1 | 1.2 | 0.18 | 1.6 | 0.01 | 2.2 | 0.6 | 0.35 | 1.3 | 2.9 |
| Sr | 0.10 | 0.08 | 0.08 | 0.001 | 0.005 | 0.10 | 0.06 | 0.06 | 0.002 | 0.004 | 0.03 |
| Ba | 0.15 | 0.01 | 0.002 | n.m. | n.m. | 0.15 | 0.11 | 0.10 | n.m. | n.m. | n.m. |
| Zn | 1.80 | 0.35 | 0.9 | 0.065 | 0.035 | | | | | | |
| B | 22.20 | 1.35[a] | 0.32 | 0.33 | 0.55 | 27.45 | 0.42 | 0.25 | 0.4 | 0.5 | 0.4 |
| Al | 2.40 | 9.4 | 9.5 | 17.9 | 10.2 | 3.05 | 9.5 | 11.5 | 7.7 | 9.2 | 10.2 |
| Mn | 0.45 | n.m. | n.m. | n.m. | n.m. | 0.45 | n.m. | n.m. | n.m. | n.m. | n.m. |
| Fe | 1.80 | 6.85[c] | 9.5 | 8.1 | 7.4 | 3.60 | 8.0[c] | 11.4 | 18.5 | 15.1 | 15.7 |
| Zr | 0.55 | 1.85[c] | 2.0 | 0.07 | 0.15 | 0.55 | 1.85[c] | 2.3 | 0.07 | 0.03 | 0.04 |
| Mo | 0.75 | 0.03 | 0.02 | n.m. | n.m. | 0.80 | n.m. | n.m. | n.m. | n.m. | n.m. |
| Y | 0.06 | 0.05 | 0.05 | n.m. | n.m. | 0.07 | 0.09 | 0.08 | n.m. | n.m. | n.m. |
| La | 0.20 | 0.08 | 0.05 | 0.002 | 0.004 | 0.20 | 0.15 | 0.15 | 0.005 | 0.009 | 0.10 |
| U | 0.30 | 0.03 | 0.015 | n.m. | n.m. | 0.30 | 0.08 | 0.06 | n.m. | n.m. | n.m. |
| $x_{\mu m}$ | | 3.8 | | | | | 14.8 | | | | |

a: Conc. increasing with depth in "gel".
b: Conc. varies; minimum in "gel" zone.
c: Conc. decreasing throughout "plateau" region.
$x_{\mu m}$: Approx. depth of leached layer.
n.m.: Not measured.

Table 2

Typical chemical analysis of bentonite
( moisture free basis )

| constituent | percent by weight ( varies between ) |
|---|---|
| Silica ( $SiO_2$ ) | 58.0 - 64.0 |
| Alumina ( $Al_2O_3$ ) | 18.0 - 21.0 |
| Ferric Oxide ( $Fe_2O_3$ ) | 2.5 - 2.8 |
| Magnesia ( MgO ) | 2.5 - 3.2 |
| Lime ( CaO ) | 0.1 - 1.0 |
| Soda ( $Na_2O$ ) | 1.5 - 2.7 |
| Potash ( $K_2O$ ) | 0.2 - 0.4 |
| Ferrous Oxide ( FeO ) | 0.2 - 0.4 |
| Titanium Oxide ( $TiO_2$ ) | 0.1 - 0.2 |
| Other minor constituents | 0.5 - 0.8 |
| Chemically-held water ( $H_2O$ ) | 5.6 |
| Mechanically-held water ( $H_2O$ ) | 0.0 |

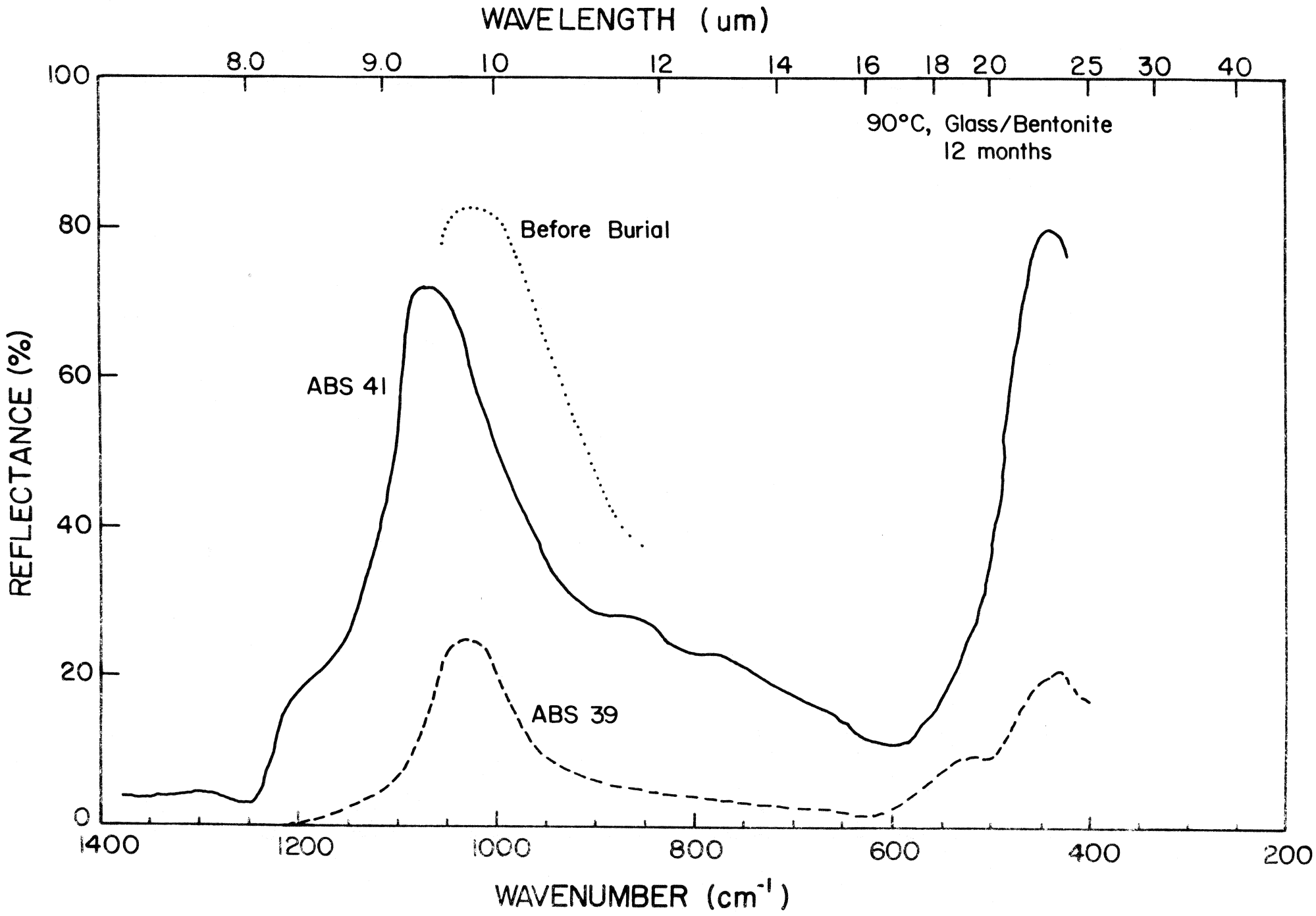
WAVELENGTH (um)
8.0
9.0
10
12
14
16
18
20
25
30
40
100
80
60
40
20
0
REFLECTANCE (%)
90°C, Glass/Bentonite
12 months
Before Burial
ABS 41
ABS 39
1400
1200
1000
800
600
400
200
WAVENUMBER (cm-1)

Fig. 1

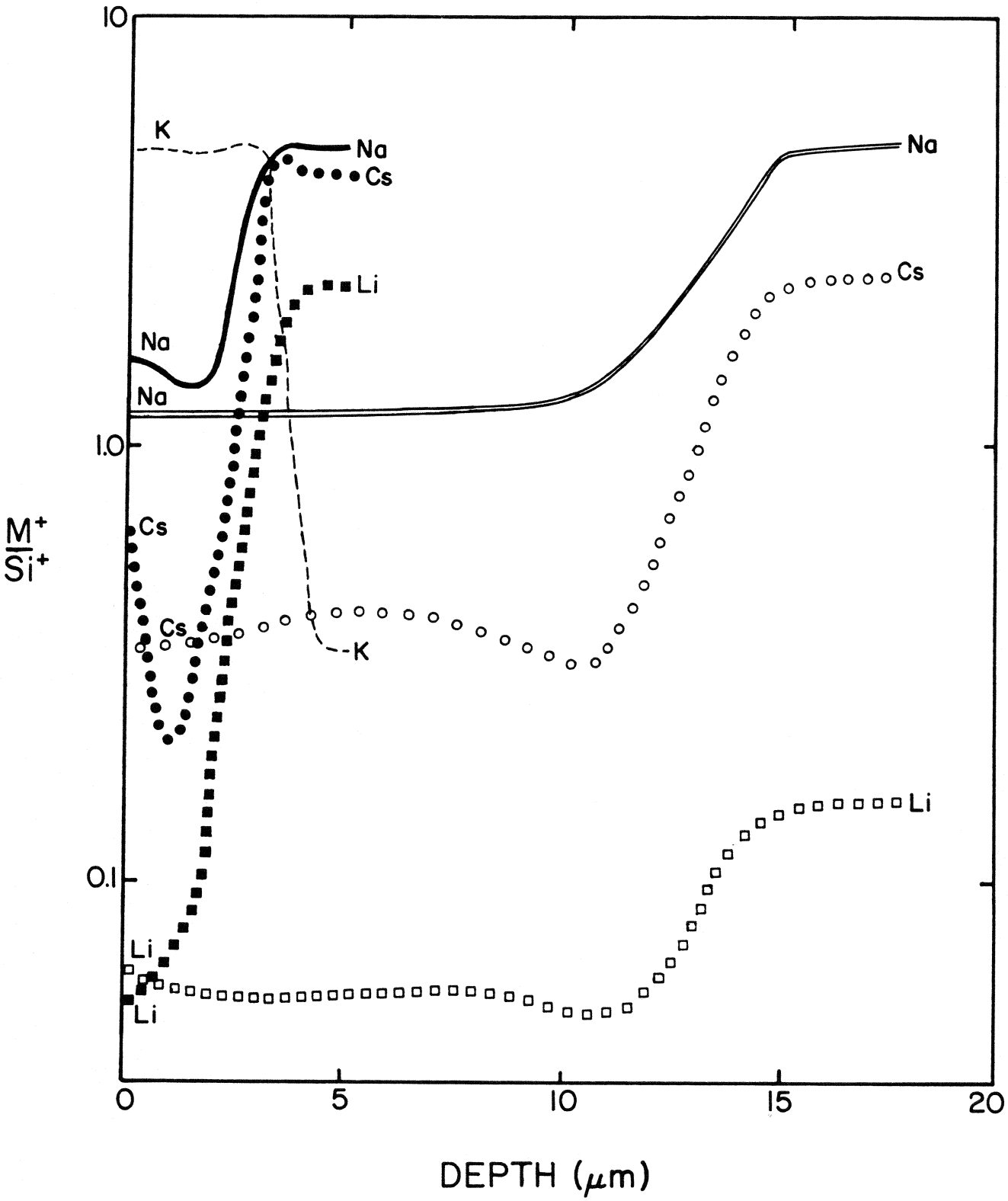


Fig. 2

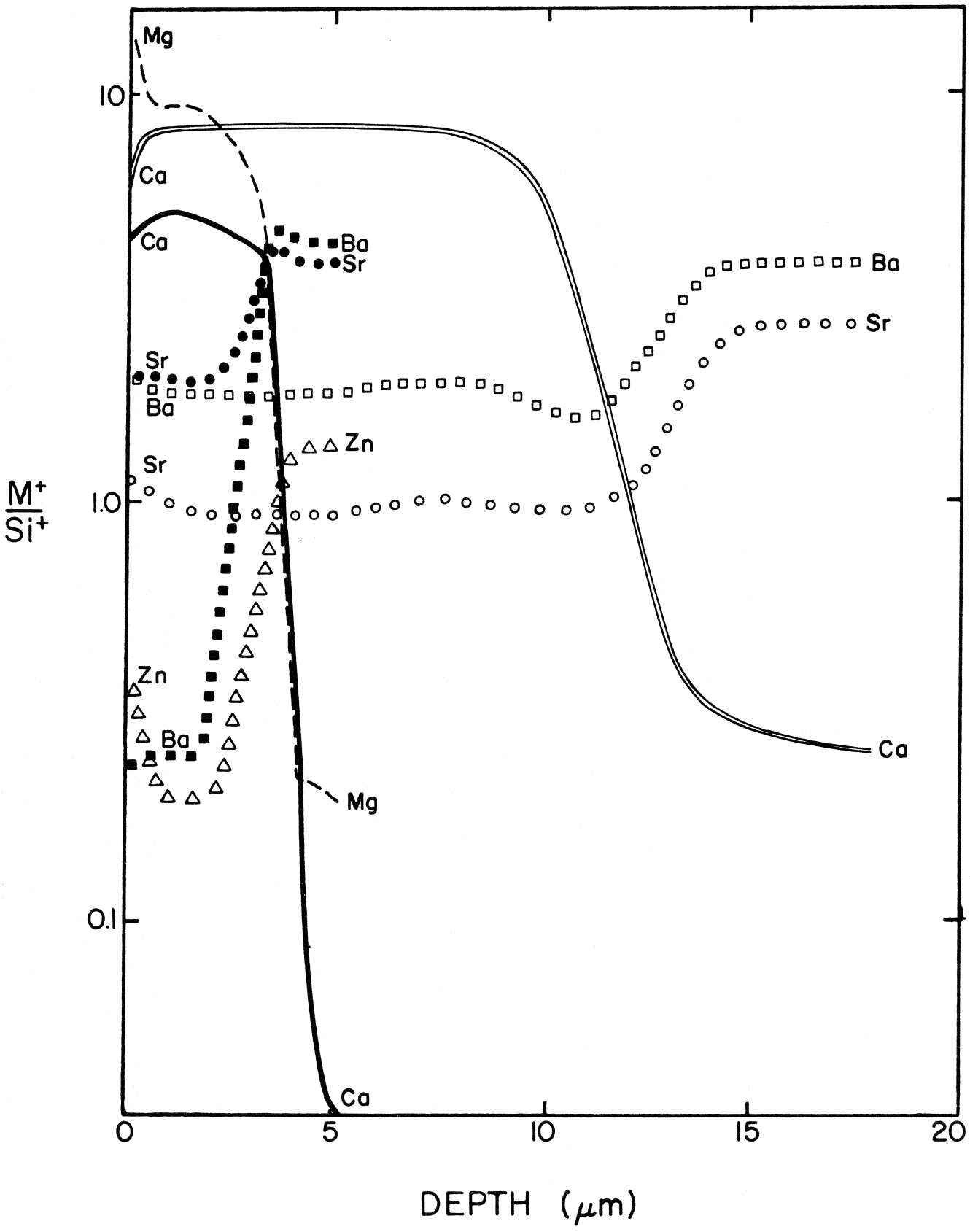
Mg
10
Ca
Ca
Ba
Sr
Sr
Ba
Zn
Sr
1.0
Zn
Ba
Mg
0.1
Ca
Ba
Sr
Ca
0
5
10
15
20
DEPTH (μm)
M+/Si+

Fig. 3.

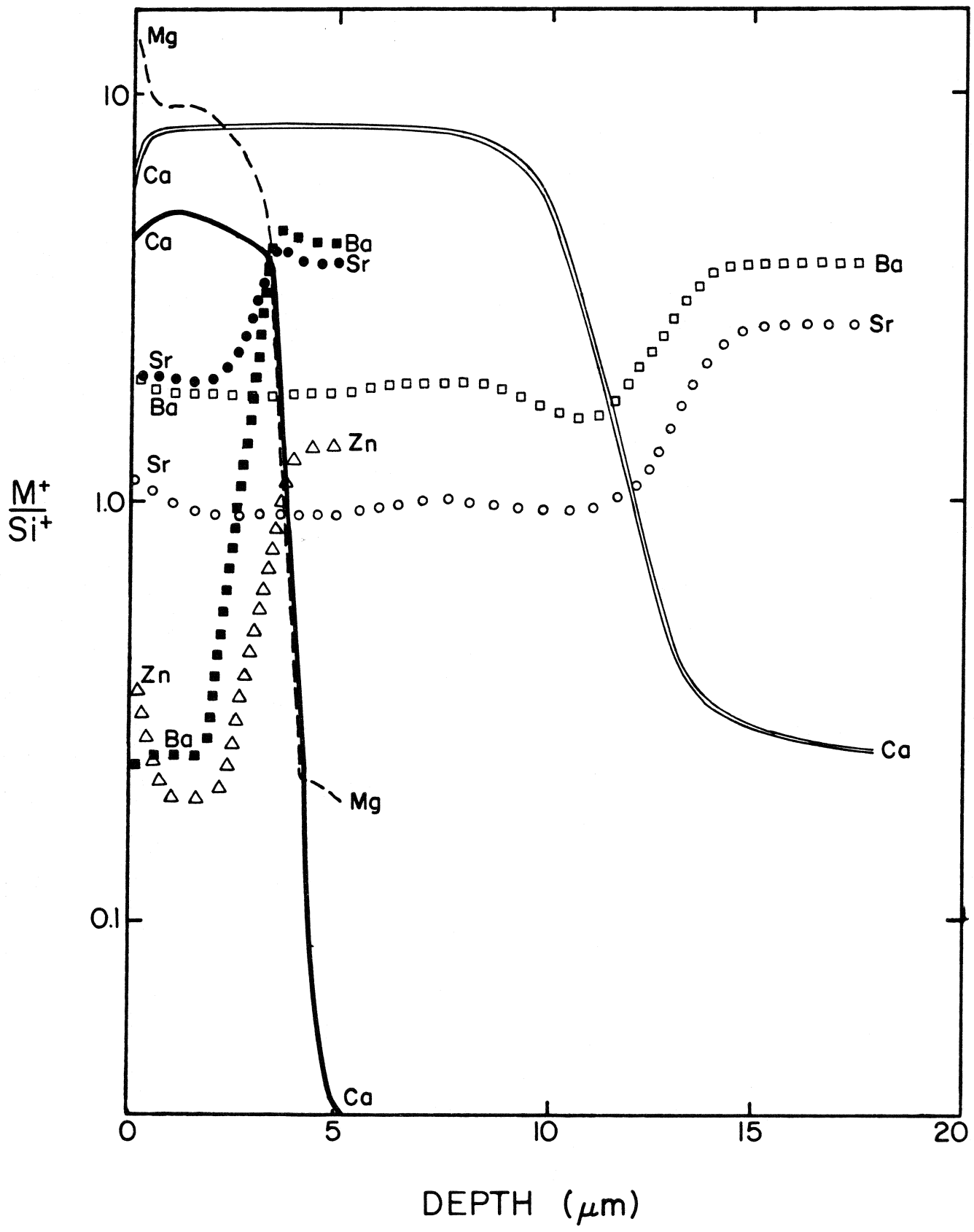
Mg
10
Ca
Ca
Ba
Sr
Sr
Ba
Ba
Sr
Zn
Sr
M+/Si+
1.0
Zn
Ba
Mg
Ca
0.1
0
5
10
15
20
DEPTH (μm)

Fig. 3.

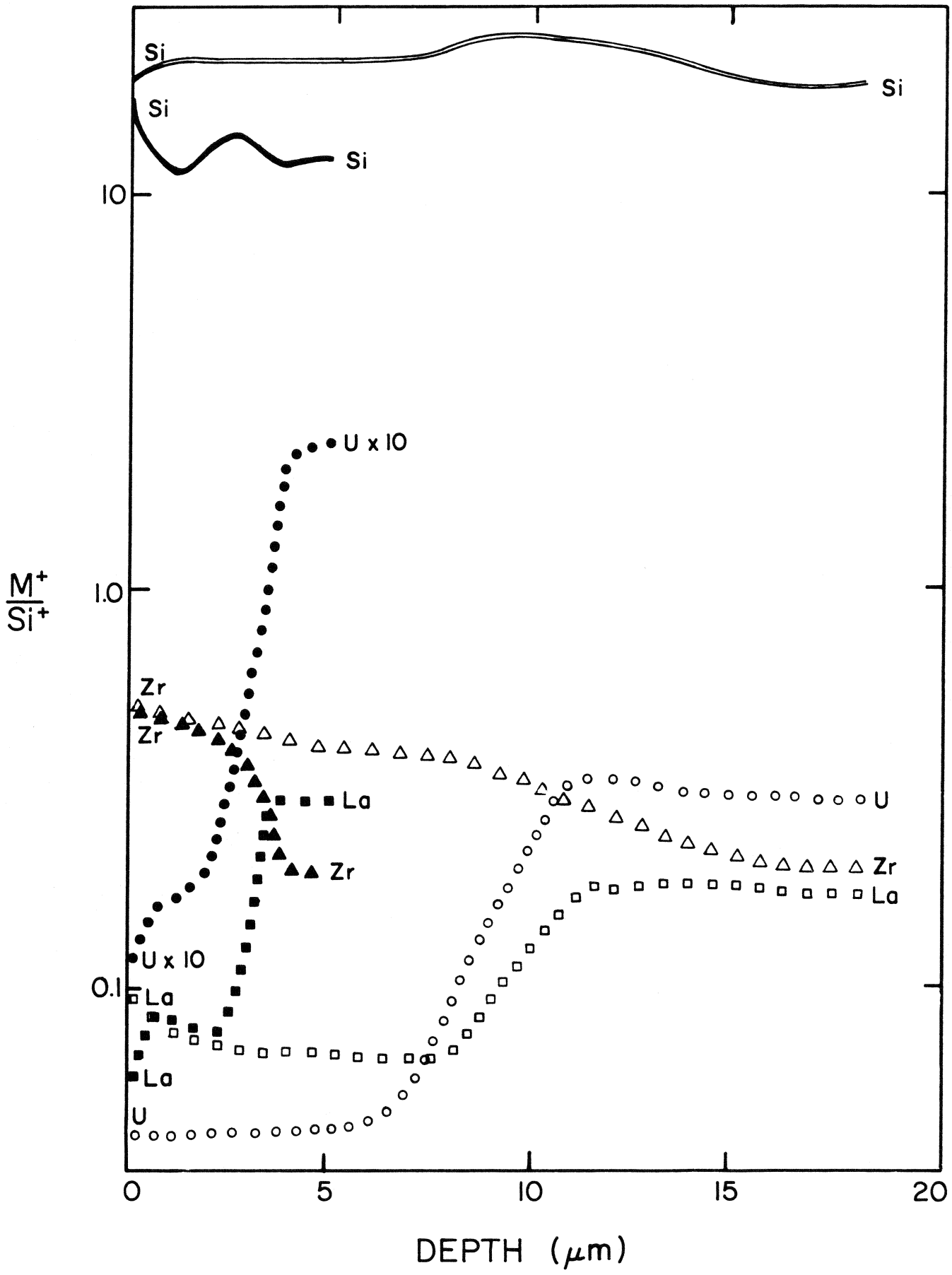
Si
Si
Si
Si
10
U x 10
1.0
M+/Si+
Zr
Zr
La
Zr
U
Zr
La
U x 10
0.1
La
La
U
0
5
10
15
20
DEPTH (μm)

Fig. 5.

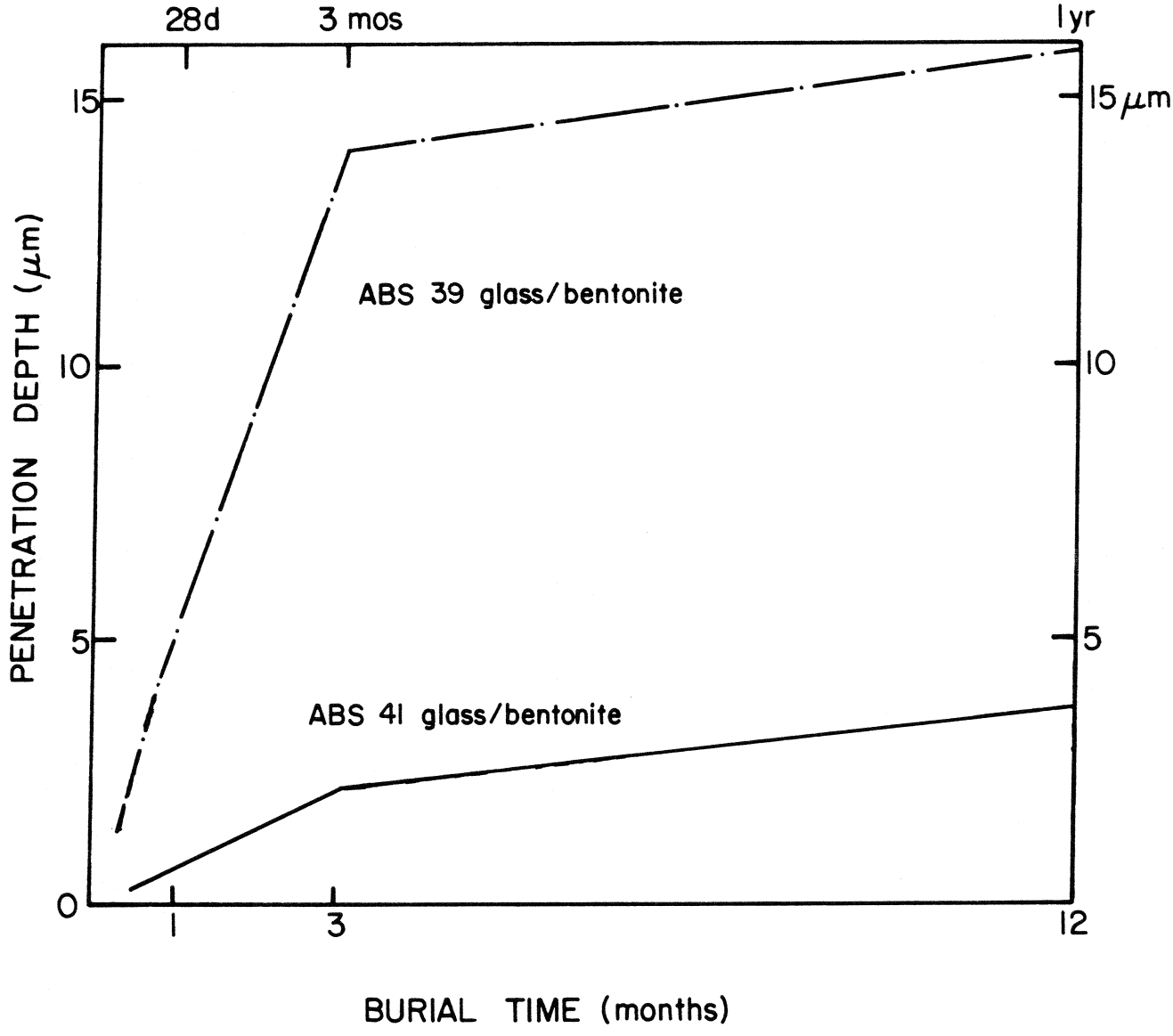
28d
3 mos
1 yr
15
10
5
0
15 μm
10
5
PENETRATION DEPTH (μm)
ABS 39 glass/bentonite
ABS 41 glass/bentonite
1
3
12
BURIAL TIME (months)

Fig. 6.

# Nuclear Waste Glass Interfaces After One Year Burial in STRIPA Part 3: Glass/Granite

by

Larry L. Hench
Department of Materials Science and Engineering
University of Florida
Gainesville, Florida 32611

Lars Werme
SKBF/KBS
Stockholm, Sweden

Alexander Lodding
Chalmers University of Technology
Gothenburg, Sweden

March, 1984

## INTRODUCTION

An in-situ nuclear waste glass burial experiment at the 350 m level in STRIPA granite has been in progress for several years.[1-3] Potential repository conditions for the thermal period of storage are simulated by 90°C center-line heaters. Two alkali borosilicate glasses (Table 1) in the so-called pineapple slice configuration[1-3] are compared in the experiment with respect to their relative leach behavior in contact with: glass, bentonite, granite, copper, lead, and titanium. Previous publications have described the interfacial reaction gradients between glass-glass[3,4] and glass-bentonite[3,5] interfaces after one-year burial using secondary ion mass spectroscopy (SIMS), Fourier Transform IR Spectroscopy (FTIRRS), and optical microscopy methods. Other publications have reported the one-year interfacial reaction gradients after one-year, 90°C burial using Rutherford backscattering spectroscopy[6] and surface profiling using precision profilometry, polishing, and FTIRRS.[7] The objective of the present paper in this series is to present quantitative SIMS analysis of the glass-granite interfaces after 1 year, 90°C burial.

## METHOD

The nature of the burial experiment and use of FTIRRS and SIMS surface analyses to study the changes in the glass surface have been described in detail elsewhere.[4,8] The statistical variation in the glass burial surfaces has also been described elsewhere.[3] Data discussed in this paper are judged to be representative of the mean of the 24 glass/granite interfacial areas studied in this one-year burial experiment. Duplicate one year, 90°C burial assemblies were used to ensure reproducibility of the results.

The compositional profiles shown herein come from SIMS analysis areas of 40 μm diameter. Consequently, the profiles represent an average composition of several "phase regions" on the outer surface layer (see Table 2).

## RESULTS

Figure 1 compares the FTIRRS spectra of ABS 39 and 41 before and after exposure to polished STRIPA granite interfaces during the one-year, 90°C burial. Very much less reaction has occurred for both glasses than is observed for glass-bentonite interfaces after the same time period.[3,5] However both glasses show evidence of having developed a $SiO_2$-rich surface layer during burial. The spectral intensity between 1000-800 $cm^{-1}$ is significantly reduced for both glasses, and is nearly absent for ABS 39. This is the region where silicon non-bridging oxygen ions dominate the molecular vibrations. Consequently, the FTIRRS data show a major reduction in the concentration of non-bridging oxygens in the surface. In contrast, the shift of the silicon-bridging oxygen-silicon peak to higher wavenumbers is characteristic of an increase in the concentration of $SiO_2$ in the surface layer formed during burial. The same type of enriched silica layer has been observed on glass-glass and glass-bentonite interfaces after burial.[1-5]

SIMS compositional profiles of the two glasses show major differences in both the depth of ion exchange and the concentration of chemical species in the surface layers (Figs. 2-5). Figure 2 compares the profiles of $M^+$ species in the surface, Fig. 3 compares $M^{2+}$ species, Fig. 4 compares $M^{3+}$, and Fig. 5 compares La and higher valence species. Since SIMS produces an elemental analysis, the assignment here of a single valence state for elements with variable oxidation states, such as Fe, is only an estimate used for comparative purposes.

Alkali ion exchange extends to approximately 1.8 μm for glass ABS 39 (Fig. 2 and Table 1) whereas it is less than 0.5 μm for glass ABS 41. Two of the alkali ions (Na and Cs) are depleted from ABS 39 but two others (K and Li) are enriched within the reaction interfaces. All four of the alkalis have an increase in relative concentration in the outer 0.2 μm of the surface layer.

This "precipitated layer" on ABS 39 is designated as Regions I and II in Figs. 2-5 and the elemental compositions for four such regions are shown in Table 2. In Table 2, S denotes the analysis of the outer surface. Region I is at an approximate depth of 0.07 μm; Region II is just inside the surface phases at 0.2 μm and corresponds to the beginning of the so-called "gel" zone. The middle of the gel zone at 0.65 μm depth is designated as Region III. Region IV corresponds to the inner border of the gel zone where the concentration of B and Na is just beginning to increase towards their bulk (B) value which is reached at Region V on the figures.

The reaction zone of glass ABS 41 is so much thinner that it was not possible to identify five reaction layers. Instead there appears to be only an outer layer of ~0.1 μm depth, and a gel zone of ~0.25 depth. Figure 2 shows that three of the alkali elements (Li, Na, and Cs) are depleted within the gel zone whereas K is enriched. All four tend to concentrate within the outermost reaction layer.

The concentration profiles of the $M^{2+}$ elements, Fig. 3, also vary for the different elements in both glasses. Three elements (Mg, Ca, and Sr) are greatly enhanced within the gel zone for glass ABS 39 whereas only Mg and Ca are enhanced for glass ABS 41. Barium is depleted in the gel layer for both glasses. However, Sr is slightly increased for ABS 39 and significantly depleted for ABS 41.

All of the $M^{2+}$ elements show an increased concentration in the outer precipitated layer on ABS 39. In contrast, only Mg is greatly concentrated within the outermost layer of ABS 41. However, underneath the enriched Mg layer on ABS 41 is a Ca enriched layer. Both are only ~0.1 μm thick.

Substantial differences are also present in the $M^{3+}$ compositional profiles. Boron is depleted in both glasses throughout the depth of the reaction zone. However, both glasses ABS 39 and 41 have an increase in Al in the reaction interface. This is especially the case for Regions I, II,and III of ABS 39 (Fig. 4). However, Table 1 shows that both glasses increase Al concentrations by about 2X. The largest difference however is in Fe concentrations. A very large Fe precipitation layer is present on ABS 39 with nearly a 10X increase over the bulk composition. Although Fig. 4 shows a decrease in Fe/Si ratio in the outer layer of ABS 41 this is primarily due to the large Si increase which makes the Fe/Si ratio drop. Table 1 indicates that there is a 2X increase of Fe within the gel zone for ABS 41.

Differences in elemental Si profiles, Fig. 5, typify the two glasses. Glass ABS 41, which is significantly more leach resistant,[1,3] has formed a Si-rich reaction layer ~0.3 μm thick. There is nearly a 2X increase in Si content of this reaction layer (Table 1). In contrast, the Si enrichment of ABS 39 is considerably less (Table 1) and the thickness of the layer considerably more (~1.8 μm). This corresponds to a 5X increase in reaction rate for glass ABS 39 over ABS 41.

The rare earths, La and Y, are depleted from the middle of the reaction zone for both glasses (Fig. 5). Thus, the rare earths appear to migrate within the reaction zone at about a 2X slower rate than B and Na. Both Zr and U concentrate within Regions I, II and III for glass ABS 39 and thus become

components of the precipitation layer on the outer surface. However, there is less concentration of U within the outer layer for glass ABS 41.

The thin multiple layers of greatly varying composition formed during burial give rise to complex optical features on the glasses when viewed at 120X magnification. Figure 6 shows that ABS 41 glass/granite interfaces may have very little evidence of reaction (6A) or a varigated appearance (6B) where heterogeneous surface reactions have occurred. Because of the greater thickness of the reaction layers on ABS 39 (Table 1) the range of optical microscopic features is even more varied. Figure 6C shows extensive multiple birefringent patterns due to the dehydration and cracking of the surface layers after removal from the wet bore holes and cleaning with ethanol. Portions of the cracked surface layers have spalled off (dark regions) in 6C. Other portions of the glass-granite interface (6D) show evidence of pitting attack of the glass although the total thickness of the reaction zone is only 5 μm.

## DISCUSSION

A summary of the time dependence of the thickness of the reaction layer for both glasses is given in Figs. 7 and 8. Figure 7 compares the effect of the glass/glass interface, the glass/bentonite interface, and the glass/granite interface for ABS 39. Figure 8 makes the same comparisons for glass ABS 41.

After one year at 90°C burial the thickness of the glass/granite reaction layer is substantially less than the other interfaces for both glasses. For ABS 41 the results are a reaction rate of only $3.6 \times 10^{-7}$ m/year for Na and B depletion in contact with granite. The loss rates of Cs, rare earths, and U as respectively: $\sim 2 \times 10^{-7}$ m/year, $1.8 \times 10^{-7}$ m/year, and $1.5 \times 10^{-7}$ m/year

in contact with granite. For glass ABS 39 the loss rates are all approximately 5X higher.

One of the most dramatic features in Figs. 7 and 8 is the large difference in thickness of reaction layers between glass/granite and glass/bentonite. After one year the difference is a factor of 10X for glass ABS 41 and 8X for ABS 39. These differences are almost entirely due to the accelerated rate of cation exchange during the first 3 months of burial. After one year at 90°C burial the sequence of reaction layers is nearly the same. Three silicate-rich zones are formed but they are very much thinner when the glasses are in contact with granite. This is because of the reduced solubility and ion exchange of granite as compared with compacted bentonite.

The reaction layer thickness and rates of reaction of glass/glass interfaces are about a factor of 2X greater than the glass/granite interfaces. This difference is likely to be due to the enhanced Al and Fe concentration in the outer layer of the glass/granite interface. At one year the glass/glass interfaces have only a 1.5X increase in Al and Fe concentration[4] whereas there is more than a 2X increase of both elements in the glass/granite interfaces (Table 1). Glass ABS 39 in fact has almost a 10X increase in Fe content. The presence of some soluble Al and Fe from the granite has been documented[9] and consequently the combined loss from glass and granite during cation exchange presumably leads to a more rapid saturation of these species. Grambow has shown[10] that the consequence of the saturation of Fe, Al as well as Ca and Mg will result in a sequence of reaction layers. Other studies have shown the evidence of these layers.[11-17] Nogues, et al. have also shown[18] that when a critical concentration of Si + Al + Fe is exceeded a dramatic rise in glass leach resistance occurs. One of the authors (LLH) has shown that these conditions

can give rise to a highly protective glass surface, termed a Type IIIB surface.[18] Aluminum ions in solution provide an alumino-silicate rich reaction layer which slows down leach rates considerably.[19,20] The presence of granite at the glass interface appears to enhance the formation of the Type IIIB surface during 90°C burial. However, lab simulation studies[9] of the glass-granite effect indicate that this favorable behavior may be sensitive to localized surface area to solution volume (SA/V) ratios and flow rates. Additional studies will be required to confirm the specific reaction mechanisms responsible for granite decreasing the rates of glass reaction during 90°C STRIPA burial.

## CONCLUSIONS

One year 90°C burial of alkali borosilicate nuclear waste glasses in contact with granite results in a substantially lower rate of surface reaction than glass/glass or glass/bentonite interfaces. The reaction thickness of glass ABS 41 after one year is only 0.36 μm and glass ABS 39 is only 1.8 μm. The difference between the two glasses is primarily due to the more rapid rate of cation exchange during the first 3 months of exposure. However, the rates between three and twelve months are also lower for the glass/granite interface. The lower rate of glass/granite attack appears to be due to a large increase of Fe and Al within the glass surfaces exposed to granite. Cs and U also are incorporated within the glass reaction layer formed in contact with granite which further reduces the reaction rate of these simulated radionuclides.

ACKNOWLEDGMENTS

The authors gratefully acknowledge the financial support of SKBF/Project KBS during the course of this study the optical microscopy of J. Wilson-Hench and FTIRRS spectroscopy of D. Spilman and G. LaTorre. One of the authors (LLH) also acknowledges partial support of the U.S. Department of Energy and part of the work was supported by a grant (to AL) from the Swedish Board of Technical Development.

REFERENCES

1. L. L. Hench, L. Werme and A. Lodding, "Burial Effects on Nuclear Waste Glass," in Scientific Basis for Nuclear Waste Management-V, W. Lutze, ed., Elsevier Science Pub. Co., New York, 153-162 (1982).

2. L. Werme, L. L. Hench and A. Lodding, "Effect of Overpack Materials on Glass Leaching in Geological Burial," in Scientific Basis for Nuclear Waste Management-V, W. Lutze, ed., Elsevier Science Pub. Co., New York, 135-144 (1982).

3. L. L. Hench, A. Lodding and L. Werme, "Analysis of One Year In-Situ Burial of Nuclear Waste Glasses in STRIPA," in Advances in Ceramics, G. Wicks, ed., Am. Ceram. Soc., Columbus, Ohio (1983).

4. L. L. Hench, A. Lodding, and L. Werme, "Nuclear Waste Glass Interfaces After One Year Burial in STRIPA, Part 1: Glass/Glass," accepted J. Nuclear Materials (1984).

5. A. Lodding, L. L. Hench and L. Werme, "Nuclear Waste Glass Interfaces After One Year Burial in STRIPA, Part 2: Glass/Bentonite," accepted J. Nuclear Materials (1984).

6. L. L. Hench, D. B. Spilman, and A. D. Buonaquisti, "Rutherford Back Scattering Surface Analysis of Nuclear Waste Glasses After One Year Burial in STRIPA," accepted J. Nuclear and Chem. Waste Management (1984).

7. L. L. Hench and M.J.R. Wilson, "Nuclear Waste Glass Interfaces After One Year Burial in STRIPA, Part 4: Comparative Surface Profiles," to be published.

8. A. Lodding and H. Odelius, "Applications of SIMS in Interdisciplinary Materials Characterization," Microchim. Acta Suppl. 10, 21-49 (1983).

9. L. L. Hench and A. Jurgensen, "Effects of Granite on the Performance of Nuclear Waste Glasses: Part 1--Leaching of Granite and Constituent Minerals," to be published.

10. B. Grambow, "The Role of Metal Ion Solubility in Leaching of Nuclear Waste Glasses," in Scientific Basis for Nuclear Waste Management-V, W. Lutze, ed., Elsevier Science Pub. Co., New York, 93-102 (1982).

11. G. G. Wicks, B. M. Robnett and W. E. Rankin, "Chemical Durability of Glass Containing SRP Waste--Leachability Characteristics, Protective Layer Formation, and Repository System Interactions," in Scientific Basis for Nuclear Waste Management-V, W. Lutze, ed., Elsevier Science Pub. Co., New York, 15-24 (1982).

12. D. E. Clark, C. A. Maurer, A. R. Jurgensen and L. Urwongse, "Effects of Waste Composition and Loading on the Chemical Durability of a Borosilicate Glass," in Scientific Basis for Nuclear Waste Management-V, W. Lutze, ed., Elsevier Science Pub. Co., New York, 1-14 (1982).

13. R. M. Wallace and G. G. Wicks, "Leaching Chemistry of Defense Borosilicate Glass," in Science Basis for Nuclear Waste Management-VI, D. G. Brookins, ed., Elsevier Pub. Co., New York, 167-174 (1983).

14. L. L. Hench, D. E. Clark and E. Lue Yen-Bower, "Corrosion of Glasses," Nuclear and Chemical Waste Management, 1, 59-75 (1980).

15. G. Malow, "The Mechanisms for Hydrothermal Leaching of Nuclear Waste Glasses: Properties and Evaluation of Surface Layers," in Scientific Basis for Nuclear Waste Management-V, W. Lutze, ed., Elsevier Science Pub. Co., New York, 347-354 (1982).

16. G. L. McVay and C. Q. Buckwalter, Nuclear Technologies, 51 (1980).

17. D. E. Clark, H./ Christensen, H-P. Hermansson, S-B. Sundvall and L. Werme, "Effects of Flow on Corrosion and Surface Film Formation on an Alkali Borosilicate Glass," presented at the Second International Symposium on Ceramics in Nuclear Waste Management, April 24-027, 1983, Chicago, Illinois.

18. J. L. Nogues, L. L. Hench and J. Zarzycki, "Comparative Study of Seven Glasses for Solidification of Nuclear Wastes," in Scientific Basis for Nuclear Waste Management-V, W. Lutze, ed., Elsevier Science Pub. Co., New York, 211-218 (1982).

18. L. L. Hench, "Glass Surfaces - 1982," J. de Physique, Coloque C9, Suppl. au. no. 12, Tome 43, 625-636 (1982).

19. M. F. Dilmore, D. E. Clark and L. L. Hench, "Aqueous Corrosion of Lithia-Alumina-Silicate Glasses," Bull. Am. Ceram. Soc., 57, 1040-1044 (1978).

20. M. F. Dilmore, D. E. Clark and L. L. Hench, "Corrosion Behavior of Lithia Disilicate Glass in Aqueous Solutions of Aluminum Compounds," Am. Ceram. Soc. Bull, 58(11), 1111-1114 (1979).

FIGURE CAPTIONS

1. Fourier Transform IR Reflection Spectra of ABS 39 and 41 before and after 1 year 90°C burial in STRIPA.

2. SIMS compositional profile of ABS 39 (darker lines extending to 2 μm) and ABS 41 (lighterlines extending to 0.5 μm) comparing depletion depth of $M^{+}$ cations after 1 year 90°C STRIPA burial.

3. SIMS compositional profiles of $M^{2+}$ after 1 year 90°C STRIPA burial. Glass ABS 39 has dark curves extending to 2 μm. ABS 41 has light curves extending to 0.5 μm.

4. SIMS compositional profiles of $M^{3+}$ after 1 year 90°C STRIPA burial. ABS 39 has dark lines; ABS 41 light lines.

5. SIMS compositional profile of $[Si^{+}]$, and other higher valent cations after 1 year 90°C STRIPA burial. ABS 39 has dark lines; ABS 41 light lines.

6. Optical micrographs (120X) after glass ABS 41 (A) and (B) and glass ABS 39 (C) and (D) after one year 90°C STRIPA burial.

7. Time dependence of reaction layer thickness (μm) for glass ABS 39 after one year 90°C burial in STRIPA comparing glass/granite interfaces with glass/glass and glass/bentonite interfaces.

8. Time dependence of reaction layer thickness (μm) for glass ABS 41 after one year 90°C burial in STRIPA comparing glass/granite interfaces with glass/glass and glass/bentonite interfaces.

TABLE 1

One-Year, 90°C Glass Against Granite
SIMS Surface Compositional Analysis
(at % of cations)
X denotes the extent of the corroded zone

| | ABS 41 | | | ABS 39 | | | |
|---|---|---|---|---|---|---|---|
| | Bulk | Gel Mid-Plateau | Outer Region | Bulk | Gel Mid-Plateau | Outer Region | |
| Si | 42.1 | 75.0 | 74.5 | 40.7 | 64.9 | 43.7 | Si |
| Li | 9.8 | 0.35 | 0.25 | 0.01 | 0.04 | 0.2 | Li |
| Na | 15.55 | 4.2 | 6.9 | 20.85 | 7.0 | 6.0 | Na |
| K | 0.05 | 0.7 | 0.9 | 0.04 | 0.65 | 0.6 | K |
| Cs | 0.30 | 0.35 | 0.4 | 0.30 | 0.30 | 0.25 | Cs |
| Mg | 0.03 | 0.5 | 1.8 | 0.02 | 0.70 | 5.0 | Mg |
| Ca | 0.01 | 1.1 | 0.7 | 0.01 | 1.0 | 0.6 | Ca |
| Sr | 0.10 | 0.06 | 0.04 | 0.10 | 0.2 | 0.1 | Sr |
| Ba | 0.15 | 0.11 | 0.07 | 0.15 | 0.03 | 0.03 | Ba |
| Zn | 1.80 | 2.25 | 2.5 | - | - | - | Zn |
| B | 22.2 | 4.0 | 0.6 | 27.5 | 2.8 | 1.9 | B |
| Al | 2.4 | 3.9 | 4.7 | 3.05 | 7.8 | 7.7 | Al |
| Mn | 0.45 | 0.35 | 0.15 | 0.45 | 0.12 | 0.3 | Mn |
| Fe | 1.80 | 3.9 | 2.2 | 3.6 | 7.5 | 29.6 | Fe |
| Zr | 0.55 | 0.8 | 0.8 | 0.55 | 1.1 | 1.2 | Zr |
| Mo | 0.75 | 0.2 | 0.01 | 0.8 | 1.45 | 0.2 | Mo |
| Y | 0.06 | 0.06 | 0.04 | 0.07 | 0.12 | 0.025 | Y |
| La | 0.20 | 0.2 | 0.12 | 0.20 | 0.17 | 0.01 | La |
| U | 0.30 | 0.3 | 0.2 | 0.30 | 0.55 | 1.0 | U |
| X(μm) | | 0.36 | | | 1.8 | | X(μm) |

TABLE 2

Quantification of Profiles, ABS 39 Against Granite,
1 Year's Exposure in STRIPA

Locations:
- S) Outer surface (outside surface phases)
- I) Region of "precipitated" surface phases (at approximate depth of 0.07 μm)
- II) Just inside of surface phases; beginning of "gel" zone (ca 0.2 μm under outer surfaces)
- III) Middle of "gel zone (ca 0.65 μm depth)
- IV) Inner border of "gel" zone (B and Na conc. just beginning to rise; depth ca 1.1 μm)
- B) Bulk glass. Onset of uncorroded ca 1.8 μm depth.

Concentrations in Atom-Percent of Cations (Neglecting H).

| Element | S | I | II | III | IV | B |
|---|---|---|---|---|---|---|
| Si | 43.7 | 44.6 | 63.7 | 64.9 | 61.5 | 40.7 |
| Li | 0.2 | 0.25 | 0.15 | 0.04 | 0.035 | 0.01 |
| Ba | 6.0 | 8.0 | 6.8 | 7.0 | 9.6 | 20.85 |
| K | 0.6 | 0.8 | 0.7 | 0.65 | 0.5 | 0.04 |
| Cs | 0.25 | 0.35 | 0.35 | 0.3 | 0.3 | 0.3 |
| Mg | 5.0 | 2.6 | 1.1 | 0.7 | 0.4 | 0.02 |
| Ca | 0.6 | 0.65 | 0.75 | 0.95 | 1.2 | 0.01 |
| Sr | 0.1 | 0.1 | 0.25 | 0.2 | 0.2 | 0.1 |
| Ba | 0.03 | 0.035 | 0.025 | 0.025 | 0.045 | 0.15 |
| B | 1.9 | 1.65 | 2.5 | 2.8 | 6.3 | 27.45 |
| Al | 7.7 | 8.7 | 10.0 | 7.8 | 5.2 | 3.05 |
| Mn | 0.3 | 0.4 | 0.09 | 0.12 | 0.35 | 0.45 |
| Fe | 29.6 | 27.6 | 7.6 | 7.5 | 6.9 | 3.6 |
| Zr | 1.2 | 1.2 | 2.0 | 1.1 | 0.95 | 0.55 |
| Mo | 0.2 | 0.25 | 0.25 | 1.45 | 1.45 | 0.8 |
| Y | 0.025 | 0.065 | 0.095 | 0.125 | 0.13 | 0.07 |
| La | 0.01 | 0.025 | 0.035 | 0.17 | 0.35 | 0.20 |
| U | 1.0 !! | 0.7 | 0.95 | 0.55 | 0.45 | 0.30 |
| H | $2.7x(c_H)_o$ | $1.7x(c_H)_o$ | $2.2x(c_H)_o$ | $2.0x(c_H)_o$ | $1.9x(c_H)_o$ | $(c_H)_o$ |

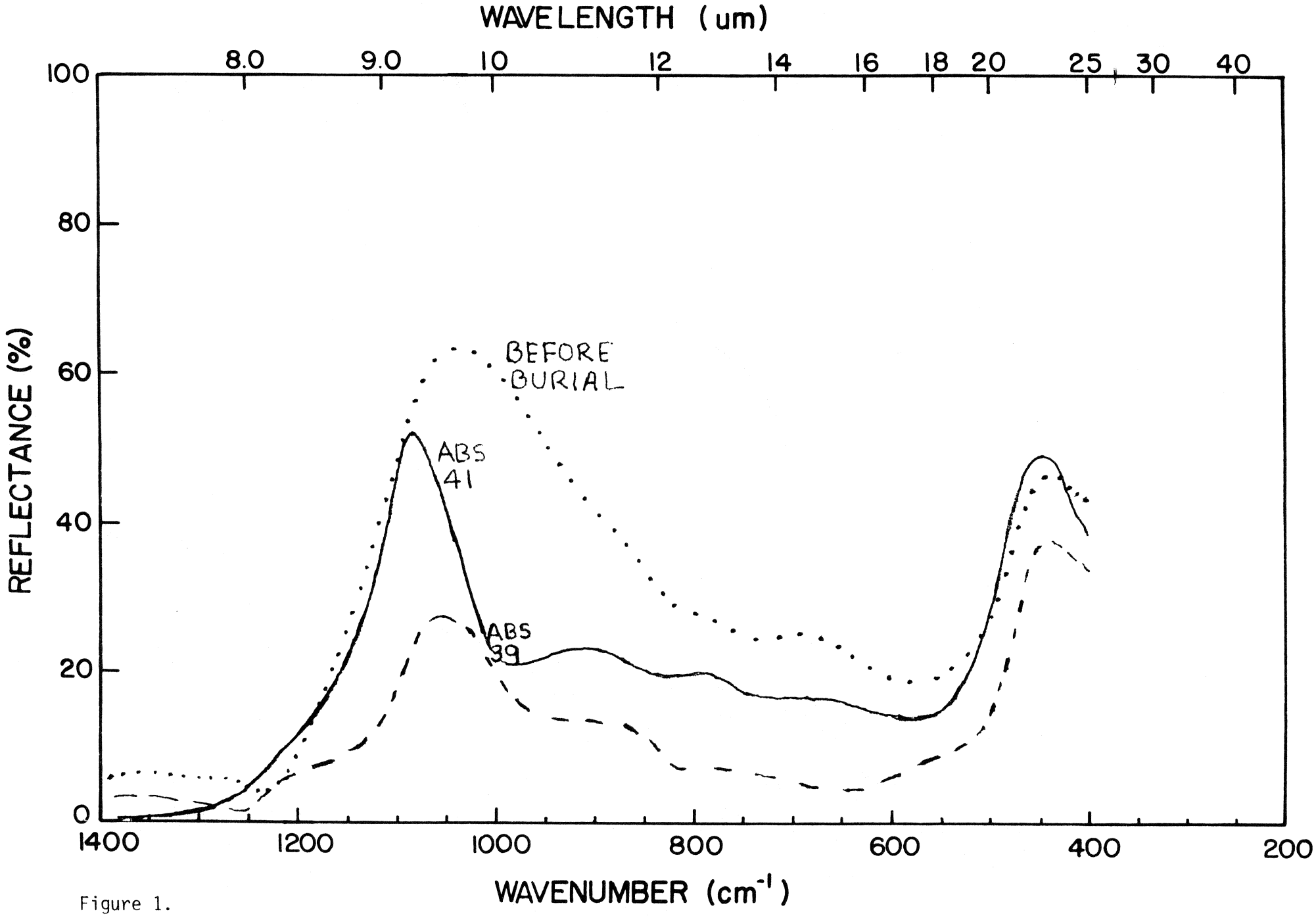
WAVELENGTH (um)
8.0
9.0
10
12
14
16
18
20
25
30
40
100
80
60
40
20
0
REFLECTANCE (%)
BEFORE BURIAL
ABS 41
ABS 39
1400
1200
1000
800
600
400
200
WAVENUMBER (cm-1)

Figure 1.

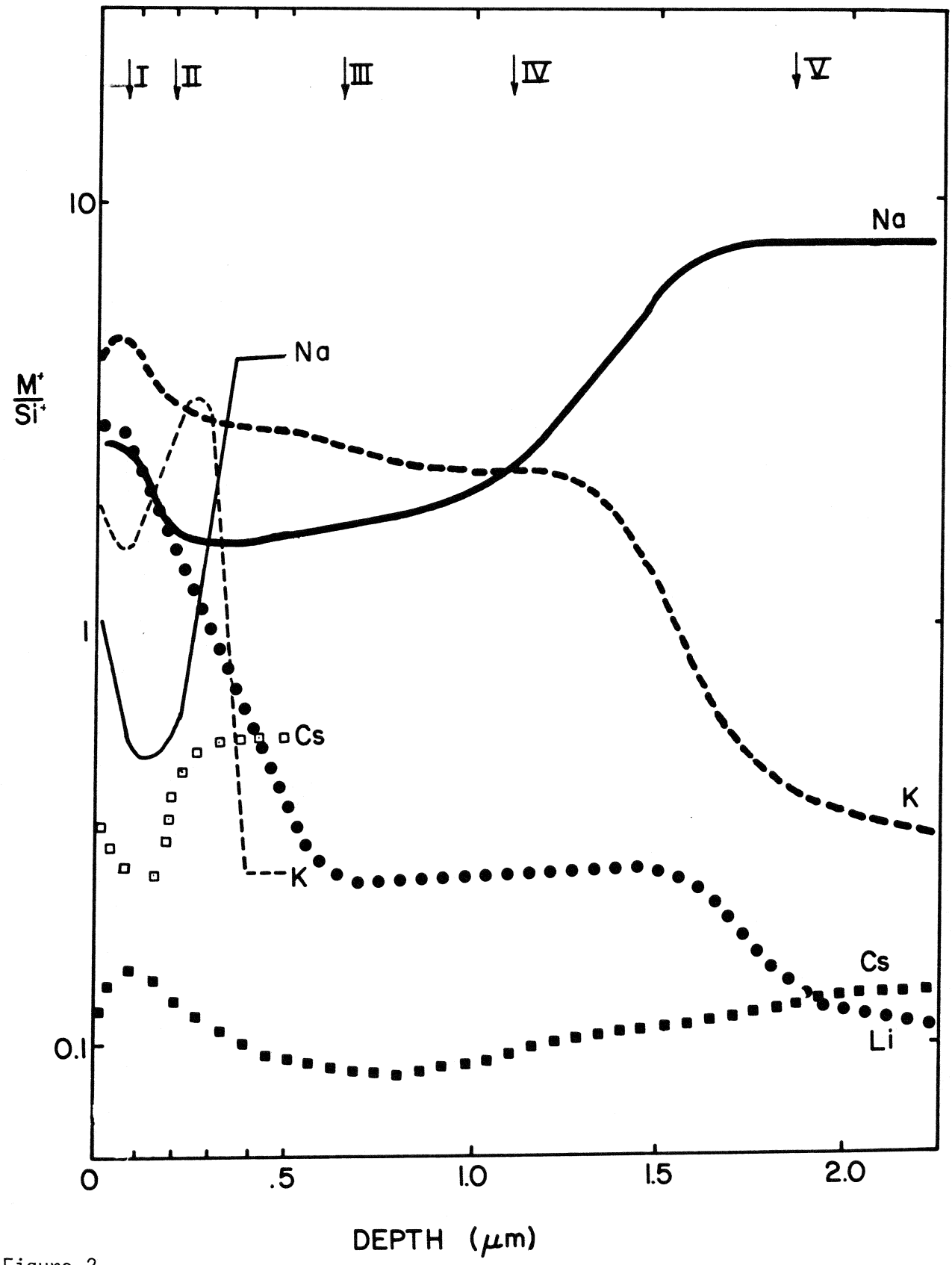


Figure 2.

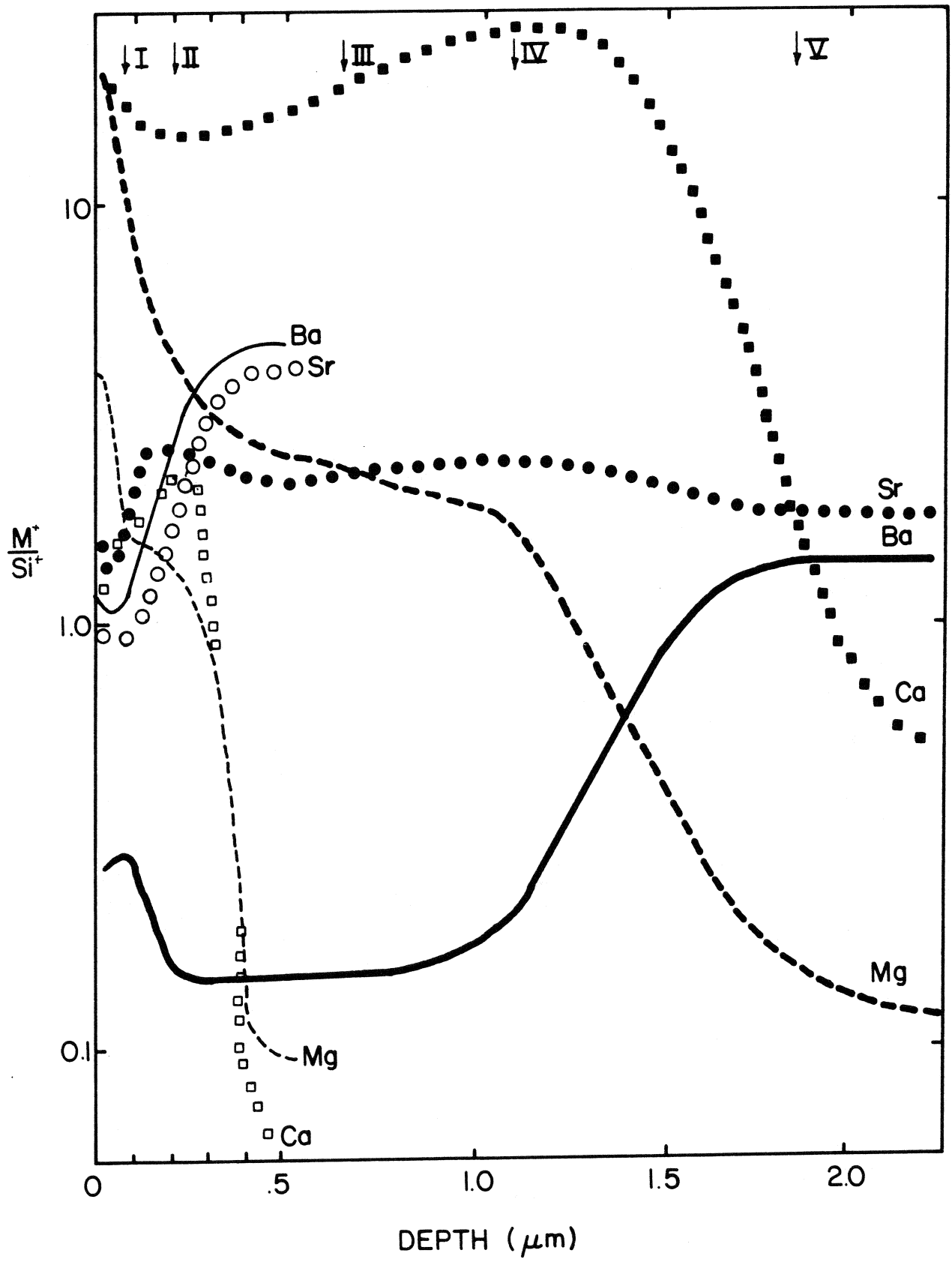


Figure 3.

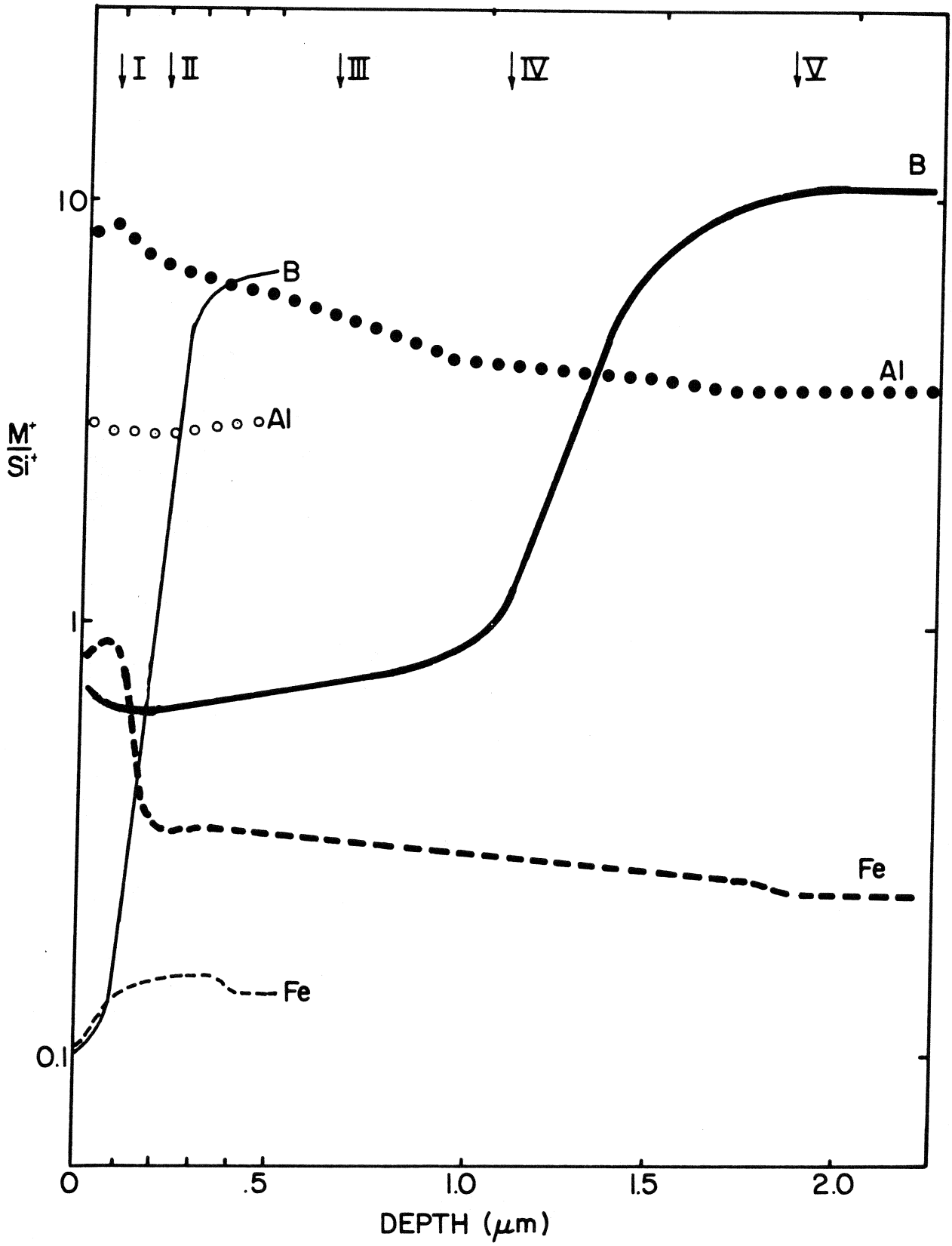


Figure 4.

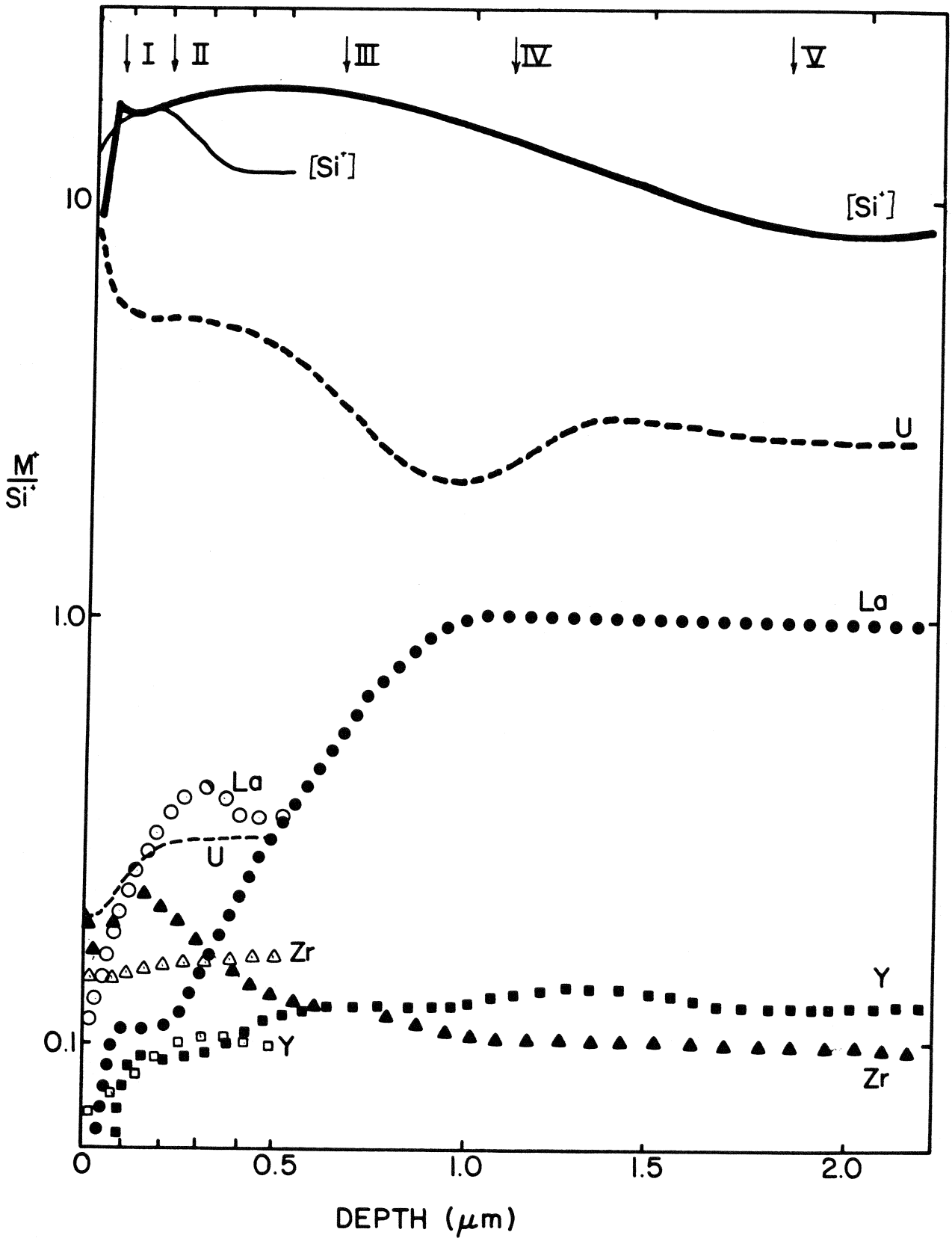
I
II
III
IV
V
[Si+]
[Si+]
10
U
M+/Si+
1.0
La
La
U
Zr
Y
Y
0.1
Zr
0
0.5
1.0
1.5
2.0
DEPTH (μm)

Figure 5

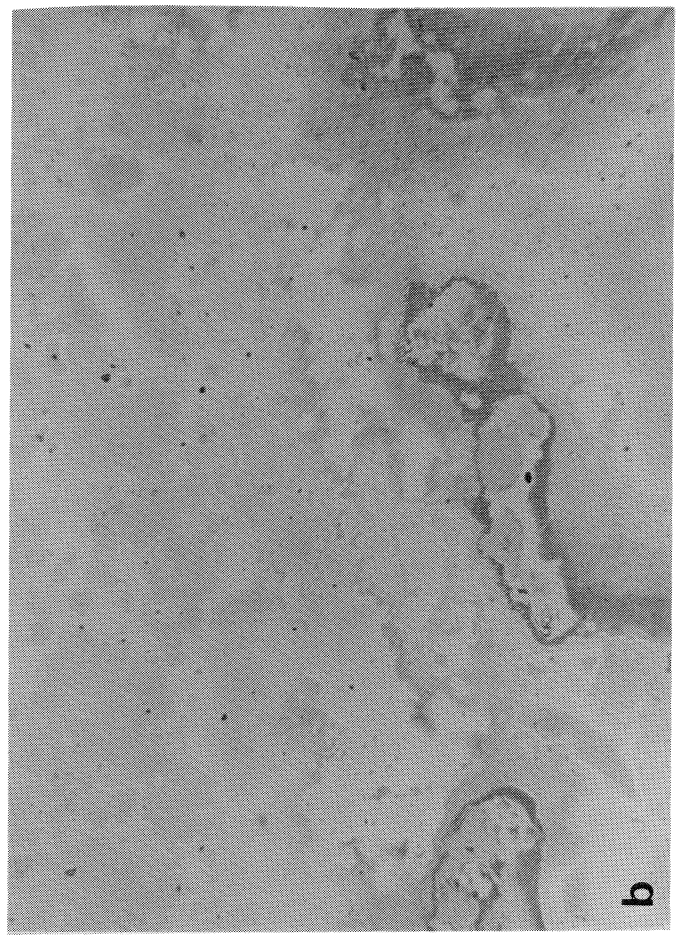


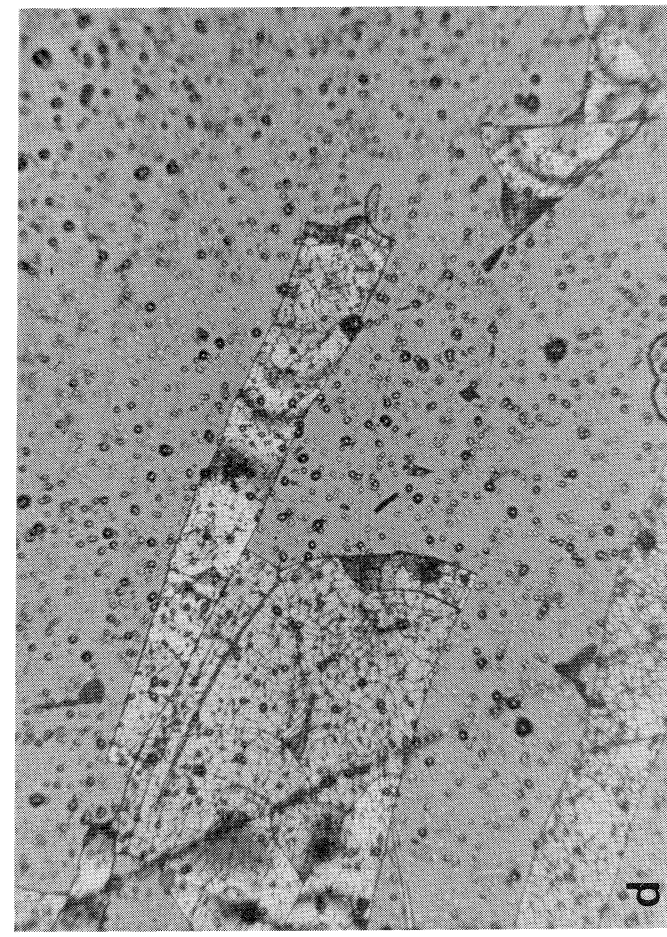


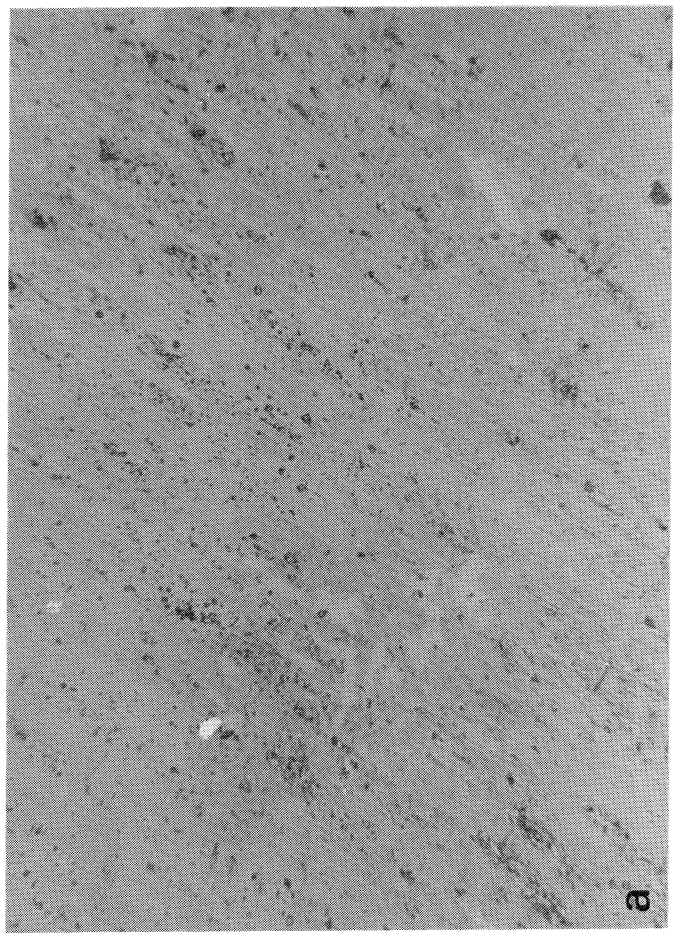


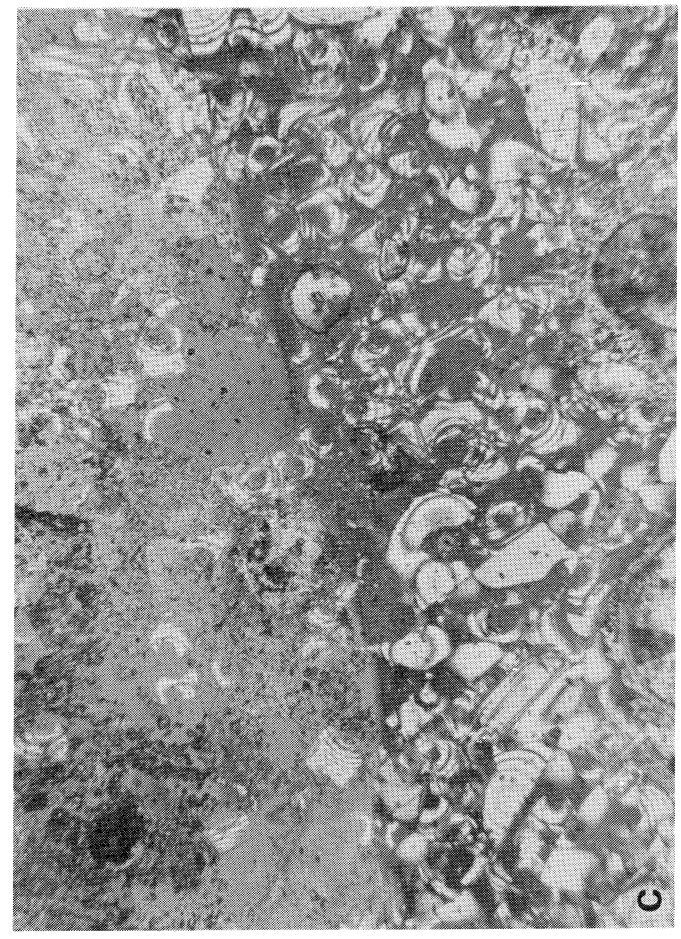


Figure 6

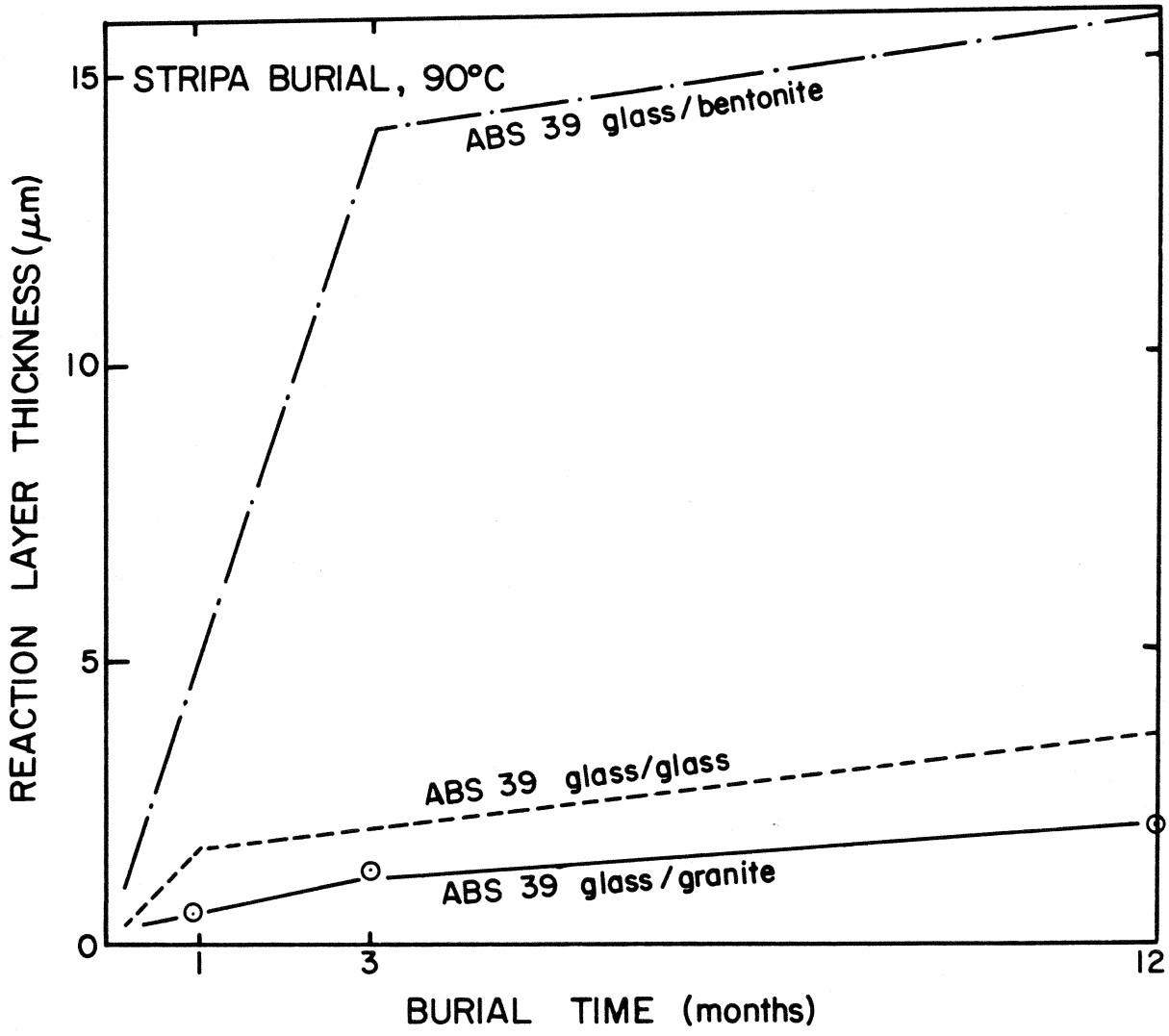
STRIPA BURIAL, 90°C
ABS 39 glass/bentonite
ABS 39 glass/glass
ABS 39 glass/granite
REACTION LAYER THICKNESS (μm)
BURIAL TIME (months)
0
5
10
15
1
3
12

Figure 7.

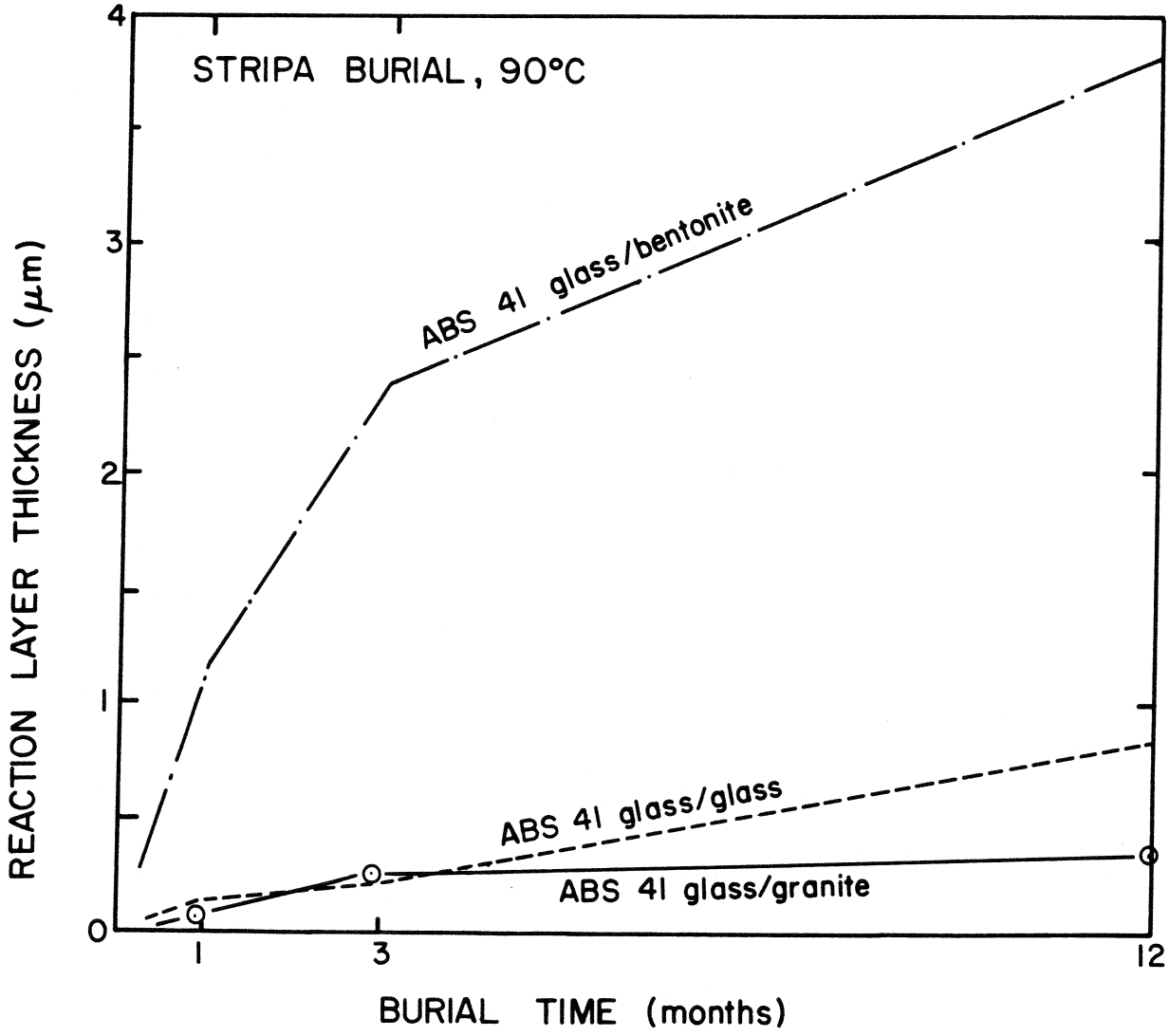
STRIPA BURIAL, 90°C
ABS 41 glass/bentonite
ABS 41 glass/glass
ABS 41 glass/granite
REACTION LAYER THICKNESS (μm)
BURIAL TIME (months)
0
1
2
3
4
1
3
12

Figure 8.

# RUTHERFORD BACK SCATTERING SURFACE ANALYSIS OF NUCLEAR WASTE GLASSES AFTER ONE YEAR BURIAL IN STRIPA

by

Larry L. Hench, Derek Spilman, and T. Buonaquisti

Ceramics Division
Department of Materials Science and Engineering
University of Florida
Gainesville, Florida 32611

Submitted to

SKBF/KBS
Stockholm, Sweden

September 9, 1983

## Introduction

Experiments to assess the effect of relevant repository conditions on the attack of nuclear waste glasses have been underway in the STRIPA mine in Sweden for some time. Two glass compositions, ABS 39 and ABS 41 (Table 1) with 9% simulated Swedish commercial waste products have now been studied for more than one year.[1-6] Three nuclear waste glass compositions with simulated U.S. defense wastes have been in place for several months.[7] In these experiments two sample configurations are compared; one is the so-called pineapple slice assembly[1] which enables 28 glass-system interfaces to be studied, and the second is a minican assembly[2] which provides 8 interfaces in addition to the cast glass-stainless steel interface present in every can. Temperatures for most of the assemblies are maintained at 90°C to simulate the thermal period of storage. In addition a fraction of the assemblies which are located 350 m deep in granite boreholes are equilibrated with the ambient mine conditions which range between 8 to 10°C. Water equilibrated with the burial hole seeps into the interfaces within the first few days of burial and the assemblies are damp upon removal after 12 mo. Therefore, this condition simulates the possible interfaces that can be exposed to repository ground water if a canister should be breached soon after burial (90°C) or long after burial (10°C).

Previous surface evaluations[1-7] of the glass samples removed after 1 mo., 3 mo., and 12 mo. burial have included optical microscopy, infrared reflection spectroscopy using a grating spectrometer, Fourier transform IR reflection spectroscopy (FTIRRS), and secondary ion mass spectroscopy (SIMS) with ion milling.

The objective of the present study is to compare the results from previous surface analyses of the 12 mo. KBS burial samples with those obtained with a Rutherford backscattering (RBS) method. RBS is a near surface analytical technique with a depth resolution of approximately 200 Å and a penetration range of up to 40,000 Å. References 8-14 describe the RBS method and summarize its application in a number of materials science areas. The method is generally most effective for heavy elements in a lighter matrix. Consequently, RBS analyses may be especially useful for determining changes in uranium surface concentration during burial. The SIMS analysis generally shows that U is lost from the glass surface at approximately the same rate as Na, and B, which are the most mobile species in the nuclear waste glasses.[1-6] There is little evidence in the SIMS data that U is concentrated in the outer glass surface reaction layer as are other multiple valence cations. Confirmation of this finding is important since it strongly influences the reaction rate constant of the loss of actinides from the glass during long term burial. Since these are long-lived elements any uncertainty in their loss rate constants is multiplied greatly during extrapolations of the glass burial data to the very long times required for secure repository behavior. In addition, the RBS method should be especially useful in evaluating glass-metal overpack interactions such as glass-Pb interfaces.

## Method

The samples used in the study were from the pineapple slice assemblies as reported previously after 12 mo. 90°C burial in STRIPA.[3-6] These include glass-glass and glass-bentonite interfaces. In addition, samples

from the ambient 10°C burial are reported. Glass-Pb interfaces are analyzed as well.

The RBS data was obtained using the van de Graaf generator and RBS collection system of the University of Florida's Major Analytical Instrumentation Center. Rutherford backscattering analysis was performed using a 2 Mev alpha particle beam. The beam current was ∿100 nA. The beam area was ∿1 $mm^2$. The scattering geometry was that of normal incidence with a scattering angle of 170°. The silicon detector had a surface area of ∿20 $mm^2$ and was positioned at ∿120 mm from the specimen. The height of the distribution between the Al/Si and the Mn/Fe/Ni shoulders was used to normalize the spectra. The comparison between spectra was made on the basis of shape distribution. Such analysis was made very carefully because of the complexity of the spectra having so many overlapping contibutions. Analysis was aided by use of kinetic calculations which indicated the channel numbers corresponding to surface scattering from each constituent element. No attempt was made to resolve species of similar mass.

## Results

Figures 1 and 2 compare the RBS spectra of nuclear waste glasses ABS 39 and 41 before corrosion and glass/glass interfaces after 12 mo. burial at 10°C and 90°C. An expanded scale of the spectral region corresponding to the heavy elements is shown in Fig. 3. The spectral location of the elements of interest in the nuclear waste glasses are indicated on the figures. Because of the close overlap of a number of elements they are discussed as groups, i.e., Mn group includes Mn, Fe, Ni; Sr group inclues Sr, Zr, Mo; Cs group includes Cs, La, Ce, Pr, and Nd.

Peak heights for the various groups and the (Al + Si)/Na ratio are reported in Table 2. The uncorroded RBS spectra of the two glasses reflect the greater $(Al_2O_3 + SiO_2)/Na_2O$ ratio for glass ABS 41. The RBS peak ratio of Al + Si/Na of ABS 41 is 5 whereas ABS 39 is 3. Conversely ABS 39 has a higher $Fe_2O_3$ content which shows up as a higher RBS peak for the Mn group of this glass. The glass compositions are roughly equivalent for the other elements and Table 2 shows that such is the case for the RBS peaks as well. This confirms that the RBS data can be used semiquantitatively to compare the relative extent of glass surface reactions even with the large number of elements in these glasses.

Table 2 shows that there is a considerable increase in the relative $SiO_2 + Al_2O_3$ content of glass ABS 39 glass-glass interfaces after 1 mo. burial at 90°C, but only a small increase due to 10°C burial. The increase in $SiO_2 + Al_2O_3$ content is due to sodium ion depeletion from the glass. A small degree of enrichment of the surface with the Mn group, probably Fe, and considerable enrichment of the entire Cs group has also occurred during the 90°C burial.

In sharp contrast ABS 41 shows almost no detectable changes in the glass surface after 12 mo. 10°C burial. A very slight $SiO_2 + Al_2O_3$ enrichment may be present.

The changes in the glass surfaces in contact with compacted bentonite are very much greater as shown in Figs. 4-7 and Table 2. At 10°C both glasses show sodium depletion. However, silica enrichment is greatest for ABS 41. Burial at 90°C results in complete absence of a Na signal for ABS 39 and a very small signal for ABS 41. Thus both compositions

are enriched in $SiO_2 + Al_2O_3$ by about a factor of 4 to 5X in contact with bentonite as compared with being in contact with glass.

Table 2 shows also that elements from the Mn group, probably Fe, and from the Sr group, probably Sr, are enriched in the ABS 39-bentonite interface after 10°C burial. However, at 90°C only the Fe enrichment is observed and Sr is depleted for this glass. Elements from the Cs group are depleted at 10°C ABS 39 bentonite interfaces but enhanced at 90°C. Uranium is lost from both the 10°C and 90°C ABS 39-bentonite interfaces by about a factor of 6X.

The effect of compacted bentonite on U migration from ABS 41 is about the same as for ABS 39; however most of the other elements are not affected as much. There is some Sr group enrichment in the ABS 41 glass-bentonite interface and a small depletion of the Mn and Cs groups.

Thus, RBS analysis shows that the predominant influence of compacted bentonite on nuclear waste glasses is loss of sodium and uranium from the glass surface, in an ion exchange with cations in the bentonite, and formation of an alumino-silicate enriched layer on the glass surface. Certain cations such as Fe and Sr tends to be complexed or adsorbed within this silicate layer with most of the others unaffected.

Effects of the 12 mo. burial on the nuclear waste glasses in contact with Pb are even more dramatic than with bentonite. Figures 8-11 and Table 2 shows that the surface of both glasses becomes essentially an $(x)PbO\cdot(y)SiO_2$ surface. Most of the other elements in the glass are not detectable after the 90°C burial of ABS 41 in contact with Pb (Figs. 9 and 11) and only a small amount of the Mn group is present for ABS 39 (Figs. 8 and 10). The Pb reaction with ABS 41 is also extensive at

10°C. However, ABS 39 still shows a measurable concentration of the lower atomic weight elements at 10°C although they are considerably depleted in comparison with the uncorroded glass.

In order to confirm that the surface layer formed in contact with Pb was primarily a lead silicate rather than a highly concentrated layer of U, an ESCA analysis of both 90°C glasses was run. The results are shown in Figs. 12 and 13 with only Pb, O, C, and Si appearing for both glasses. Consequently, we conclude that a surface composed of Pb salts and $(x)PbO\cdot(y)SiO_2$ phases is present on both glasses.

## Discussion

The RBS results obtained in this experiment confirm nearly every observation made previously[1-6] on the STRIPA burial effects of nuclear waste glasses ABS 39 and ABS 41. SIMS, FTIRRS, optical microscopy and RBS also show that a silica-rich layer forms on the glass surface with the extent of the layer increasing when the temperature is increased or when the glass is in contact with wet compacted bentonite. All the experimental methods show that the extent of the surface reaction layer is greater for glass ABS 39 than for ABS 41.

Each of the surface analyses, including RBS, show that the silica enriched surface layer results from a depletion of Na from the glass. Quantitative SIMS profiles establish that the Na and B loss is due to Ca and K ion exchange with the ground water. The presence of wet compacted bentonite at the interface also results in exchange of Al and Fe as well as Ca and K for Na and B. Both SIMS and RBS data show that U is lost from the glass surface. When bentonite is present the loss is greater due to cation exchange with the clay. Increasing the temperature increases

the extent of U loss. Quantitative SIMS results show that the U migration is somewhat slower than the Na, and B exchange and all the surface reactions are considerably less after the first 30 days of exposure to water. The decrase in rate of surface depletion is presumably due to solution saturation effects at the glass surface as described by Grambow.[15]

Previous data[2] on 1 mo. and 3 mo. glass-Pb interfaces showed a large enhancement of Pb in the glass surface to a depth of less than 1 μm. Other multiple species such as U, Fe, Ba, La and Zn were depleted within the Pb-rich layer. There was little change in the thickness of this reaction layer with time. The present RBS and ESCA data shows that the surface is almost entirely composed of Pb salts and $(x)PbO\cdot(y)SiO_2$ reaction products. The RBS spectra for the Pb enriched interfaces are consistent with a non-uniform deposit of Pb containing reaction product.[16] Previously SIMS analyses also indicates a non-uniform surface precipitation of a Pb-rich compound.[2]

## Conclusions

Rutherford backscattering analyses of glass-glass, glass-bentonite, and glass-lead interfaces after 12 mo. STRIPA burial at 10°C and 90°C confirm the previous findings of other surface analysis methods. Very thin, up to only a few μm, surface reaction layers form on the glasses due to loss of sodium and boron. Multiple valence cations are concentrated within the silica-rich surface layer with the exception of U. Bentonite accelerates these reactions and makes a thicker layer whereas Pb retards them and results in a Pb rich surface.

Acknowledgments

The authors acknowledge the financial support of SKBF/KBS, the assistance of Lars Werme and the STRIPA burial team at Lulea, Sweden, the preparation of the glass specimens by Dr. T. Lakatos, Swedish Glass Research Institute, and the use of the RBS system of the Major Analytical Instrumentation Center of the University of Florida. One of the authors (LLH) also acknowledges support of the U.S. DOE nuclear waste research program during the course of this work.

References


1. L. L. Hench, L. Werme and A. Lodding, "Burial Effects on Nuclear Waste Glass," in Scientific Basis for Nuclear Waste Management-V, W. Lutze, ed., Elsevier Science Pub. Co. (1982) pp. 153-162.

2. L. Werme, L. L. Hench and A. Lodding, "Effect of Overpack Materials on Glass Leaching in Geological Burial," in Scientific Basis for Nuclear Waste Management-V, W. Lutze, ed., Elsevier Science Pub. Co. (1982) pp. 135-144.

3. L. L. Hench, A. Lodding and L. Werme, "Analysis of One Year in Situ Burial of Nuclear Waste Glasses in Stripa," presented at the Second International Symposium on Ceramics in Nuclear Waste Management, April 24-27, 1983, Chicago, Illinois.

4. L. L. Hench, A. Lodding and L. Werme, "Nuclear Waste Glass Interfaces After One Year Burial in STRIPA, Part 1: Glass/Glass," (to be published).

5. A. Lodding, L. L. Hench, and L. Werme, "Nuclear Waste Glass Interfaces After One Year Burial in STRIPA, Part 2: Glass/Bentonite," (to be published).

6. L. L. Hench, Derek Spilman, and Lars Werme, "One-Year Burial of Nuclear Waste Glass Mini-Cans in STRIPA," (to be published).

7. D. E. Clark, B. F. Zhu, R. S. Robinson and G. G. Wicks, "Preliminary Report on a Glass Burial Experiment in Granite," presented at the Second International Symposium on Ceramics in Nuclear Waste Management, April 24-27, 1983, Chicago, Illinois.

8. W. K. Chu, J. W. Mayer, and M-A. Nicolet in Backscattering Spectrometery, Academic Press, New York, 1978.

9. J. F. Ziegler and W. K. Chu, Atomic Data and Nuclear Tables 13(5), 464 (1974).

10. L. C. Feldman, Nuclear Inst. and Methods 191(1-3), 211 (1981).

11. J. F. Ziegler, J. W. Mayer, B. M. Ullrich and W. K. Chu, "Material Analysis by Nuclear Backscattering," in New Uses of Ion Accelerators, J. F. Ziegler, ed., Chapt. 2, p. 75, Plenum Press, New York, 1975.

12. T. B. Pierce, "Accelerator Microbeam Techniques," in Characterization of Solid Surfaces, P. F. Kane and G. B. Larrabee, eds., Chapt. 17, p. 419, Plenum Press, New York, 1974.

13. M-A. Nicolet, I. V. Mitchell and J. W. Mayer, "Microanalysis of Materials by Backscattering Spectrometry," Science 177, 841 (1972).

14. W. D. Mackintosh, "Rutherford Scattering," in Characterization of Solid Surfaces, P. F. Kane and G. B. Larrabee, eds., Chapt. 16, p. 403, Plenum Press, New York, 1974.

15. B. Grambow, "The Role of Metal Ion Solubility in Leaching of Nuclear Waste Glasses," in Scientific Basis for Nuclear Waste Management-V, W. Lutze, ed., Elsevier Science Pub. Co. (1982) pp. 92-102.

16. S. U. Campisano, G. Foti, F. Grasso, and E. Rimini, Thin Solid Films 15, 431 (1975).

TABLE 1

GLASS COMPOSITIONS

| Glass | $Na_2O$ | $Li_2O$ | ZnO | $Al_2O_3$ | $B_2O_3$ | $Fe_2O_3$ | $SiO_2$ | $UO_2$ | F.P.* |
|---|---|---|---|---|---|---|---|---|---|
| ABS 39 | 12.91 | -- | -- | 3.1 | 19.12 | 5.71 | 48.54 | 1.66 | 9.0 |
| ABS 41 | 9.40 | 2.99 | 2.99 | 2.50 | 15.90 | 3.60 | 52.00 | 1.60 | 9.0 |

*F.P. - Fission Products

| Oxide | wt % |
|---|---|
| $Cs_2O$ | 9.88 |
| SrO | 2.92 |
| BaO | 5.16 |
| $Y_2O_3$ | 1.69 |
| $ZrO_2$ | 14.37 |
| $MoO_3$ | 18.30 |
| $MnO_2$ | 8.65 |
| NiO | 4.15 |
| $Ag_2O$ | 0.12 |
| SnO | 0.19 |
| $Sb_2O_3$ | 0.04 |
| $La_2O_3$ | 7.97 |
| $Nd_2O_3$ | 13.58 |
| $Pr_2O_3$ | 4.26 |
| $Ce_2O_3$ | 8.42 |
| CdO | 00.29 |
| | 100.00 |

Table 2. Effects of 12 Mo. STRIPA Burial on RBS Spectra

| | | | Peak to Peak Height | | | | | Peak Ratio |
|---|---|---|---|---|---|---|---|---|
| Glass | Interface | T(°C) | Na | AlSi | Mn Group | Sr Group | Cs Group | U (Pb) | AlSi/Na |
| ABS 39 | glass | before corrosion | 0.3 | 0.9 | (1.5) 0.35 | (0.9) 0.25 | (1.7) 0.35 | (1.2) 0.3 | 3. |
| | glass/ glass | 10 | 0.3 | 1.0 | (1.35) 0.3 | (0.95) 0.20 | (1.8) 0.45 | (1.2) 0.3 | 3.3 |
| | glass/ glass | 90 | 0.05 | 1.2 | (1.7) 0.35 | (.95) 0.2 | (2.25) 0.55 | (1.5) 0.3 | 24. |
| ABS 41 | glass | before corrosion | 0.2 | 1.0 | (1.65) 0.4 | (0.95) 0.2 | (1.70) 0.40 | (1.2) 0.25 | 5. |
| | glass/ glass | 10 | 0.2 | 1.0 | (1.7) 0.4 | (1.0) 0.2 | (1.75) 0.45 | (1.3) 0.25 | 5. |
| | glass/ glass | 90 | 0.2 | 1.1 | (1.7) 0.4 | (1.0) 0.2 | (1.75) 0.45 | (1.3) 0.3 | 5.5 |
| ABS 39 | glass/ bentonite | 10 | 0.2 | 1.0 | (2.0) 0.5 | (1.7) 0.3 | (0.7) 0.1 | (0.2) 0.1 | 5. |
| | glass/ bentonite | 90 | 0.01 | 1.0 | (2.5) 0.9 | (0.4) 0.2 | (1.9) 0.3 | (0.4) 0.1 | 100. |
| ABS 41 | glass/ bentonite | 10 | .1 | 1.0 | (1.4) 0.4 | (1.4) 0.3 | (1.6) 0.4 | (0.2) 0.05 | 10. |
| | glass/ bentonite | 90 | .05 | 1.4 | (1.5) 0.4 | (1.1) 0.3 | (1.6) 0.4 | (0.3) 0.05 | 28. |
| ABS 39 | Glass/Pb | 10 | 0.3 | 1.1 | (0.7) 0.4 | (0.4) 0.2 | (0.5) 0.2 | (5.4) 2.8 | 3.6 |
| | glass/Pb | 90 | .01 | 0.5 | (0.4) 0.2 | (0) 0.1 | (0) 0.05 | (7.8) 3.9 | 50. |
| ABS 41 | glass/Pb | 10 | .05 | 1.0 | (0.2) 0.1 | (0.1) 0.1 | (0.3) 0.2 | (2.5) 2.5 | 20. |
| | glass/Pb | 90 | .01 | 0.7 | (0) 0 | (0) 0 | (0) 0 | (8.7) 8.5 | 70. |

Note: Numbers in brackets are RBS peaks measured on expanded scale.

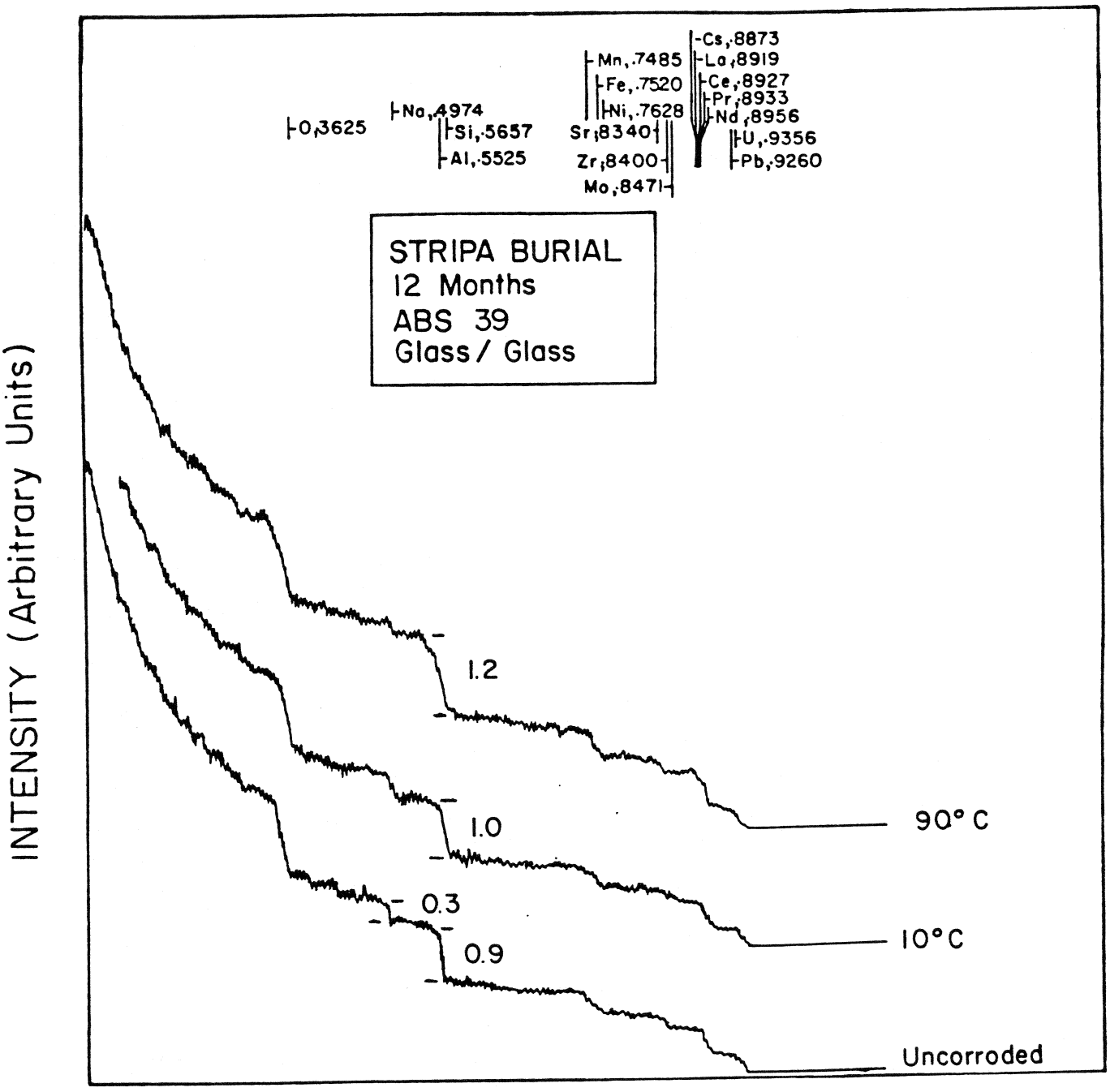
O,.3625
Na,.4974
Si,.5657
Al,.5525
Mn,.7485
Fe,.7520
Ni,.7628
Sr,.8340
Zr,.8400
Mo,.8471
Cs,.8873
La,.8919
Ce,.8927
Pr,.8933
Nd,.8956
U,.9356
Pb,.9260
STRIPA BURIAL
12 Months
ABS 39
Glass / Glass
1.2
1.0
0.3
0.9
90° C
10° C
Uncorroded
INTENSITY (Arbitrary Units)
KINEMATIC FACTOR: $\bar{K}$

FIGURE 1

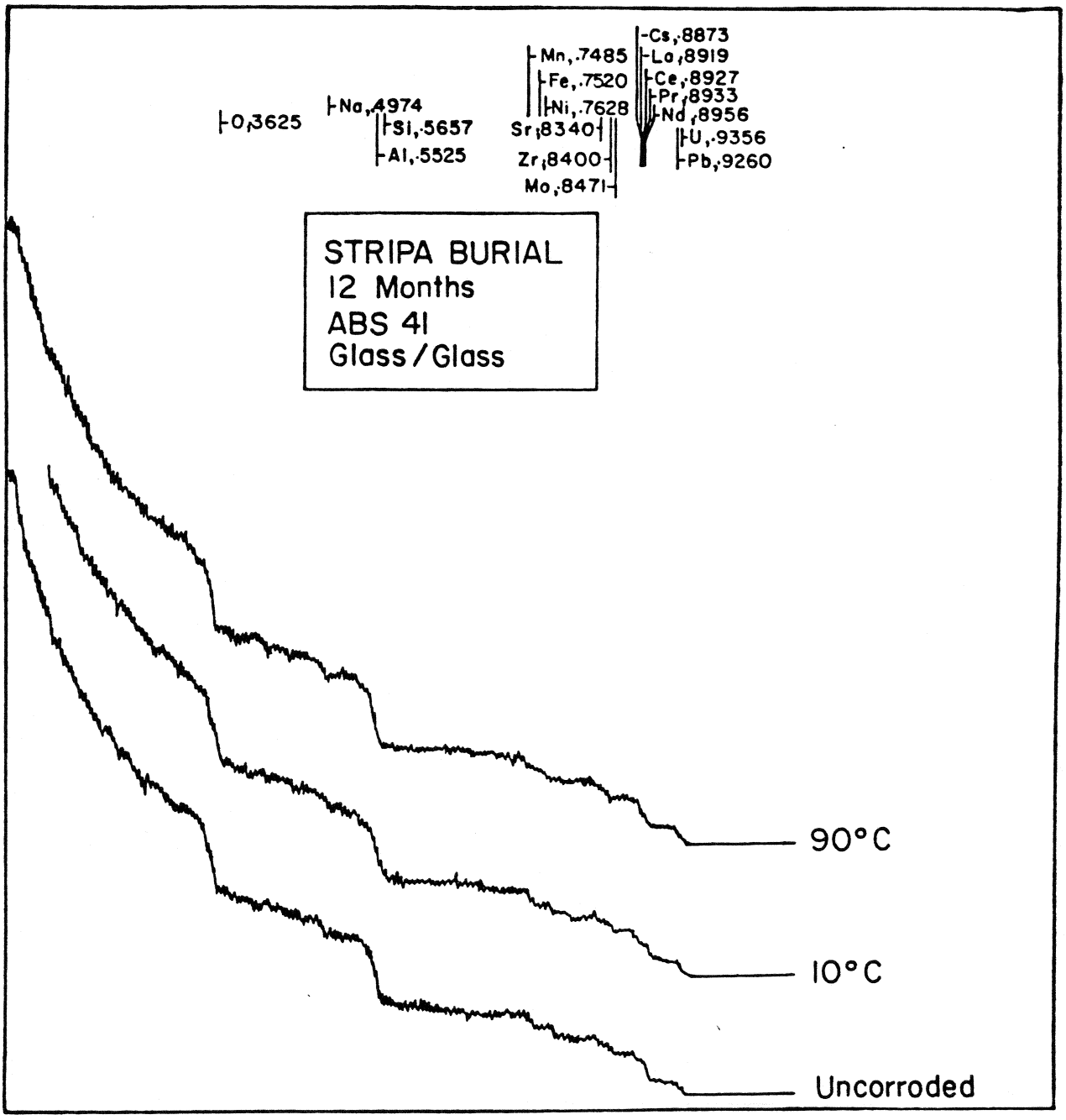
O,.3625
Na,.4974
Si,.5657
Al,.5525
Mn,.7485
Fe,.7520
Ni,.7628
Sr,.8340
Zr,.8400
Mo,.8471
Cs,.8873
La,.8919
Ce,.8927
Pr,.8933
Nd,.8956
U,.9356
Pb,.9260
STRIPA BURIAL
12 Months
ABS 41
Glass / Glass
90°C
10°C
Uncorroded
INTENSITY (Arbitrary Units)
KINEMATIC FACTOR: $\overline{K}$

FIGURE 2

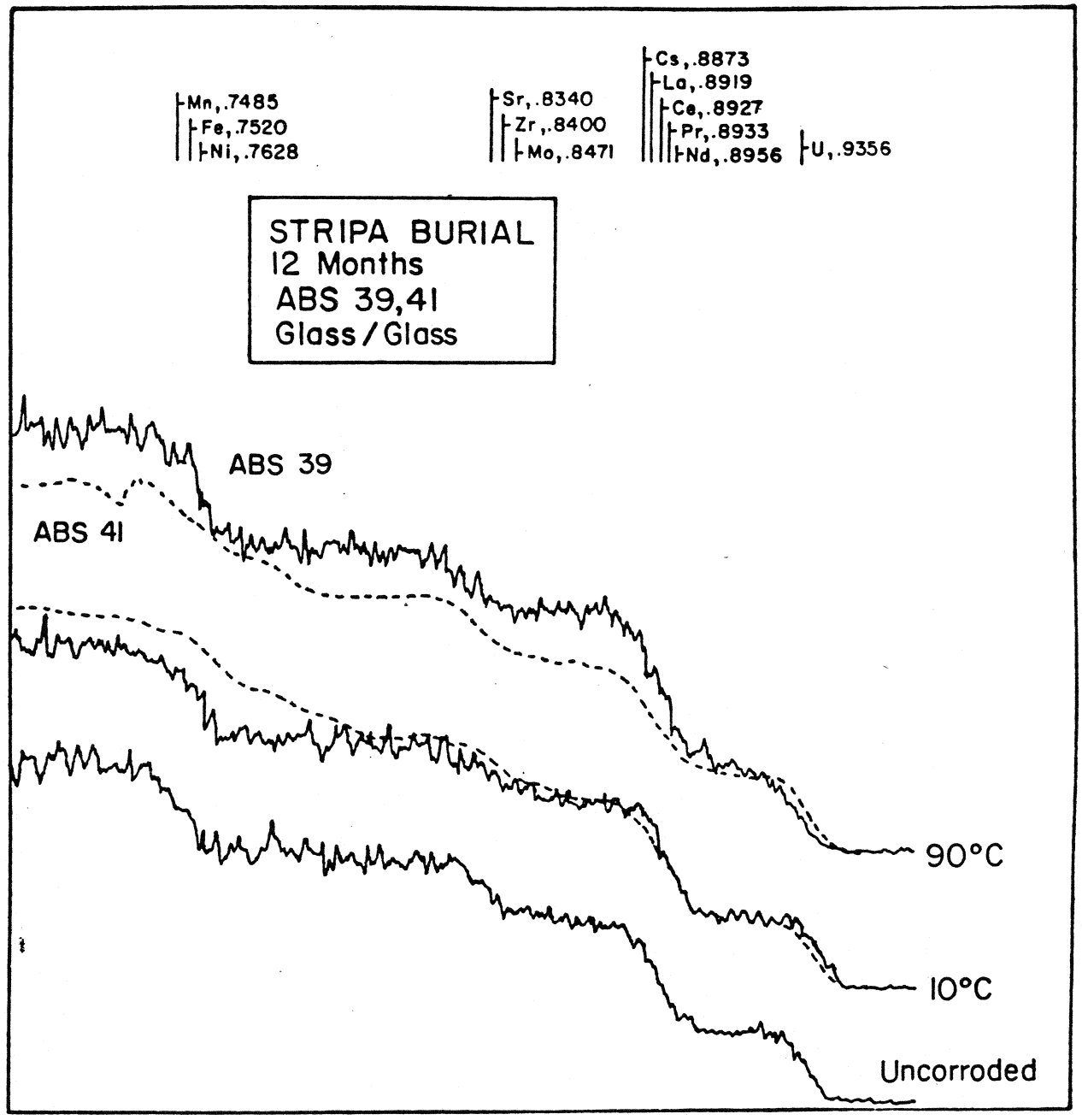
Mn,.7485
Fe,.7520
Ni,.7628
Sr,.8340
Zr,.8400
Mo,.8471
Cs,.8873
La,.8919
Ce,.8927
Pr,.8933
Nd,.8956
U,.9356
STRIPA BURIAL
12 Months
ABS 39,41
Glass / Glass
ABS 39
ABS 41
90°C
10°C
Uncorroded
INTENSITY (Arbitrary Units)
KINEMATIC FACTOR: $\bar{K}$

FIGURE 3

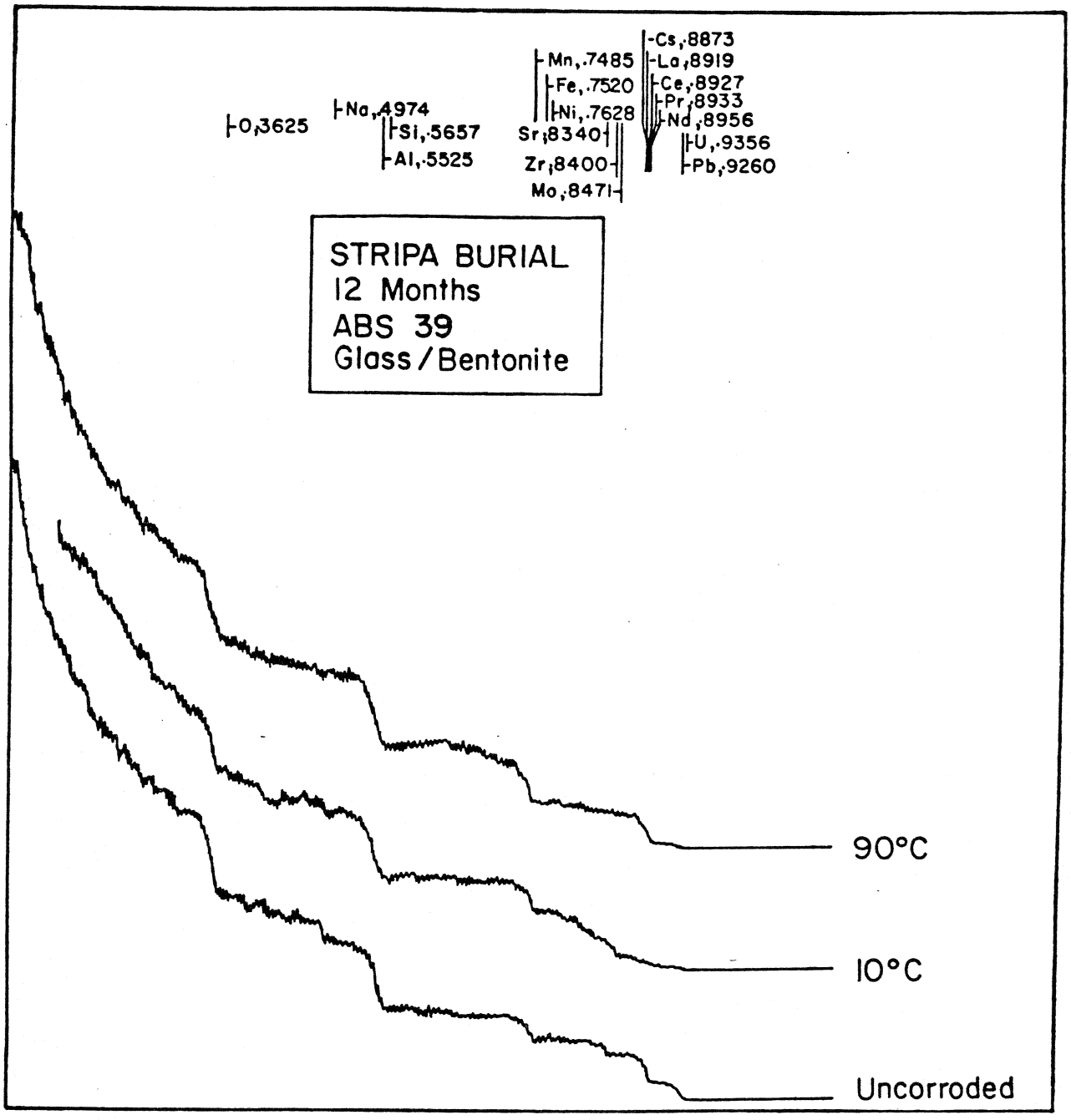
O,.3625
Na,.4974
Si,.5657
Al,.5525
Mn,.7485
Fe,.7520
Ni,.7628
Sr,.8340
Zr,.8400
Mo,.8471
Cs,.8873
La,.8919
Ce,.8927
Pr,.8933
Nd,.8956
U,.9356
Pb,.9260
STRIPA BURIAL
12 Months
ABS 39
Glass / Bentonite
90°C
10°C
Uncorroded
INTENSITY (Arbitrary Units)
KINEMATIC FACTOR: $\overline{K}$

FIGURE 4

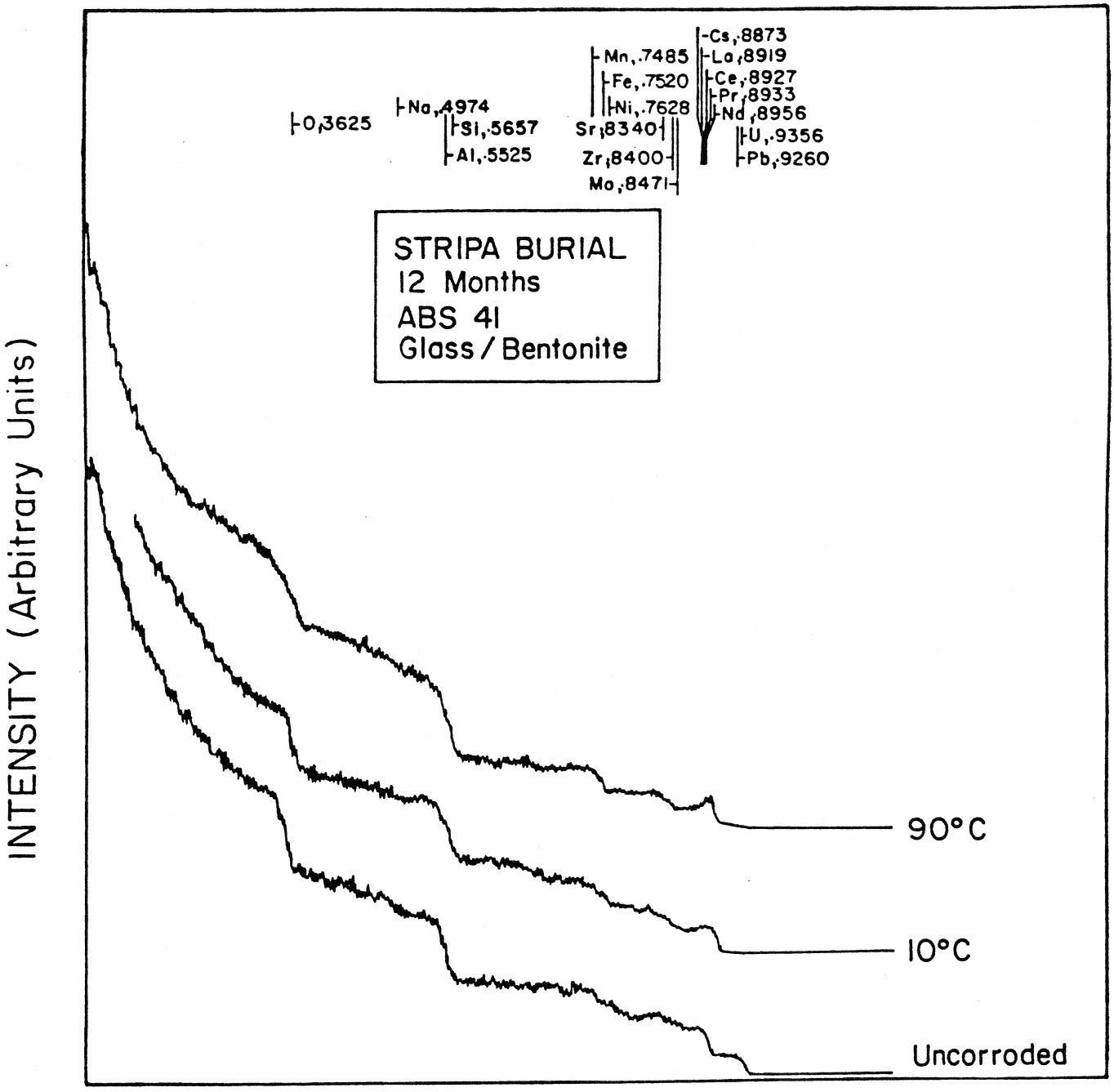
O,.3625
Na,.4974
Si,.5657
Al,.5525
Mn,.7485
Fe,.7520
Ni,.7628
Sr,.8340
Zr,.8400
Mo,.8471
Cs,.8873
La,.8919
Ce,.8927
Pr,.8933
Nd,.8956
U,.9356
Pb,.9260
STRIPA BURIAL
12 Months
ABS 41
Glass / Bentonite
90°C
10°C
Uncorroded
INTENSITY (Arbitrary Units)
KINEMATIC FACTOR: $\overline{K}$

FIGURE 5

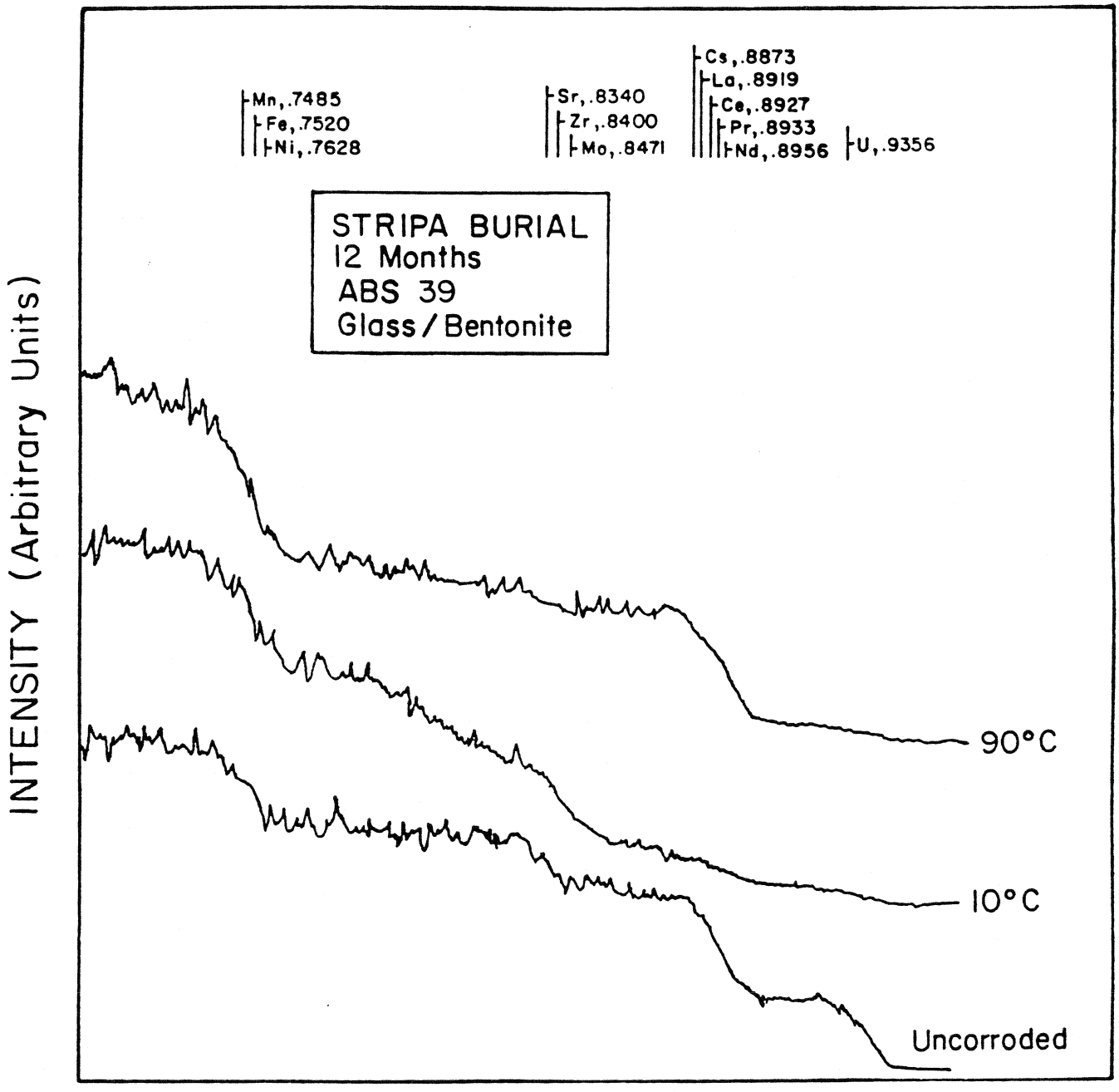
Mn, .7485
Fe, .7520
Ni, .7628
Sr, .8340
Zr, .8400
Mo, .8471
Cs, .8873
La, .8919
Ce, .8927
Pr, .8933
Nd, .8956
U, .9356
STRIPA BURIAL
12 Months
ABS 39
Glass / Bentonite
90°C
10°C
Uncorroded
INTENSITY (Arbitrary Units)
KINEMATIC FACTOR: $\bar{K}$

FIGURE 6

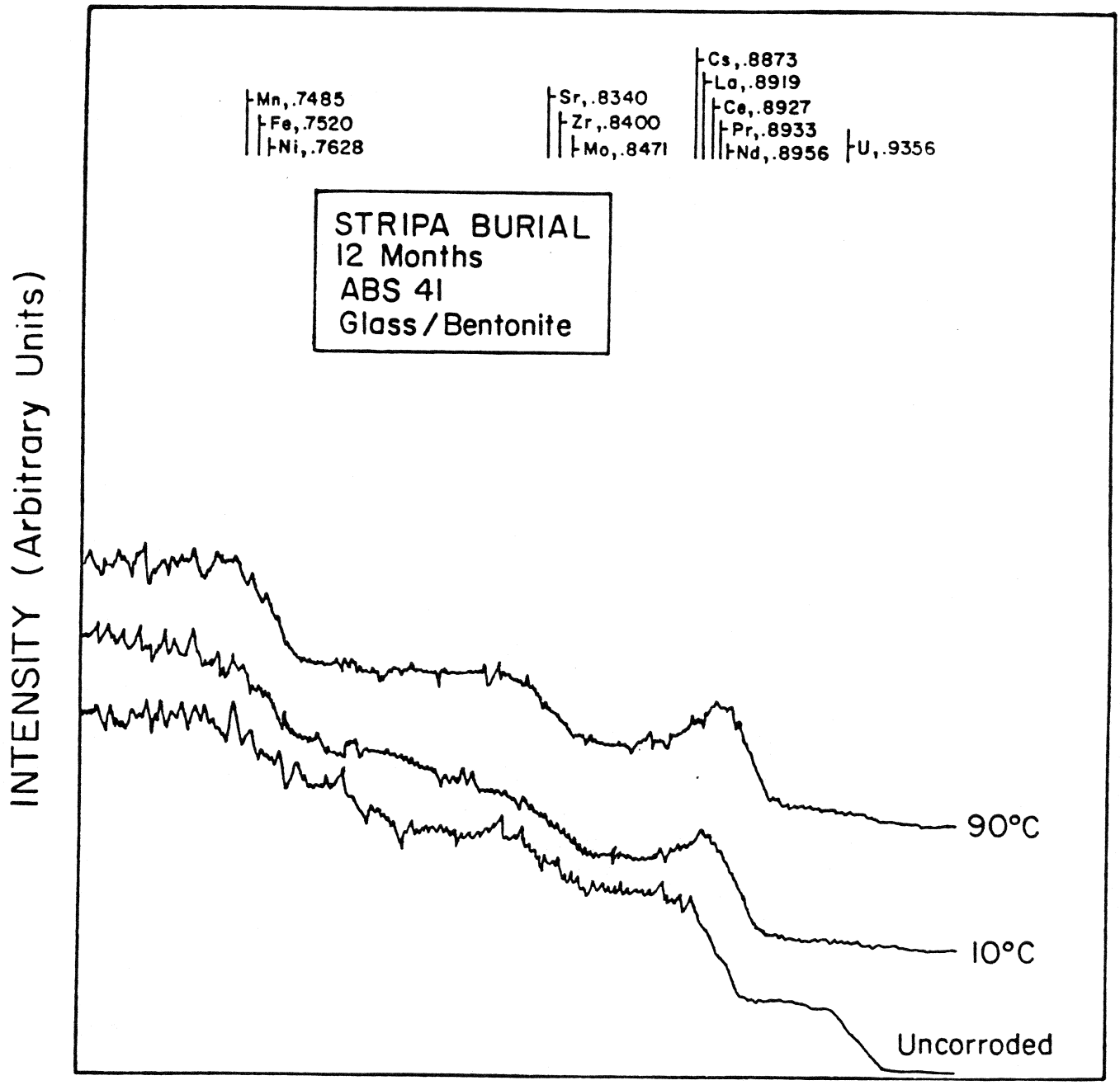
Mn,.7485
Fe,.7520
Ni,.7628
Sr,.8340
Zr,.8400
Mo,.8471
Cs,.8873
La,.8919
Ce,.8927
Pr,.8933
Nd,.8956
U,.9356
STRIPA BURIAL
12 Months
ABS 41
Glass / Bentonite
90°C
10°C
Uncorroded
INTENSITY (Arbitrary Units)
KINEMATIC FACTOR: $\bar{K}$

FIGURE 7

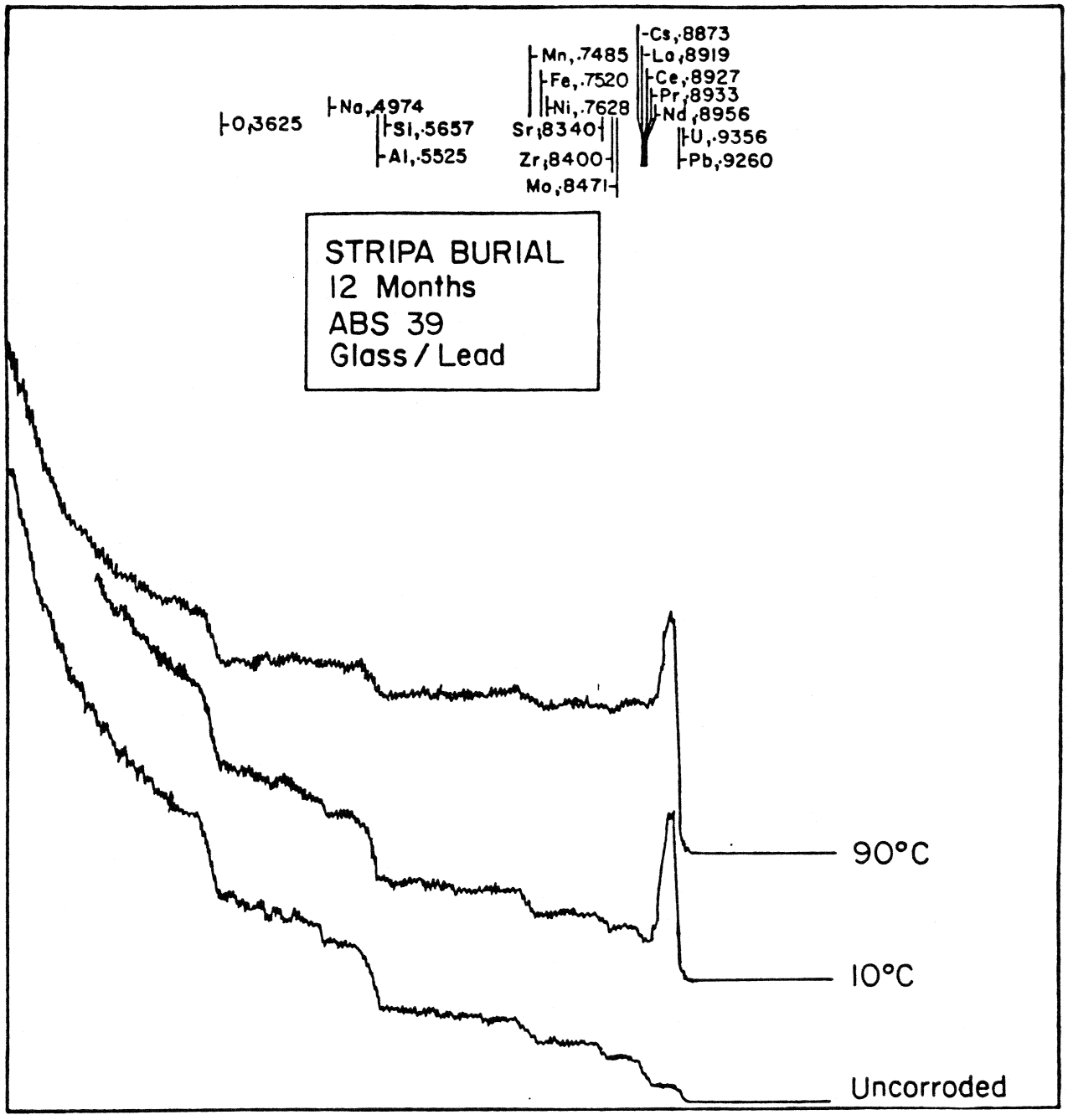
O,.3625
Na,.4974
Si,.5657
Al,.5525
Mn,.7485
Fe,.7520
Ni,.7628
Sr,.8340
Zr,.8400
Mo,.8471
Cs,.8873
La,.8919
Ce,.8927
Pr,.8933
Nd,.8956
U,.9356
Pb,.9260
STRIPA BURIAL
12 Months
ABS 39
Glass / Lead
90°C
10°C
Uncorroded
INTENSITY (Arbitrary Units)
KINEMATIC FACTOR: $\overline{K}$

FIGURE 8

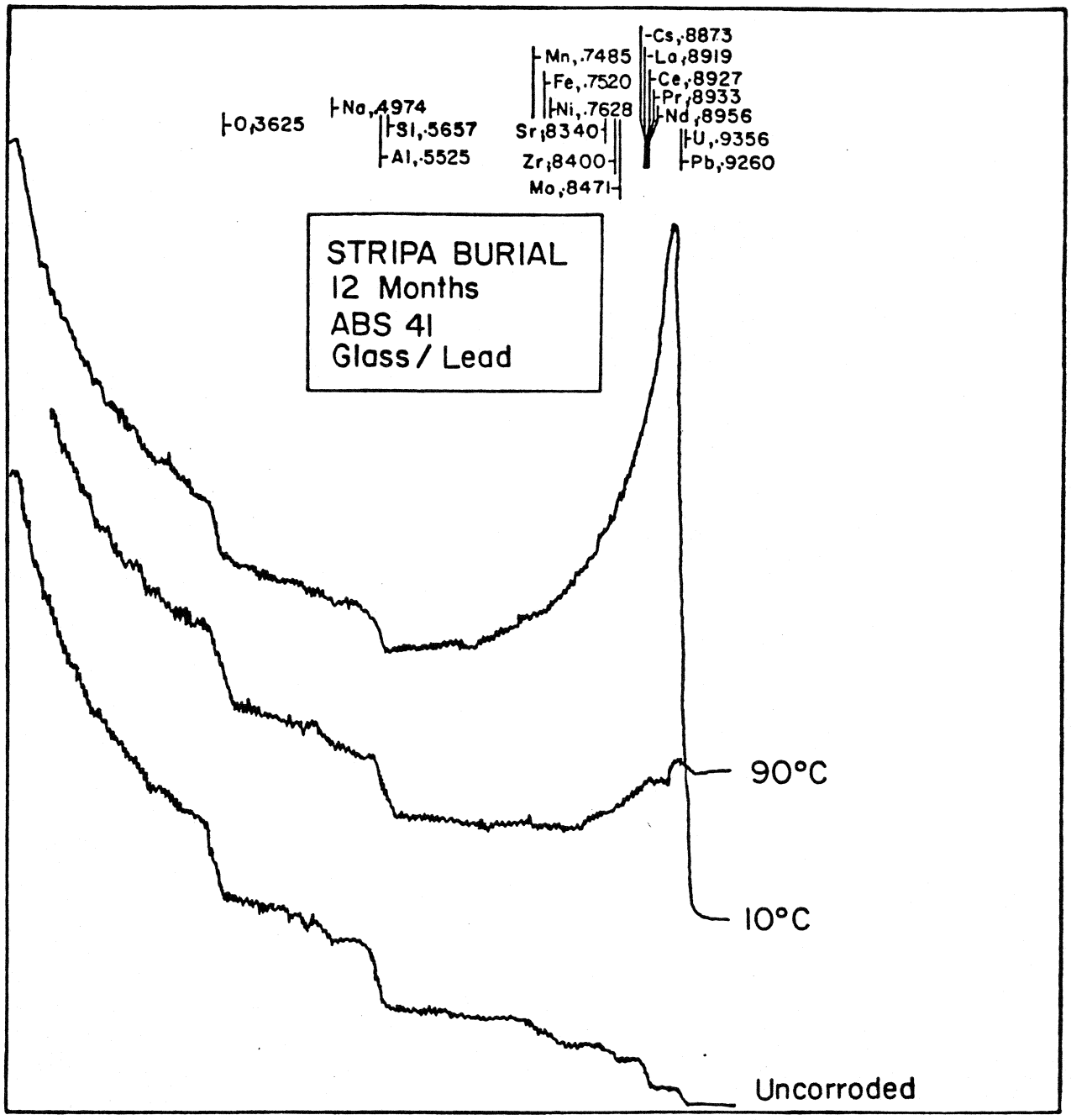
O,.3625
Na,.4974
Si,.5657
Al,.5525
Mn,.7485
Fe,.7520
Ni,.7628
Sr,.8340
Zr,.8400
Mo,.8471
Cs,.8873
La,.8919
Ce,.8927
Pr,.8933
Nd,.8956
U,.9356
Pb,.9260
STRIPA BURIAL
12 Months
ABS 41
Glass / Lead
90°C
10°C
Uncorroded
INTENSITY (Arbitrary Units)
KINEMATIC FACTOR: $\overline{K}$

FIGURE 9

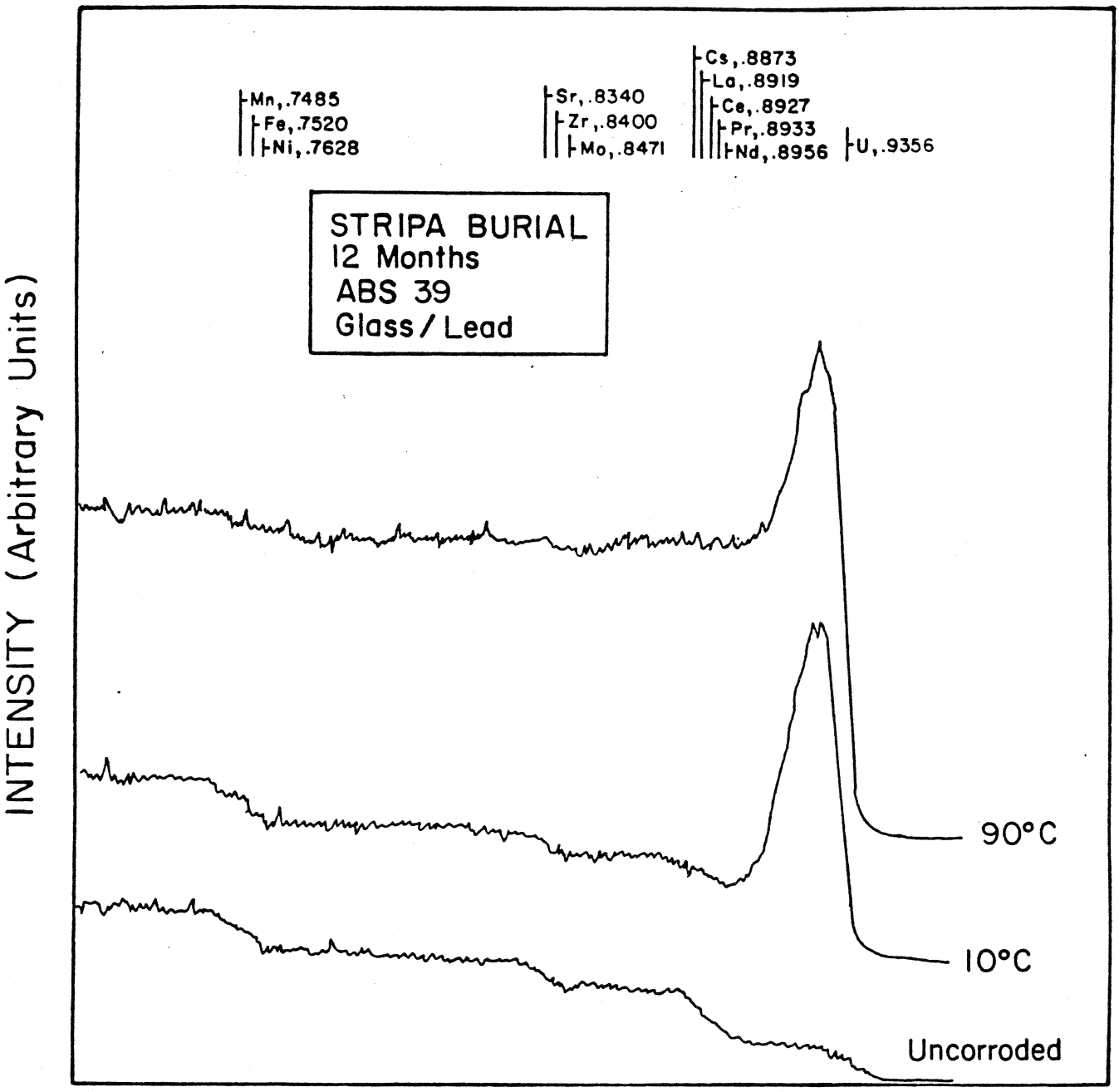
Mn,.7485
Fe,.7520
Ni,.7628
Sr,.8340
Zr,.8400
Mo,.8471
Cs,.8873
La,.8919
Ce,.8927
Pr,.8933
Nd,.8956
U,.9356
STRIPA BURIAL
12 Months
ABS 39
Glass / Lead
90°C
10°C
Uncorroded
INTENSITY (Arbitrary Units)
KINEMATIC FACTOR: $\bar{K}$

FIGURE 10

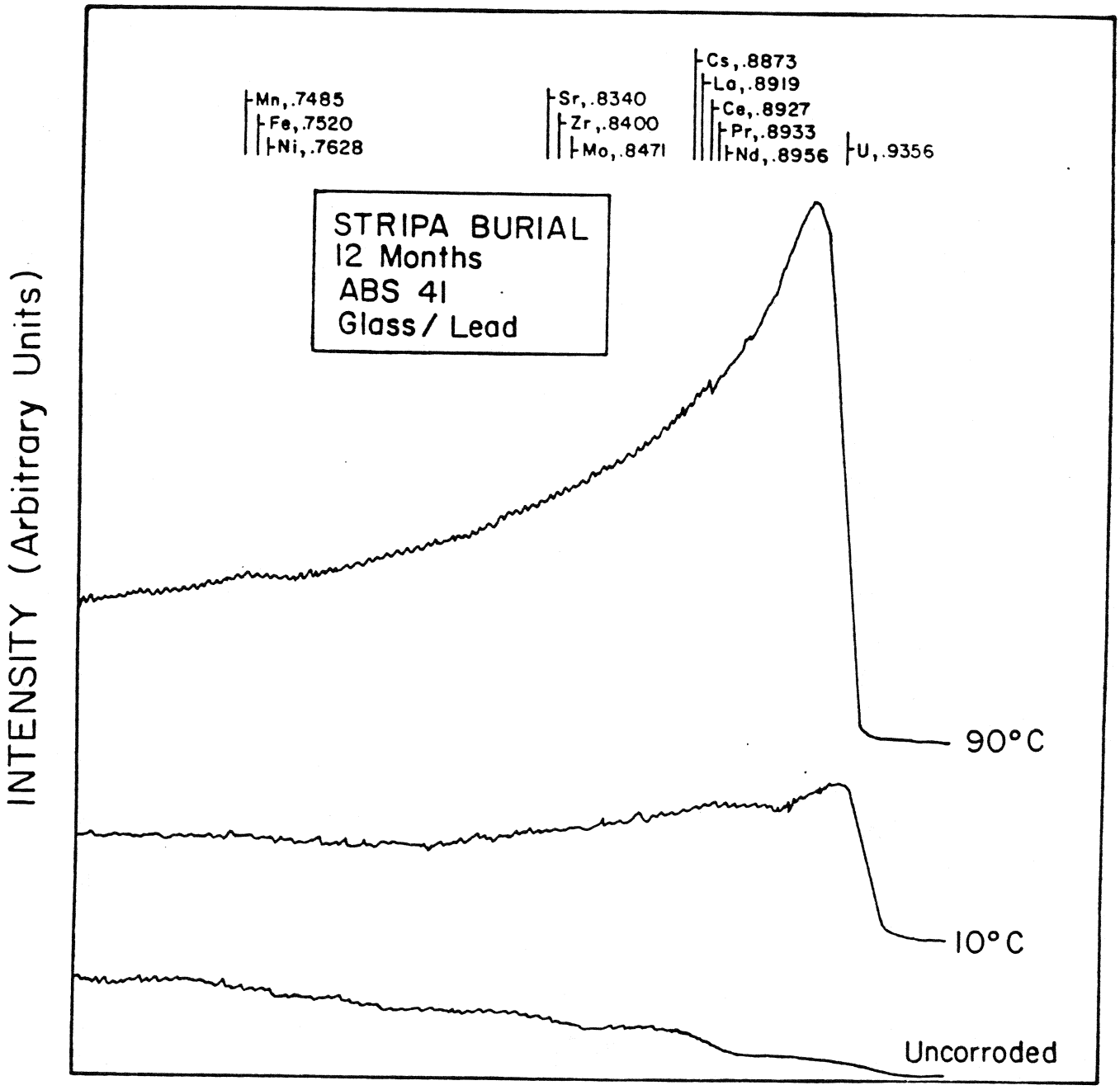
Mn,.7485
Fe,.7520
Ni,.7628
Sr,.8340
Zr,.8400
Mo,.8471
Cs,.8873
La,.8919
Ce,.8927
Pr,.8933
Nd,.8956
U,.9356
STRIPA BURIAL
12 Months
ABS 41
Glass / Lead
90°C
10°C
Uncorroded
INTENSITY (Arbitrary Units)
KINEMATIC FACTOR: $\bar{K}$

FIGURE 11

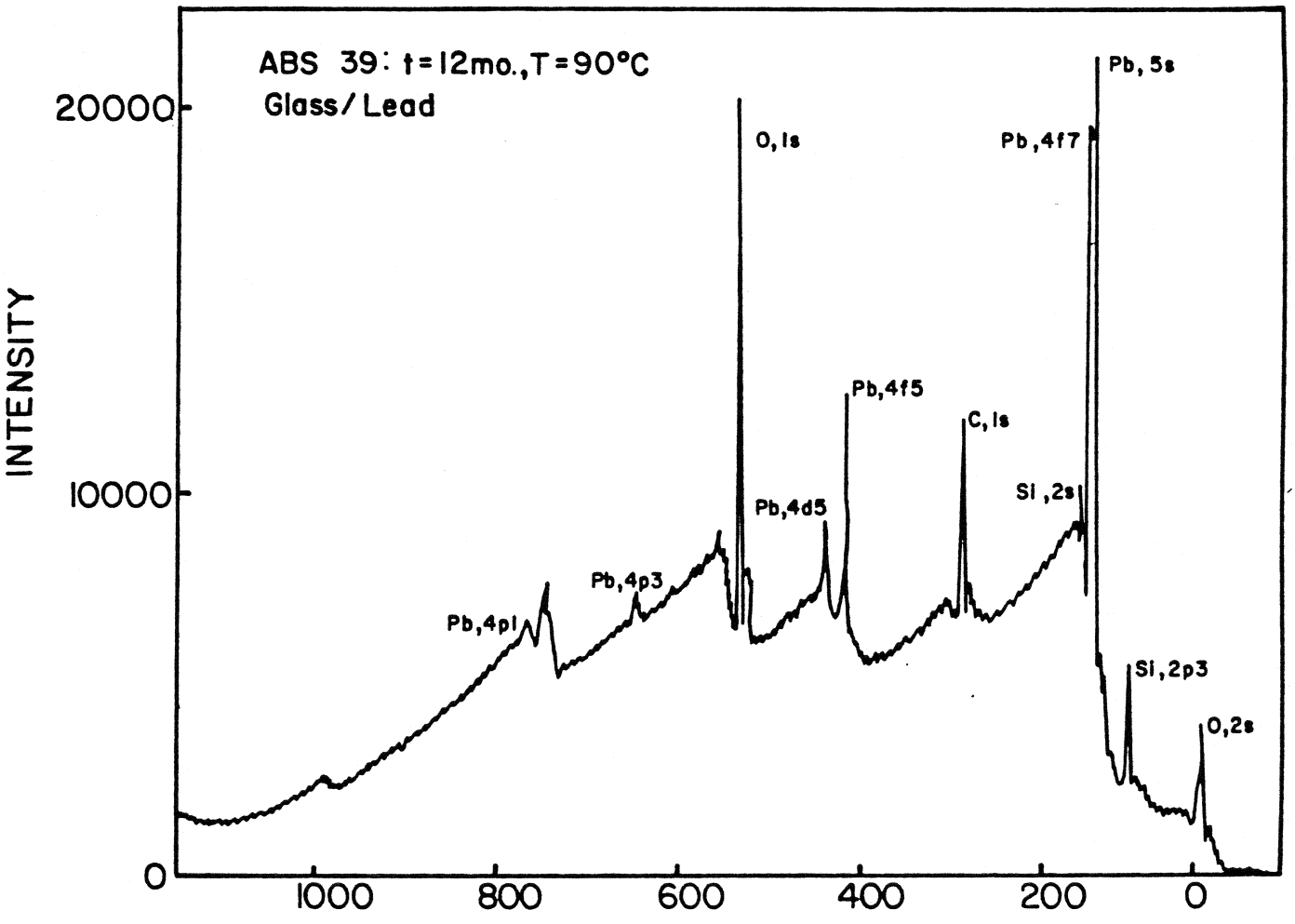
ABS 39: t=12mo.,T=90°C
Glass/Lead
20000
10000
0
INTENSITY
O,1s
Pb,4f7
Pb,5s
Pb,4f5
C,1s
Si,2s
Pb,4d5
Pb,4p3
Pb,4p1
Si,2p3
O,2s
1000
800
600
400
200
0
BINDING ENERGY (eV)

FIGURE 12

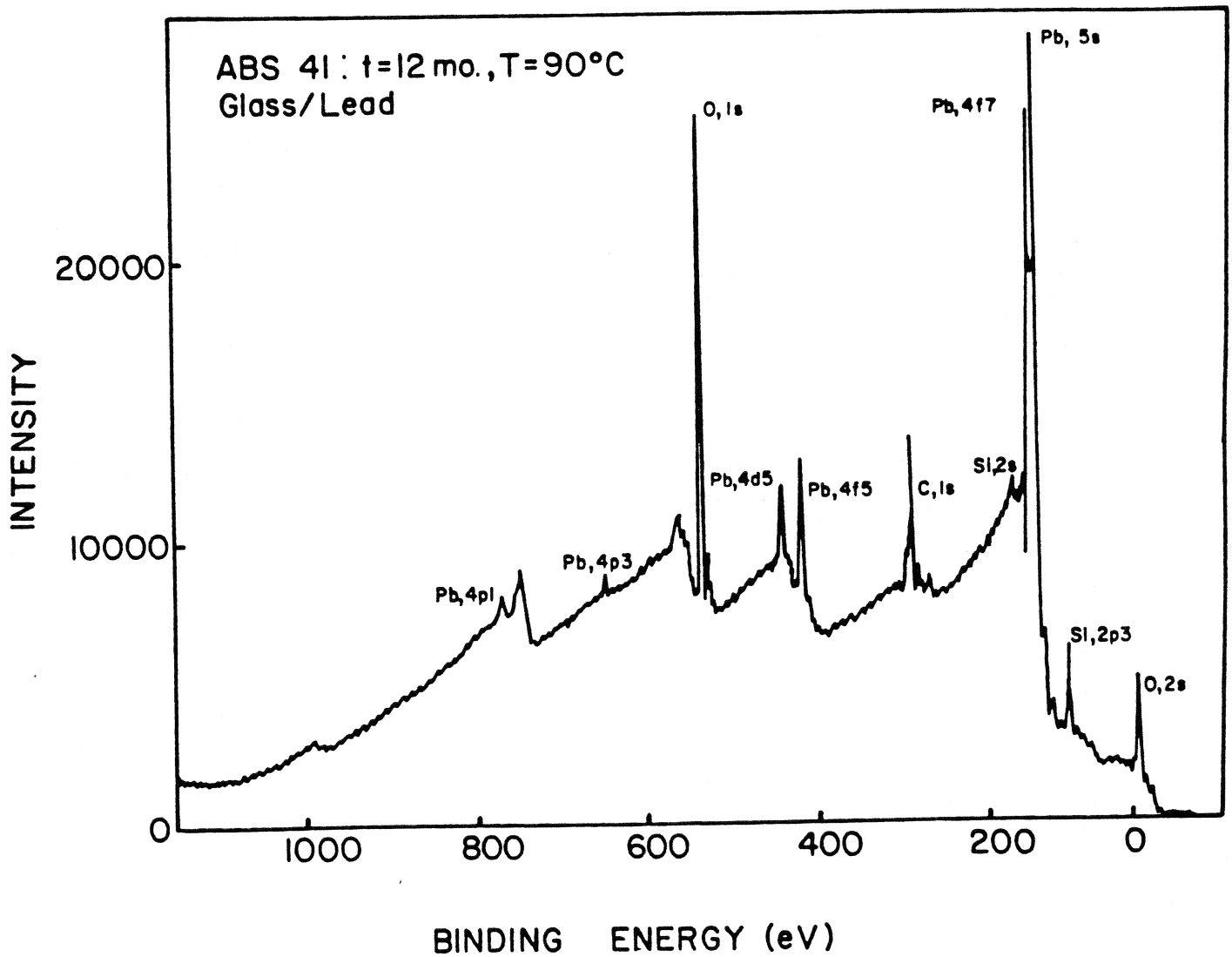
ABS 41 : t=12 mo., T=90°C
Glass/Lead
O, 1s
Pb, 4f7
Pb, 5s
Pb,4d5
Pb, 4f5
C, 1s
Si,2s
Pb,4p3
Pb,4p1
Si,2p3
O,2s
20000
10000
0
INTENSITY
1000
800
600
400
200
0
BINDING ENERGY (eV)

FIGURE 13

# NUCLEAR WASTE GLASS INTERFACES AFTER ONE YEAR BURIAL IN STRIPA MINI-CANS

by

Larry L. Hench and Derek B. Spilman
Department of Materials Science and Engineering
Univesity of Florida
Gainesville, FL 32611

and

Lars Werme
SKB/KBS
Stockholm, Sweden

## Introduction

Previous publications have described a burial experiment designed to test nuclear waste storage systems interactions.[1-5] The experiment involves burial of nuclear waste glasses of two compositions (Table I) similar to those selected by CEA [6] for solidification of commercial reprocessed wastes. Two configurations of glasses are used; both with a centerline hole suitable for insertion of a heater rod to maintain a 90°C centerline temperature, characteristic of the thermal period of storage. Samples without the heater rod are at the 8 to 10°C ambient temperature of the STRIPA mine at 330 m depth. One configuration, called the pineapple slice assembly, permits evaluation of 28 interfaces at each time period.[1] Results from 1, 3, and 12 mo. evaluation of the pineapple slice samples have already been reported.[1-5] The same

procedures have been followed in evaluating effects of burial on three U.S. defense waste glass compositions.[7]

The second configuration, termed a minican, only provides 8 interfaces for analysis at each time period.[2] However, production of the minicans more closely approximates the process of melting and casting glass into stainless steel cans which has been used in the AVM process[8] and will be employed in La Hague operations.[6] Consequently, if accelerated attack at the cast glass-steel interface is possible, it should occur in this deep granite burial experiment. Also, if the presence of a compacted bentonite backfill material together with stainless steel corrosion products should result in a rapidly accelerating attack of the glass, it should also take place in this experiment.

Early (1 month) burial results from the minicans showed very low rates of attack of the glass-glass interfaces, even at 90°C.[2] A somewhat accelerated rate of attack was observed at minican glass-bentonite interfaces,[2] equivalent to the accelerated attack at pineapple slice glass-bentonite interfaces[1,3,5] There was no evidence of enhanced attack at the minican glass-steel interfaces after 1 month burial.[2]

The objective of this paper is to present results from 90°C and 10°C minicans after one year burial in STRIPA. Because of the potential importance of the longer term burial response, a considerable extent of statistical confirmation of the surface analyses is performed as well.

## Method

The minicans were prepared by Dr. T. Lakatos, Swedish Glass Research Institute, Vaxjo, Sweden, by casting at 1150°C the two glass compositions

shown in Table I into stainless steel cans. After annealing, the glass surfaces were ground and polished dry to a 600 grit SiC finish. The minicans were assembled as shown in a previous paper,[2] and illustrated in Fig. 1, with alternating glass-glass and glass-bentonite interfaces.

Removal from the burial hole required considerable force; a hydraulic jack was used due to swelling pressure of the wet compacted bentonite sleeve between the borehole and the minican assemnbly. The assembly was wet throughout. After disassembly, each interface was cleaned in an ultrasonic bath with 100% ethanol for 15 minutes. Eight areas (5mm diameter) were selected on each minican interface for FTIRRS (Fourier Transform Infrared Reflection Spectroscopy) analysis. Each area was scanned 160 times and the resulting spectra were computer averaged and stored on floppy discs for subsequent digital comparison with other burial data. This analysis method is considerably more accurate than the single grating IR reflection spectra method employed in the one month burial experiment.[2] Details of the FTIRRS method are described elsewhere.[9]

The overall area sampled on the minican interfaces represented ~30% of the total surface area exposed. In addition, one minican representative of each composition and interface type was selected from the 90°C assembly for additional statistical comparisons of spatial dependence of attack. To do this, 12 spots of 2 mm diameter were analyzed per interface arranged spatially as shown in Fig. 2. Because of the smaller aperture size, a total of 320 FTIRRS scans were run per spot. Comparison of the spectra from the edge (E), median (M) and core (C) of the minican interfaces should establish whether preferential attack has occurred due to the glass/metal interface; i.e., the (E) position.

## Experimental Results

The compiled raw FTIRRS data for the 8 spots/interface of each minican are given in Table 2. Data include: maximum peak position (Pm) of the silicon-bridging oxygen molecular stretching vibration (S peak located at ~1050 $cm^{-1}$)[10-12] and intensity of the peak (Im). The mean, Pm and Im, and the upper and lower limits of the primary spectral feature and the standard deviation (n=8) of each is also given for each interface in Table 2.

Glass interfaces 1 and 4 and 5 and 8 are glass/bentonite and glass interfaces 2 and 3 and 6 and 7 are glass/glass as shown in Fig. 1.

The FTIRRS spectra characteristic of the glass surfaces before burial and the 90°C and 10°C glass-glass post burial interfaces are compared in Fig. 3 for glass ABS 41 and in Fig. 4 for glass ABS 39. It is quite clear from this data that there is little change in the glass surface of either composition after 10°C burial. By contrast, the change occurring at 90°C is easily distinguished.

However, when the range of results is examined, Table 2 and Figs. 5-6 it is evident that some attack has occurred at the 10°C glass/glass interfaces, with the extent being a function of position on the minican interface. There is only a small, ~2.7 $cm^{-1}$, variation in peak position (Table 2 and Figs. 5-6) but a larger range of reflection intensity ($\sigma$ = 0.4 to 5) for the glasses. The small peak shift and small difference in magnitude of shift indicates that the silica-rich film that has formed is very thin and is consistent from sample to sample, glass to glass, and spot to spot on a given sample. However, there is some variation of roughness of the surface which results in the intensity differences. Comparison of the spectral data shows that there

is excellent reproducibility between interfaces for both ABS 41 (samples 41-2 and 3) and ABS 39 (samples 39-6 and 7). Glass ABS 41 has a 5 $cm^{-1}$ greater increase in S peak location indicating that a more silica-enriched film has formed on that glass.(10-12)

In comparison with the 10°C results, Figures 3 and 4 and Table 2 show there is a substantially greater shift in the location of the S peak towards higher wavenumbers after 90°C burial for both glass compositions. There is also considerable loss of reflection intensity in the region 900 $cm^{-1}$ after 90°C burial for both glasses. The loss of intensity around 900 $cm^{-1}$ is due to incongruent loss of alkali and boron ions from the glass surface.(10-13) Incongruent dissolution gives rises to a silica-rich layer on the glass surface and the shift to higher wavenumbers is proportional to the concentration of Si-O-Si bonds on the surface.(10-12)

Glass ABS 41 shows excellent reproducibility of the peak position Pm between samples (Table 2, samples 41-2, 3) although there is considerable variation from spot to spot on the surface (Fig. 7). The range of reflection intensity for the various areas analyzed, Fig. 2, is represented by the upper and lower curves on Fig. 6 (10°C) and Fig. 7 (90°C). The area that most closely represents the mean of the spectral location and intensity is plotted as the middle curve in these figures. For example, we see in Fig. 7 that spot (e) has an intensity of 23.2 and peak location at 1077 $cm^{-1}$ with considerably less loss in intensity at 900 $cm^{-1}$. Spots (g) and (c), which are generally more characteristic of the ABS 41 glass/glass interface are somewhat lower in intensity and are located several wavenumbers lower. Spot (b) on sample 41-3, is considerably lower and represents the lowest limit for ABS 41 glass/glass interfaces.

The same range of spectral features is present on the ABS 39 glass/glass interfaces after 1 yr 90°C burial (Table 2, and Fig. 8). However, the mean peak location for glass ABS 39 is 18 $cm^{-1}$ lower. This is due to the lower $SiO_2$ content of this glass and a substantially lower concentration of Si-O-Si bonds in the glass ABS 39 surface after 1 year burial. This finding is consistent with previous burial[1-5] and laboratory leaching studies of these two nuclear waste glasses. It is noteworthy that even when an area on glass ABS 41 shows a roughened surface and low intensity, such as 41-3c (Fig. 7), the peak location is still higher than occurs on glass ABS 39. As discussed below, this difference is due to variations in the incorporation of multivalent cations in the glass reaction layer formed during burial.

The glass bentonite interfaces show considerably more attack after 1 year 10°C burial, Figs. 9-14, than the equivalent 10°C glass/glass interfaces, Figs. 3-6. The higher temperature, 90°C, exposure produces more surface reaction than 10°C, as expected, Figs. 9 and 10, for both glasses. However, it is especially important that the extent of the glass/bentonite reaction at 90°C after 12 months is not substantially greater than was present after 1 month.[2] It is also significant that the 90°C glass/bentonite interface after 12 months shows only somewhat greater attack than the glass/glass interfaces, Table 2. Both ABS 41 and ABS 39 minicans in the middle of the 90°C assembly in contact with bentonite show the greatest change (Table 2). This is similar to the stack location effect reported for the pineapple slice assemblies and is suspected to be due to a small temperature gradient with the ends being slightly cooler. Note that there is no difference in results as a function of location in the assembly for the ambient, 10°C, assemblies (Table 2).

Variations from spot to spot on the 10°C glass/bentonite interfaces are quite large for both glasses and both locations of minicans, Figs. 11-12. The large peak developed at 900 $cm^{-1}$ for many of the samples indicates development of an amorphous surface phase enriched in $M^{2+}$ cations. Nearly all spots analyzed on the 10°C glass/bentonite interface show evidence of the new surface phase.

There is less evidence of the new amorphous surface phase on the 90°C glass/bentonite interfaces after 12 mo. burial (Figs. 13-14). Instead a major new peak developed at 530 $cm^{-1}$ on 3 of the 4 minicans suggests that a new mineral phase is developing on the surface. This finding is consistent with the surface compositional changes reported previously for equivalent 12 mo. interfaces involving the pineapple slice configuration.[3,5]

In order to test the susceptibility of the glass/metal interface at the edge of the minicans to accelerated attack during 90°C burial an extensive series of 2 mm diameter spot to spot analyses was made according to the geometric array shown in Fig. 2. The results of this study are presented in Table 3. The range of spectra as well as the spectrum representing the mean are similar for the glass/glass interfaces and the glass/bentonite interfaces shown in Figs. 3-14 for the 5 mm diameter spots. The spectra for minicans ABS 41-3 and 39-7 glass/glass interfaces are compared in Table 3. Also edge and cventer locations for minicans ABS 41-4 and 39-8 with glass/bentonite interfaces are compared in Table 3.

It is evident in Table 3 that ABS 41 shows a higher peak location for all three locations than does ABS 39. There is also relatively little difference between the means of the edge, middle, and center peak locations for ABS 41. Use of students' t-test showed no statistical difference in peak location or peak height locations for ABS 41 at a 99% confidence level.

Thus, there is no preferential edge attack at the glass/stainless steel interface of the minicans with glass ABS 41 during 12 months 90°C burial when glass/glass interfaces are in contact.

An equivalent analysis of edge, middle, and center spectra for ABS 39, (Table 3) showed more location sensitivity after the 90°C 12 months burial. However, there was no statistically significant difference, 99% confidence level, between the peak location of the edge vs the middle for ABS 39 even though there was a difference for peak height. There was a significant difference in peak location between middle and center for the ABS 39 minican, but not in height. Both peak location and height of the edge location was significantly different from the center.

Consequently, ABS 39 minicans do show significant variations among various spot locations on the glass surface. However, this variation exists at various locations on the surface and not just at the glass/metal edge. This means that there is no systematic sensitivity of the ABS 39 glass to corrosion attack at the stainless steel-can interface during 12 months 90°C burial.

However, the presence of bentonite leads to a statistically significant difference between the edge and center of minicans ABS 41-4, and ABS 39-8.

## Discussion

Statistical distribution plots are a convenient way to compare the two glass compositions, two types of interfaces, and two burial temperatures. Figures 15-18 show such graphical comparisons. In these figures the center of the bar graph is the statistical mean of the peak location ($cm^{-1}$) and the width is ± one standard deviation of peak location. The asterisk in the graph

is the mean of the peak height and the width of the upper segment of the height is the ± standard deviation of the height. Thus, when two bar graphs overlap there is no statistical difference between the two samples; when they do not overlap there is a significant difference.

Figure 15, which illustrates glass/glass interfaces, shows that both 90°C glass compositions have been shifted to significantly higher peak locations as a result of the 12 mo. burial. Both glasses are statistically different in their behavior. The difference between the two compositions shows up even after the 10°C burial. A dramatic increase in wavenumber exists between the 90°C and 10°C burial samples. This is because there is considerably more sodium and boron ion exchange from the glass surface at 90°C than at 10°C. Thus, the glass surface develops an increased concentration of Si-O-Si bonds to form a silica-rich surface layer at 90°C. This finding is equivalent to that reported in detail for the pineapple slice burial assemblies using SIMS analysis.

Figure 16 shows that the equivalent pairs of ABS 39 and 41 minicans in both 90°C and 10°C assemblies behave the same as those shown in Fig. 15. This is an important finding since it shows that there is reproducibility from minican to minican. Thus, a routine melting and casting operation of two compositions of nuclear waste glasses result in statistically equivalent surface behavior after one year of burial in both thermal (90°C) and post-thermal (10°C) conditions.

The differences in behavior between the two glass compositions is also repeatable for the equivalent pairs of samples. These results also correspond to the findings of pineapple slice assemblies.[1-5] The statistical equivalence between various sample configurations, duplicate samples, and

compositional dependence yield considerable confidence that the results from these burial experiments are representative of the behavior of these nuclear waste glasses under relevant repository conditions.

The presence of compacted bentonite at the glass interface not only accelerates the initial rate of cation exchange, but also introduces more variability in the surface behavior. Figures 17 and 18 illustrate this point. However, at 10°C burial there is no statistical difference between duplicate ABS 39 and 41 minicans. The composition difference of the two glasses present without bentonite is diminished when bentonite is present, as also shown in the pineapple slice assemblies,[1-5] but is still statistically significant.

After 90°C burial, the glass reaction with bentonite produces sufficiently thick layers, see Ref. 5, that there is inconsistency between the duplicate minicans; i.e., compare Figs. 17 and 18. This is likely to be due to the formation of a hydrated mineral phase on the surface rich in $M^{2+}$ and $M^{3+}$ cations, as discussed by Lodding et al.[5]. Secondary ion mass spectroscopy (SIMS) profiles of the 12 mo glass surfaces show that there is silica enrichment of the glass surface with extensive amounts of $Ca^{2+}$, $Al^{3+}$, and $Fe^{3+}$ cations.[5] Depletion depths of Na and B from these surfaces provide the basis for long-term extrapolation of glass burial behavior.

## Conclusions

The present FTIRRS results show that the quantitative SIMS data on pineapple slice assemblies can be extended to nuclear waste glasses cast into stainless steel canisters replicating the production steps required for solidification of commercial or defense wastes. There is no significant

corrosion effects associated with the steel canister glass interface. Glass ABS 41 shows a slower rate of attack at both 10°C and 90°C than ABS 39, as shown previously. Burial at post thermal, 10°C, ambient conditions, produces barely detectable surface changes for glass-glass interfaces even after 1 year of burial. This finding confirms data from 1 year pineapple slice assemblies that show surface depletion rates of less than 0.1-0.5 μm/yr. Bentonite accelerates the early stage of cation exchange of the glass minicans but not the long term attack.

## Acknowledgements

The authors acknowledge financial support of SKBF/Project KBS throughout this study, Dr. T. Lakatos, Swedish Glass Research Institute for preparation of the minicans, and the STRIPA operations team at Lulea, Sweden. One of the authors, L. L. H., also acknowledges support of the U.S. D.O.E. Nuclear Waste Research Program for use of the Nicolet FTIR and data analysis system.

## References


1. L. L. Hench, L. Werme and A. Lodding, "Burial Effects on Nuclear Waste Glass," in Scientific Basis for Nuclear Waste Management-V, W. Lutze, ed., Elsevier Science Pub. Co., (1982) pp. 153-162.

2. L. Werme, L. L. Hench and A. Lodding, "Effect of Overpack Materials on Glass Leaching in Geological Burial," ibid., pp. 135-144.

3. L. L. Hench, A. Lodding and L. Werme, "Analysis of One Year In Situ Burial of Nuclear Waste Glasses in Stripa," presented at the Second International Symposium on Ceramics in Nuclear Waste Management, April 24-27, 1983, Chicago, Illinois.

4. L. L. Hench, A. Lodding, and L. Werme, "Nuclear Waste Glass Interfaces After One Year burial in STRIPA, Part 1: Glass/Glass

5. A. Lodding, L. L. Hench, and L. Werme, "Nuclear Waste Glass Interfaces After One Year Burial in STRIPA, Part 2: Glass/Bentonite,"

6. Radioactive Glasses: Research and Testing, CEA Group Anon., Editions MSA 20 rue Therese, 75001 Paris (1982) 269 pp.

7. D. E. Clark, B. F. Zhu, R. S. Robinson and G. G. Wicks, "Preliminary Report on a Glass Burial Experiment in Granite," presented at the Second International Symposium on Ceramics in Nuclear Waste Management, April 24-27, 1983, Chicago, Illinois.

8. C. Sombret, R. Bonniard and A. Jovani, "Large Scale Waste Glass Production," in Proceedings of the Conference on High Level Radioactive Solid Waste Forms, L. A. Casey, ed. U.S. Nuclear Reg. Comm., Washington, D.C. (1979).

9. L. L. Hench, G. LaTorre, L. Storz, D. E. Clark, and H. Yamanaka, "Use of Fourier Transform IR Reflection Spectroscopy (FTIRRS) in Non-Destructive Quality Assurance of Glasses and Ceramics," Advances in Ceramics, Am. Ceram. Soc., Columbus, Ohio, 1985.

10. D. E. Clark, C. F. Pantano and L. L. Hench, Glass Corrosion, Books for Industry, publishers, N.Y., NY (1979).

11. D. M. Sanders and L. L. Hench, "Mechanisms of Glass Corrosion," J. Am. Ceram. Soc., 56[7] (1973) 373-377.

12. D. E. Clark, E. C. Ethridge and L. L. Hench, "Effects of Glass Surface Area to Solution Volume Ratio on Glass Corrosion," Physics and Chemistry of Glasses, 20[2] (1979) 35-40.

13. D. M. Sanders, W. B. Person and L. L. Hench, "New Methods for Studying Glass Corrosion Kinetics," Appl. Spectroscopy, 26[5] (1972) 530-536.

Table 1

Compositions of Nuclear Waste Glasses and Simulated Fission Product Oxides (F.P.O.)

| Glass | $Na_2O$ | $Li_2O$ | ZnO | $Al_2O_3$ | $B_2O_3$ | $Fe_2O_3$ | $SiO_2$ | $UO_2$ | F.P.O. |
|---|---|---|---|---|---|---|---|---|---|
| ABS 39 | 12.91 | -- | -- | 3.1 | 19.12 | 5.71 | 48.54 | 1.66 | 9.0 |
| ABS 41 | 9.40 | 2.99 | 2.99 | 2.50 | 15.90 | 3.60 | 52.00 | 1.60 | 9.0 |

| Simulated Fission Product Oxides | wt % |
|---|---|
| $Cs_2O$ | 9.88 |
| SrO | 2.92 |
| BaO | 5.16 |
| $Y_2O_3$ | 1.69 |
| $ZrO_2$ | 14.37 |
| $MoO_3$ | 18.30 |
| $MnO_2$ | 8.65 |
| NiO | 4.15 |
| $Ag_2O$ | 0.12 |
| SnO | 0.19 |
| $Sb_2O_3$ | 0.04 |
| $La_2O_3$ | 7.97 |
| $Nd_2O_3$ | 13.58 |
| $Pr_2O_3$ | 4.26 |
| $Ce_2O_3$ | 8.42 |
| CdO | 00.29 |
| | 100.00 |

Table 2

FTIRRS* Results of 12 Month Minican Burial in STRIPA

| ABS Glass Type and Location | Interface | Temp °C | No. of Analysis | S Peak Location (P) ($cm^{-1}$) | | | | S Peak Intensity (I) | | | |
|---|---|---|---|---|---|---|---|---|---|---|---|
| | | | | Upper Limit | Lower Limit | Mean $P_m$ | Standard Deviation | Upper Limit | Lower Limit | Mean $I_{P_m}$ | Standard Deviation $\sigma_I$ |
| 41-1 | glass/bentonite | 10 | 8 | 1066 | 1058 | 1061 | 2.6 | 20.8 | 8.7 | 15.0 | 4.9 |
| 41-2 | glass/bentonite | 10 | 8 | 1041 | 1033 | 1037 | 2.8 | 26.7 | 17.4 | 21.4 | 4.0 |
| 41-3 | glass/bentonite | 10 | 8 | 1042 | 1034 | 1037 | 2.8 | 25.2 | 18.4 | 22.3 | 2.6 |
| 41-4 | glass/bentonite | 10 | 8 | 1064 | 1057 | 1061 | 2.2 | 10.9 | 9.9 | 10.4 | 0.4 |
| 39.5 | glass/bentonite | 10 | 8 | 1061 | 1050 | 1054 | 3.5 | 11.7 | 4.7 | 8.8 | 2.7 |
| 39.6 | glass/glass | 10 | 8 | 1033 | 1027 | 1030 | 2.9 | 26.3 | 22.0 | 25.1 | 1.4 |
| 39-7 | glass/glass | 10 | 8 | 1038 | 1028 | 1033 | 3.1 | 26.2 | 24.9 | 25.5 | 0.5 |
| 39-8 | glass/bentonite | 10 | 8 | 1056 | 1052 | 1054 | 2.4 | 16.0 | 6.7 | 12.4 | 2.8 |
| 41-1 | glass/bentonite | 90 | 8 | 1067 | 1060 | 1065 | 2.5 | 10.3 | 1.3 | 6.9 | 3.4 |
| 41-2 | glass/glass | 90 | 8 | 1093 | 1066 | 1075 | 7.9 | 23.2 | 11.3 | 16.2 | 5.2 |
| 41-3 | glass/glass | 90 | 8 | 1084 | 1065 | 1075 | 5.9 | 24.2 | 4.9 | 16.3 | 5.7 |
| 41-4 | glass/bentonite | 90 | 8 | 1065 | 1017 | 1043 | 16.7 | 11.1 | 4.8 | 7.6 | 2.6 |
| 39-5 | glass/bentonite | 90 | 8 | 1047 | 1023 | 1034 | 10.0 | 12.5 | 4.0 | 6.9 | 3.2 |
| 39-6 | glass/glass | 90 | 8 | 1065 | 1045 | 11057 | 7.5 | 21.7 | 15.2 | 18.0 | 2.4 |
| 39-7 | glass/glass | 90 | 8 | 1064 | 1045 | 1056 | 6.3 | 21.9 | 8.5 | 16.0 | 4.4 |
| 39-8 | glass/bentonite | 90 | 8 | 1063 | 1044 | 1053 | 7.2 | 14.2 | 5.7 | 11.2 | 2.8 |

*(5 mm spots, 160n scans/spot)

Table 3

Geometric Dependence of FTIRRS* Results of 12 Month Minican Burial in STRIPA

| ABS Glass Type and Location | Interface | Temp °C | No. of Analysis | S Peak Location (P) ($cm^{-1}$) Upper Limit | Lower Limit | Mean $P_m$ | Standard Deviation | S Peak Intensity (I) Upper Limit | Lower Limit | Mean $I_{P_m}$ | Standard Deviation $\sigma_I$ |
|---|---|---|---|---|---|---|---|---|---|---|---|
| 41-3(E) | glass/glass | 90 | 4 | 1080 | 1070 | 1074 | 4.3 | 21.4 | 14.2 | 18.0 | 2.9 |
| 41-3(M) | glass/glass | 90 | 4 | 1083 | 1066 | 1077 | 7.3 | 21.3 | 12.1 | 17.1 | 3.8 |
| 41-3(C) | glass/glass | 90 | 4 | 1083 | 1072 | 1079 | 4.8 | 21.2 | 15.4 | 17.7 | 2.7 |
| 39-7(E) | glass/glass | 90 | 4 | 1065 | 1060 | 1062 | 2.2 | 16.8 | 7.2 | 10.0 | 4.7 |
| 39-7(M) | glass/glass | 90 | 4 | 1061 | 1056 | 1059 | 2.1 | 23.6 | 17.6 | 21.6 | 2.8 |
| 39-7(C) | glass/glass | 90 | 4 | 1068 | 1066 | 1067 | 0.8 | 21.7 | 19.7 | 21.0 | 0.9 |
| 41-4(E) | glass/bentonite | 90 | 6 | 1045 | 1006 | 1017 | 14.8 | 18.1 | 6.1 | 12.3 | 3.9 |
| 41-4(C) | glass/bentonite | 90 | 6 | 1071 | 1035 | 1056 | 13.3 | 8.4 | 1.2 | 4.2 | 2.7 |
| 39-8(E) | glass/bentonite | 90 | 6 | 1065 | 1026 | 1044 | 16.0 | 16.1 | 10.2 | 12.8 | 2.4 |
| 39-8(C) | glass/bentonite | 90 | 6 | 1065 | 1046 | 1058 | 7.4 | 18.5 | 1.7 | 10.7 | 8.0 |

*(5 mm spots, 160 scans/spot)

Table 4

Statistical Comparison of 1 Year Minicans

| | C.L. | Vmax | |
|---|---|---|---|
| 90' mc41-1 to 90' mc41 | 0.01 | YES | |
| 90' mc39-5 to 90' mc39 | 0.01 | YES | YES |
| mc39-7E to mc39-7M | 0.01 | NO | YES |
| mc39-7E to mc39-7C | 0.01 | YES | YES |
| mc39-7M to mc39-7C | 0.01 | YES | NO |
| mc39-8E to mc39-8C | 0.01 | YES | NO |
| mc39-7E to mc39-8E | 0.01 | YES | NO |
| mc39-7C to mc39-8C | 0.01 | YES | YES |
| mc39-7E to mc41-3E | 0.01 | YES | YES |
| mc39-7M to mc41-3M | 0.01 | YES | NO |
| mc39-7C to mc41-3C | 0.01 | YES | NO |
| mc41-3E to mc41-3M | 0.01 | NO | NO |
| mc41-3E to mc41-3C | 0.01 | NO | NO |
| mc41-3M to mc41-3C | 0.01 | NO | NO |
| mc41-4E to mc41-4C | 0.01 | YES | YES |
| mc41-3E to mc41-4E | 0.01 | YES | YES |
| mc41-3C to mc41-4C | 0.01 | YES | YES |
| mc39-8E to mc41-4E | 0.01 | YES | NO |
| mc39-8C to mc41-4C | 0.01 | NO | YES |

Figure 1.

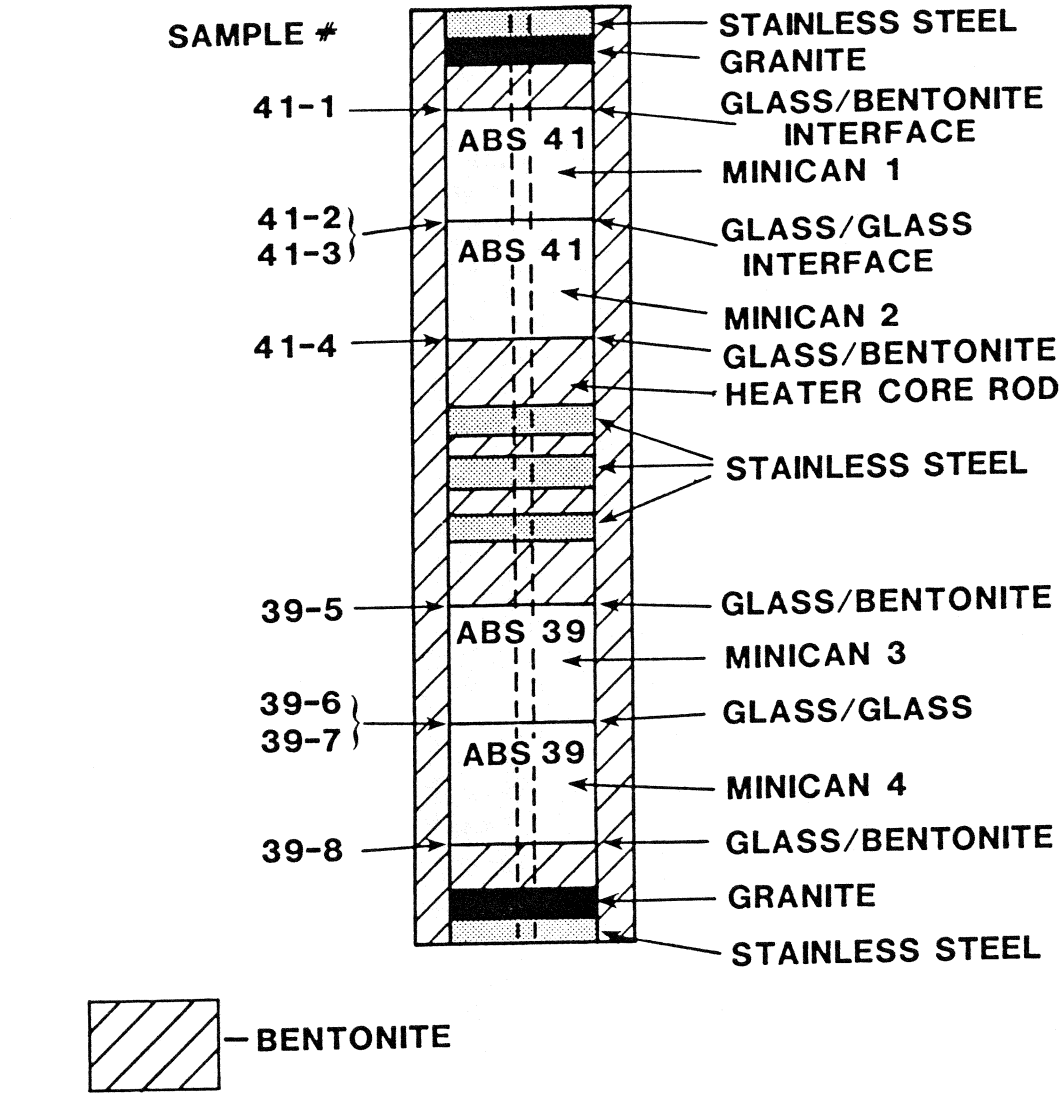


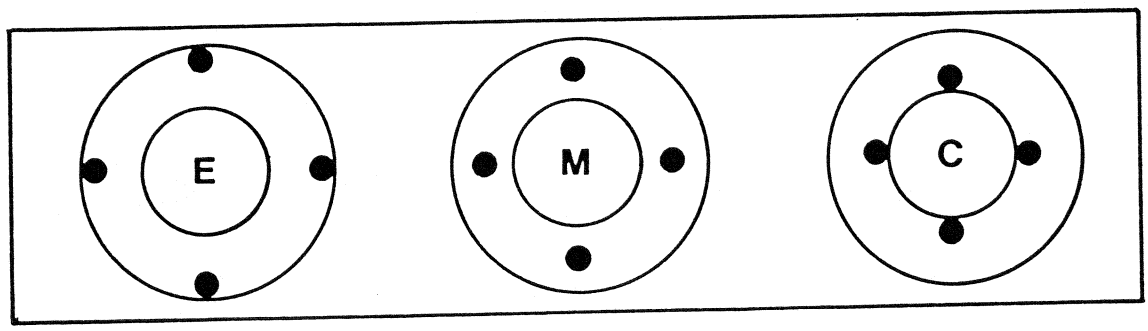


Figure 2.

MINI-CAN ASSEMBLY

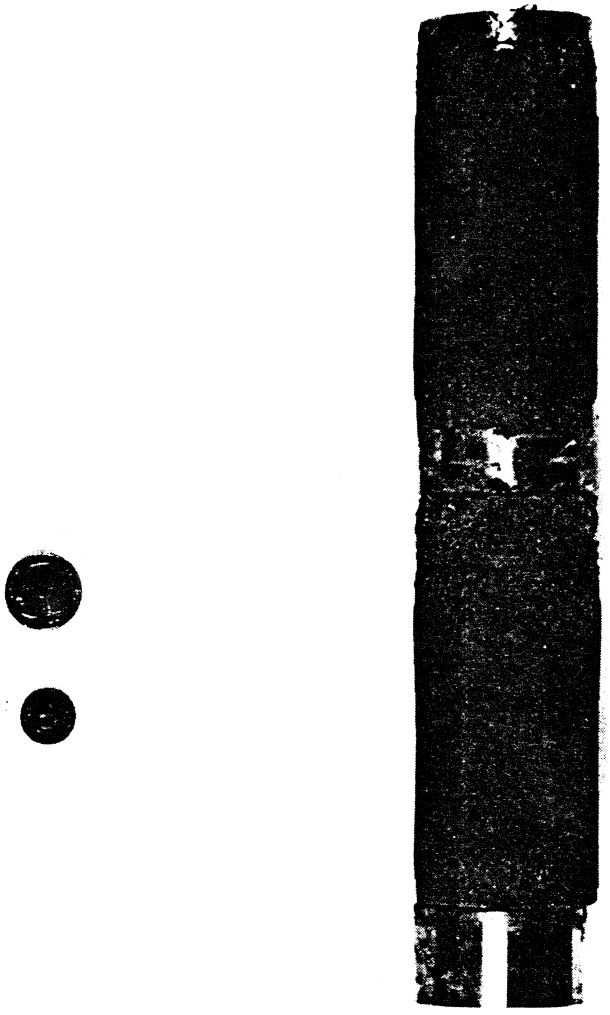

Post Burial-1 Month-90 C

Figure 2a. Post Burial Minican Assembly

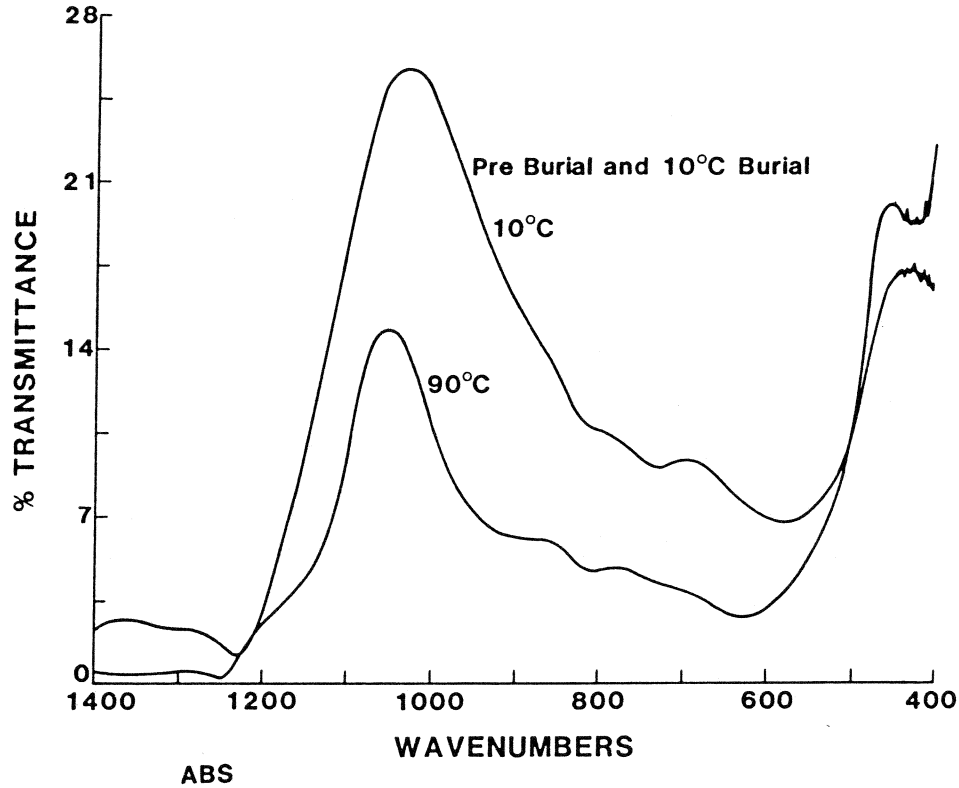


Figure 3. 39-7 Glass/Glass

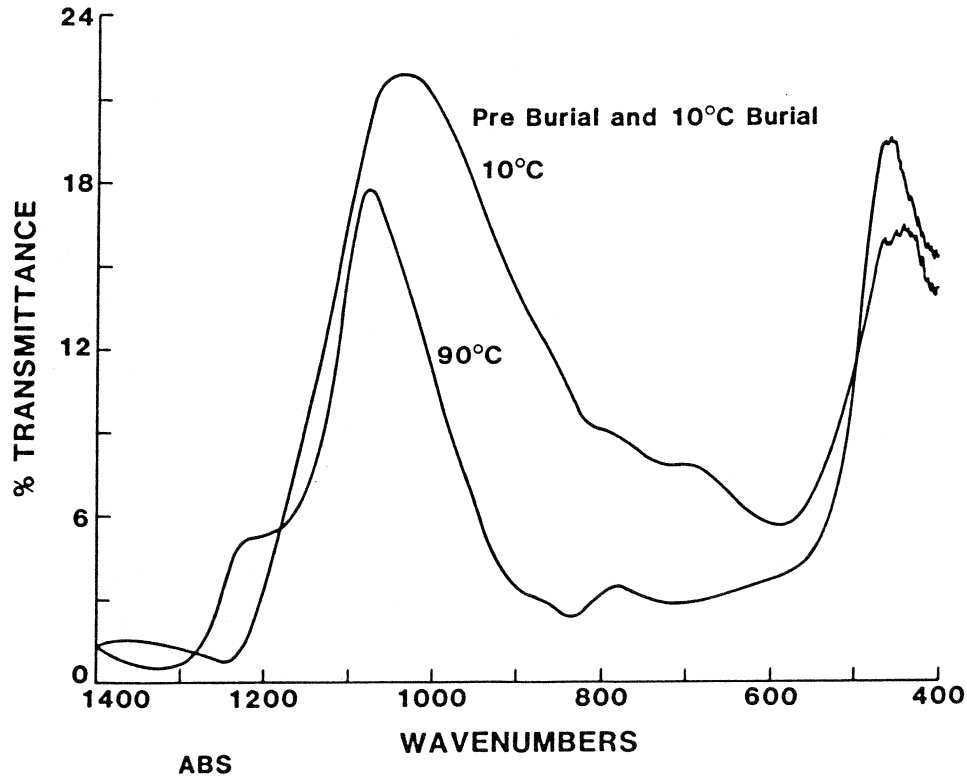


Figure 4. 41-3 Glass/Glass

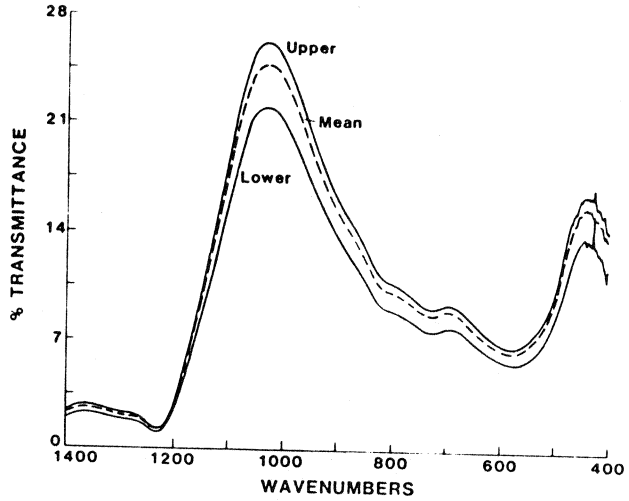


ABS d
Figure 5. 10-39-6 f Glass/Glass 10°C
c

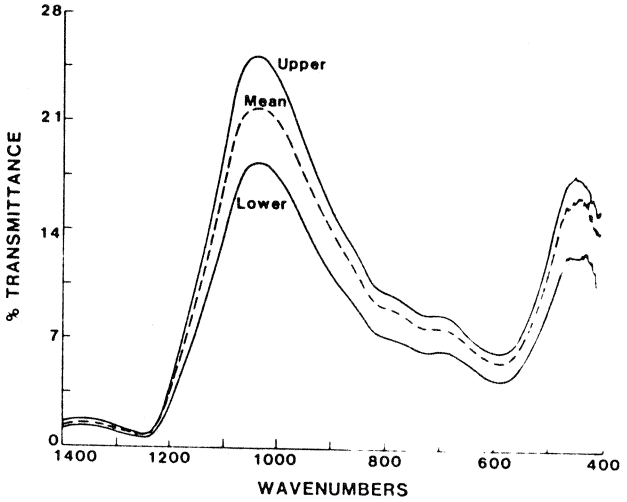


ABS c
Figure 6. 10-41-3 f Glass/Glass 10°C Median
b

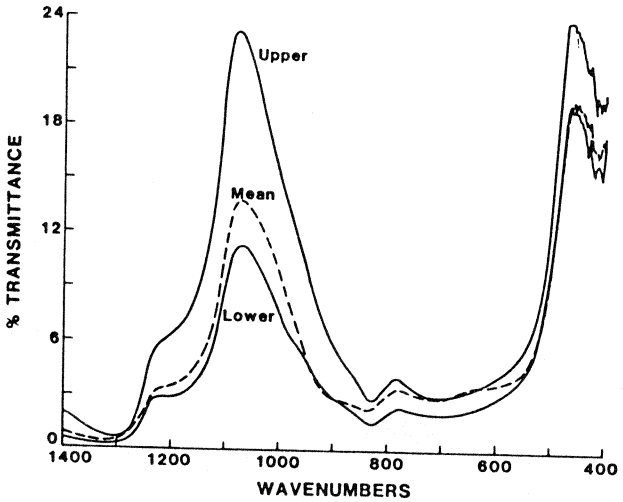


ABS e
Figure 7. 90-41-2 g Glass/Glass 90°C
c

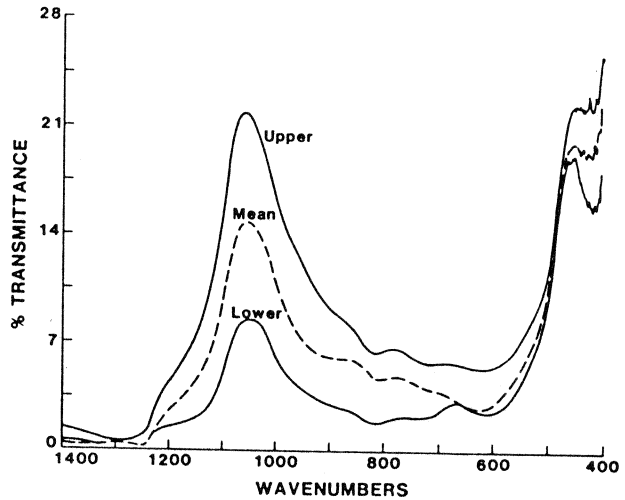


ABS e
Figure 8. 90-39-7 d Glass/Glass 90°C
a

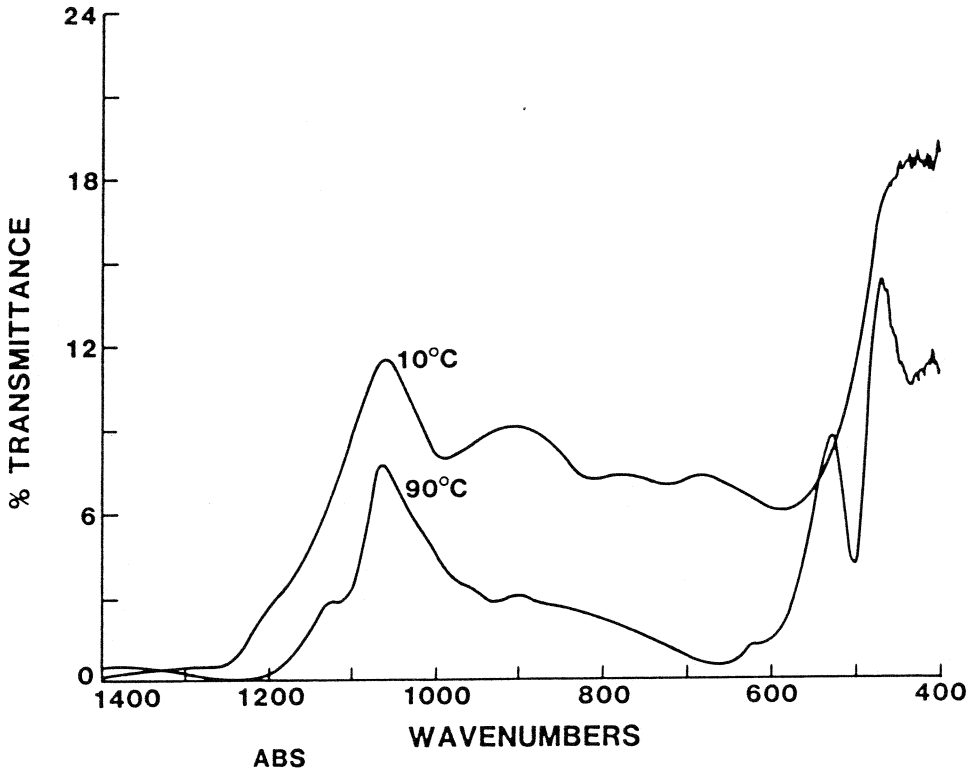


Figure 9. 41-1 Glass/Bentonite

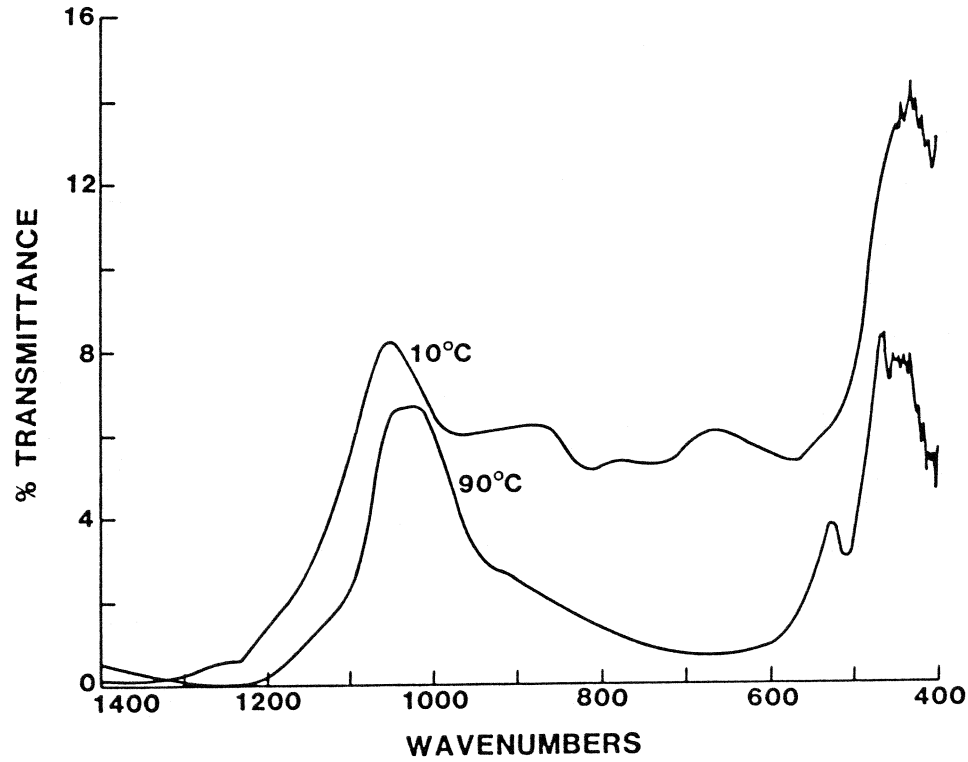


Figure 10. 39-5 Glass/Bentonite

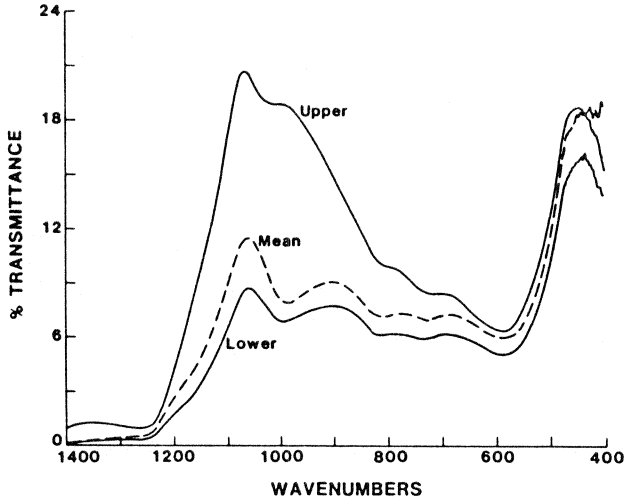


ABS g
Figure 11. 10-41-1 a Glass/Bentonite 10°C
e

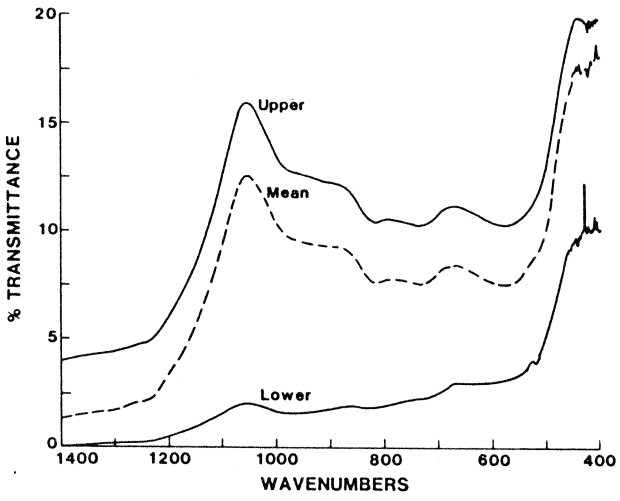


ABS f
Figure 12. 10-39-8 e Glass/Bentonite 10°C
h

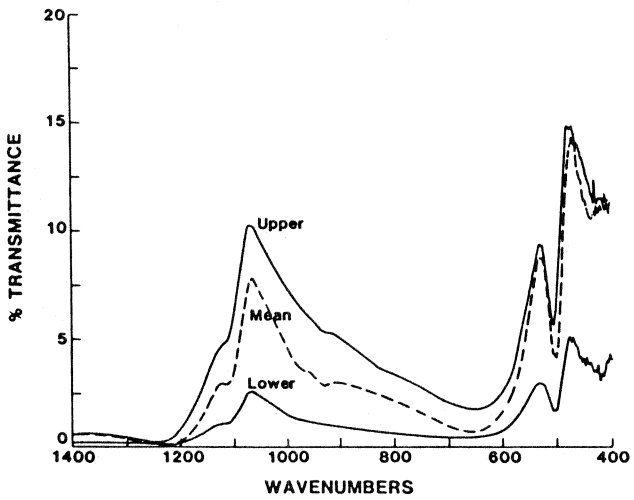


ABS c
Figure 13. 90-41-1 h Glass/Bentonite 90°C
e

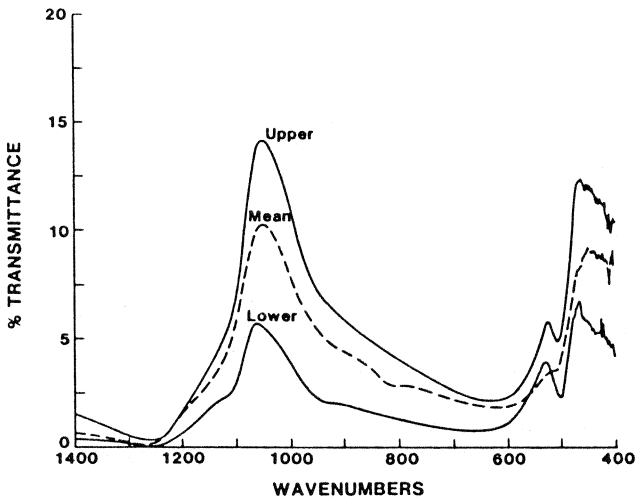


ABS e
Figure 14. 90-39-8 a Glass/Bentonite
c

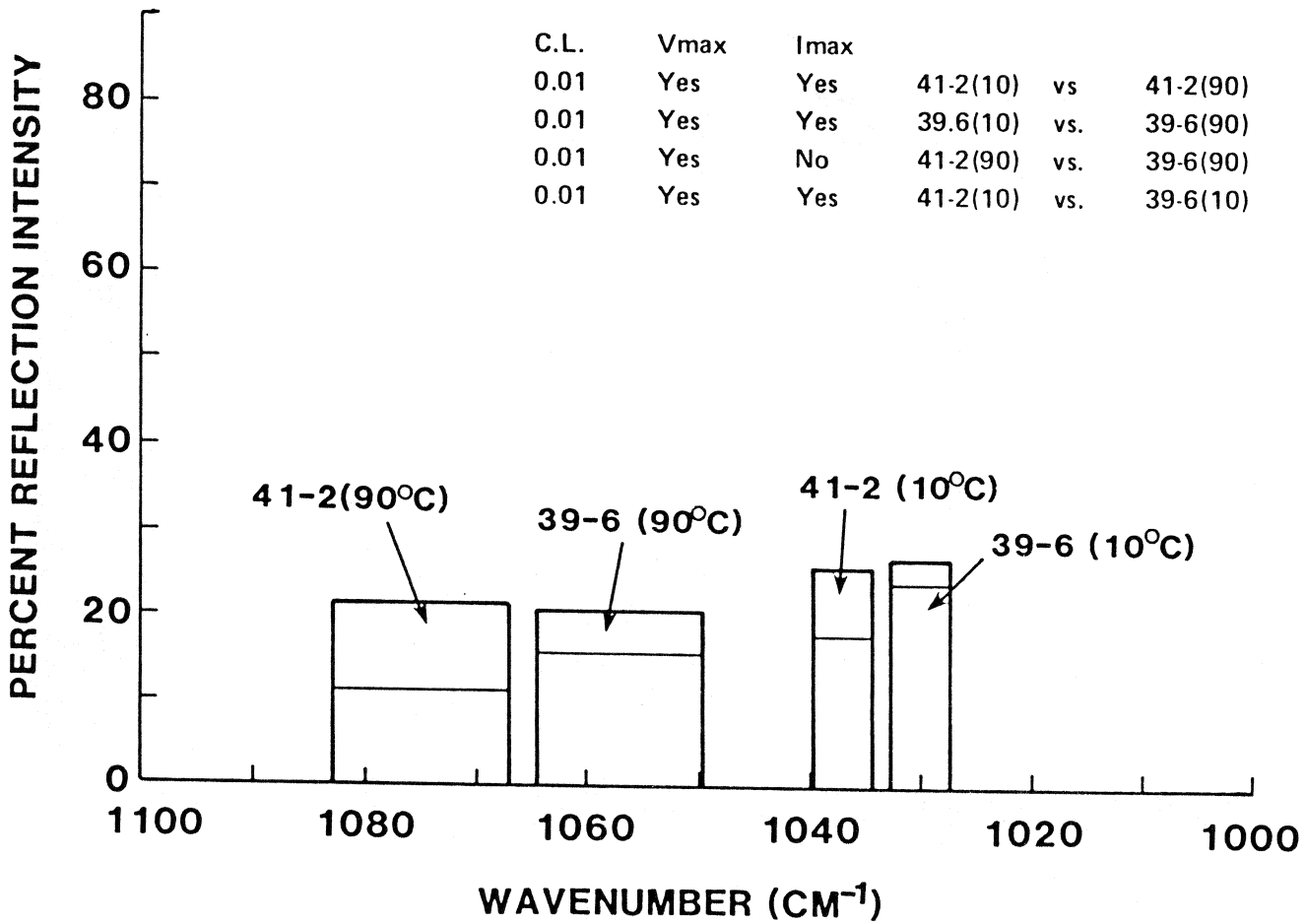
C.L. Vmax Imax
0.01 Yes Yes 41-2(10) vs 41-2(90)
0.01 Yes Yes 39.6(10) vs. 39-6(90)
0.01 Yes No 41-2(90) vs. 39-6(90)
0.01 Yes Yes 41-2(10) vs. 39-6(10)
PERCENT REFLECTION INTENSITY
80
60
40
20
0
41-2(90°C)
39-6 (90°C)
41-2 (10°C)
39-6 (10°C)
1100
1080
1060
1040
1020
1000
WAVENUMBER (CM⁻¹)

Figure 15.

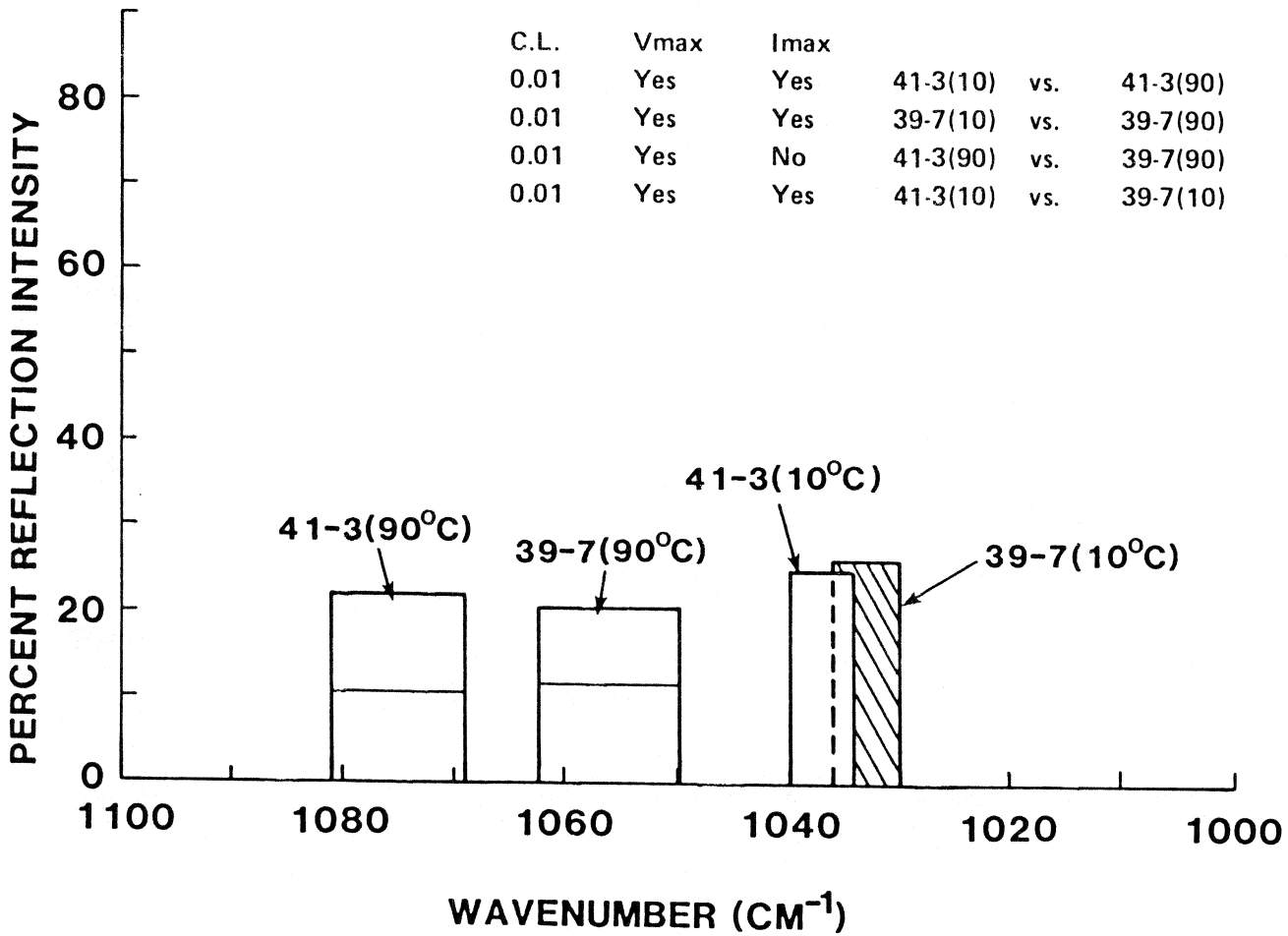
C.L. Vmax Imax
0.01 Yes Yes 41-3(10) vs. 41-3(90)
0.01 Yes Yes 39-7(10) vs. 39-7(90)
0.01 Yes No 41-3(90) vs. 39-7(90)
0.01 Yes Yes 41-3(10) vs. 39-7(10)
PERCENT REFLECTION INTENSITY
80
60
40
20
0
41-3(90°C)
39-7(90°C)
41-3(10°C)
39-7(10°C)
1100
1080
1060
1040
1020
1000
WAVENUMBER (CM-1)

Figure 16.

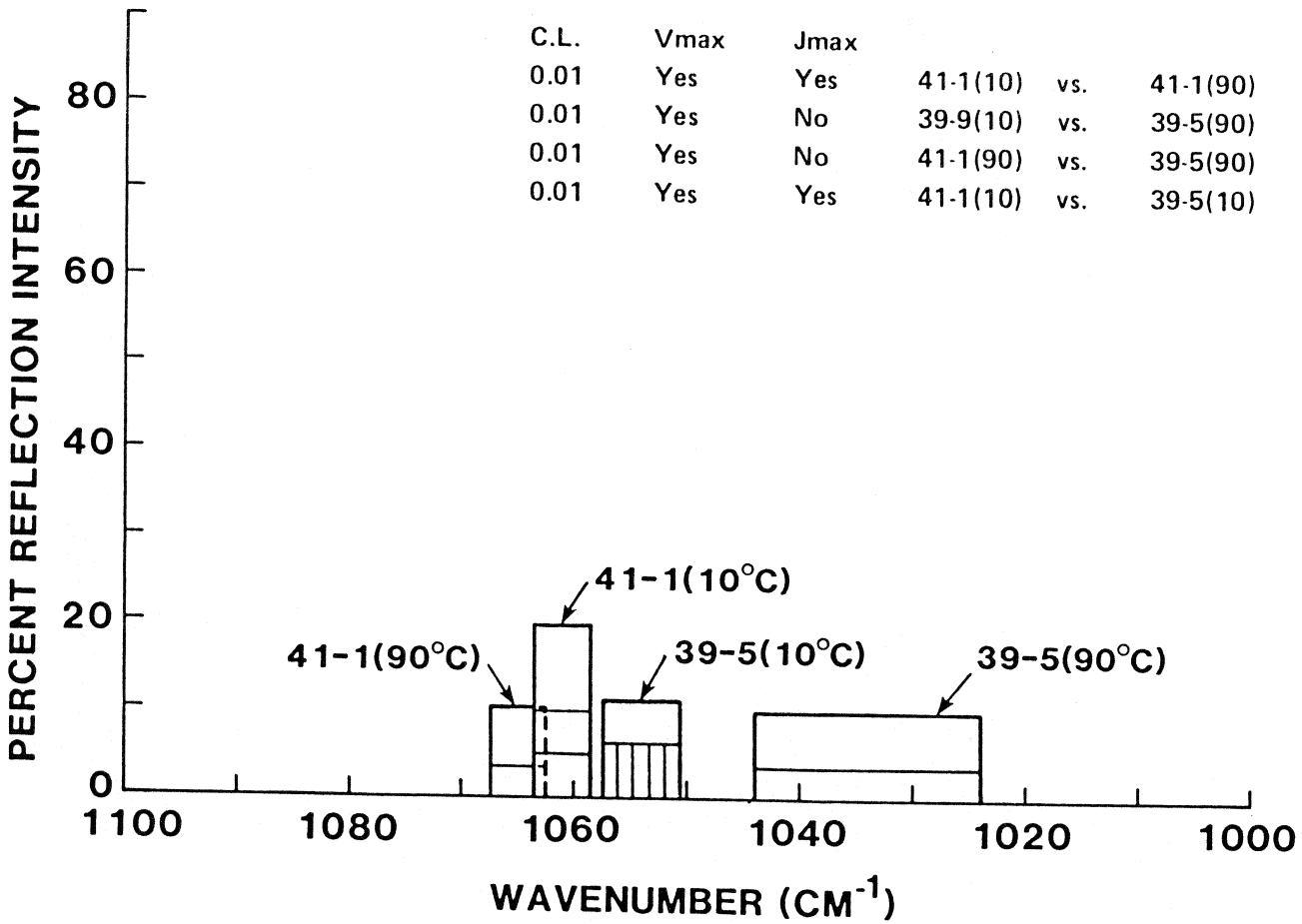
C.L. Vmax Jmax
0.01 Yes Yes 41-1(10) vs. 41-1(90)
0.01 Yes No 39-9(10) vs. 39-5(90)
0.01 Yes No 41-1(90) vs. 39-5(90)
0.01 Yes Yes 41-1(10) vs. 39-5(10)
PERCENT REFLECTION INTENSITY
80
60
40
20
0
41-1(10°C)
41-1(90°C)
39-5(10°C)
39-5(90°C)
1100
1080
1060
1040
1020
1000
WAVENUMBER (CM-1)

Figure 17.

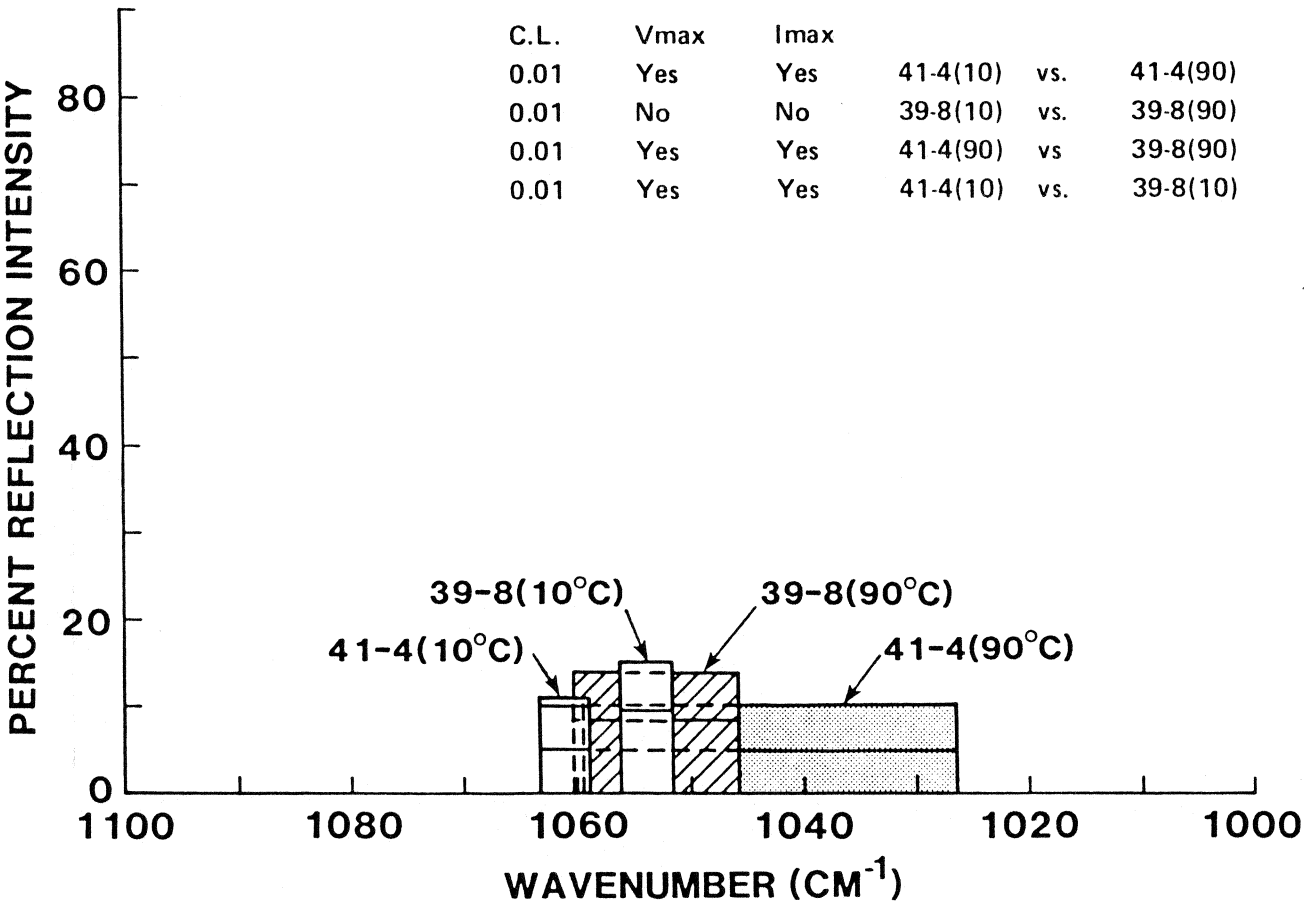
C.L. Vmax Imax
0.01 Yes Yes 41-4(10) vs. 41-4(90)
0.01 No No 39-8(10) vs. 39-8(90)
0.01 Yes Yes 41-4(90) vs 39-8(90)
0.01 Yes Yes 41-4(10) vs. 39-8(10)
PERCENT REFLECTION INTENSITY
0
20
40
60
80
39-8(10°C)
39-8(90°C)
41-4(10°C)
41-4(90°C)
1100
1080
1060
1040
1020
1000
WAVENUMBER (CM-1)

Figure 18

# *List of Technical Reports*

*1977–78*
TR 121
**KBS Technical Reports 1 – 120.**
Summaries. Stockholm, May 1979.

*1979*
TR 79–28
**The KBS Annual Report 1979.**
KBS Technical Reports 79-01 – 79-27.
Summaries. Stockholm, March 1980.

*1980*
TR 80–26
**The KBS Annual Report 1980.**
KBS Technical Reports 80-01 – 80-25.
Summaries. Stockholm, March 1981.

*1981*
TR 81–17
**The KBS Annual Report 1981.**
KBS Technical Reports 81-01 – 81-16.
Summaries. Stockholm, April 1982.

*1982*
TR 82–28
**The KBS Annual Report 1982.**
KBS Technical Reports 82-01 – 82-27.
Summaries. Stockholm, July 1983.

*1983*
TR 83–77
**The KBS Annual Report 1983.**
KBS Technical Reports 83-01 – 83-76
Summaries. Stockholm, June 1984.

*1984*
TR 85–01
**Annual Research and Development Report 1984**
Including Summaries of Technical Reports Issued during 1984. (Technical Reports 84-01–84-19)
Stockholm June 1985.

*1985*
TR 85–01
**Annual Research and Development Report 1984**
Including Summaries of Technical Reports Issued during 1984.
Stockholm June 1985.

TR 85–02
**The Taavinunnanen gabbro massif. A compilation of results from geological, geophysical and hydrogeological investigations.**
Bengt Gentzschein
Sven-Åke Larson
Eva-Lena Tullborg
Swedish Geological Company
Uppsala, January 1985

TR 85–03
**Porosities and diffusivities of some non-sorbing species in crystalline rocks.**
Kristina Skagius
Ivars Neretnieks
The Royal Institute of Technology
Department of Chemical Engineering
Stockholm, 1985-02-07

TR 85–04
**The chemical coherence of natural spent fuel at the Oklo nuclear reactors.**
David B. Curtis
New Mexico, USA, March 1985

TR 85–05
**Diffusivity measurements and electrical resistivity measurements in rock samples under mechanical stress.**
Kristina Skagius
Ivars Neretnieks
The Royal Institute of Technology
Department of Chemical Engineering
Stockholm, 1985-04-15

TR 85-06
**Mechanical properties of granitic rocks from Gideå, Sweden**
Christer Ljunggren
Ove Stephansson
Ove Alm
Hossein Hakami
Ulf Mattila
Div of Rock Mechanics
University of Luleå
Luleå, Sweden, October 1985

TR 85-07
**Complex forming properties of natural occurring fulvic acids**
**Part 1. Complexes with cadmium, copper and calcium**
Jacob A. Marinsky,
A. Mathuthu,
M. Bicking and
J. Ephraim
State University of New York at Buffalo
Buffalo, New York 14214,
July 1985